9-3-2013

Incipient motion of mixed sediment load on the Rio Chama

Angela Gregory

Angela Gregory
Candidate

Civil Engineering
Department

This thesis is approved, and it is acceptable in quality and form for publication.

Approved by the Thesis Committee:

Dr. Mark Stone, Chairperson

Dr. Julie Coonrod

Dr. Grant Meyer

Incipient Motion of Mixed Sediment Load on the Rio Chama

BY

Angela Gregory

Bachelor of Science
Department of Civil Engineering
New Mexico State University, 2008

Submitted in Partial Fulfillment of the
Requirements for the Degree of

Master of Science
Civil Engineering

The University of New Mexico
Albuquerque, New Mexico

July, 2013

Incipient Motion of Mixed Sediment Load on the Rio Chama

BY

Angela Gregory

B.S. CIVIL ENGINEERING, NEW MEXICO STATE UNIVERSITY, 2008

M.S. CIVIL ENGINEERING, UNIVERSITY OF NEW MEXICO, 2013

ABSTRACT

Discharge and sediment supply are the primary controls affecting the ability of rivers to adjust. When these are modified to manage water resources for human needs, the ecosystem that relied on them is often negatively impacted. The river that once knew a specific dynamic equilibrium is forced to change. The result is usually changes in hydraulic geometry, a decrease in heterogeneity, bed armoring, disconnected floodplains, vegetative establishment and ecological impacts. Environmental flows are a way to find a middle ground for water resource managers and the physical and ecological needs of the river.

The Rio Chama, between El Vado Dam and Abiquiu Reservoir was designated as a Wild and Scenic River in 1988. Along with the desire to protect this reach, came the hope to manage and protect the habitat of brown trout that were introduced for sports fishing. The Rio Chama Instream Flow Assessment, completed by the Bureau of Land Management, aimed to determine flows necessary for brown trout habitat for all life stages but failed to determine the flows that would be required to maintain appropriate sediment conditions for the brown trout and macroinvertebrate food sources (BLM, 1992).

The objectives of this study were to spatially evaluate incipient motion of sediments for environmental flows and to determine the flow required to mobilize the channel bed. To accomplish the objective, topographic data collected at the Archuleta and Cebolla sites was used to develop a 2-D mesh in Surface-water Modeling Solution (SMS) and model hydraulic conditions using the Bureau of Reclamation's Sediment and River Hydraulics Two-Dimensional Model (SRH-2D). Wolman Pebble counts were completed at each site and particle sizes ranged from < 2 to 256 mm along the intermediate axis. Discharge for model runs within SRH-2D ranged from 14 m^3/s to 170 m^3/s in 14 m^3/s increments. Results from SRH-2D were used to calculate the particle size of incipient motion using Neill's method (1968) and implicit calculations of Shields equation and the Shields-Rouse dimensionless diameter equations (Guo, 2002). It was determined using Neill's method that for 85 m^3/s and 170 m^3/s, incipient motion for the full range of particle sizes is possible. For 85 m^3/s, the mean particle size of entrainment at Archuleta and Cebolla is 41 mm and 57 mm, respectively. However, there is significant spatial variability within each reach and it is likely that the predominant mode of transport is partial movement for all flows.

This research suggested that there is a strong connection between channel geometry and the ability of a channel to transport sediments at a given flow. The modeling efforts for this study showed that the most effective use of environmental flows for sediment transport would resemble a natural flow regime in terms of variability. Variability of flood size would accomplish movement of a broader range of sediment size classes as spatial conditions changed with distance downstream of a dam.

Table of Contents

List of Tables

List of Figures

Introduction

Heterogeneity within streams is the principal driver of the health and diversity of aquatic communities (Hynes, 1968; Sarriquet et al., 2007; Townsend & Hildrew, 1994; Sheldon, 1986). To maintain physically stable conditions, rivers rely on their historical water and sediment supply that allows them to morphologically adjust (Pitlick & Wilcock, 2001). Given no other changes occur that impact the watershed and its river, the river is able to maintain a state of dynamic equilibrium. Dynamic equilibrium is the state at which a landform changes with the energy and water/sediment supply that is exerted (Leopold et al., 1964; Schumm & Lichty, 1965; Hack, 1960). However, when dams are built to manage rivers, the result downstream is often reduction in flows, flood frequency and sediment supply. The river adapts towards a new state of dynamic equilibrium. Depending on the hydrology, geology and location of the dam, the adjusted flow and sediment regime can result in changes in hydraulic geometry, a decrease in heterogeneity, bed armoring, disconnected floodplain, vegetative establishment and ecological impacts (Williams & Wolman, 1984). While the extent of degradation varies by river, the impact that infrastructure in rivers has had as a whole is well documented.

The effect of dam construction on salmon populations along the west coast of the U.S. is a prime example of ecological impacts caused by dams. On the Trinity River in northern California, the installation of Lewiston Dam resulted in a reduction of peak flows and of nearly 100% of downstream sediment supply (Kondolf & Minear, 2004). The decrease in sediment supply and discharge caused the channel bed to be negatively affected due to sediment sorting and armoring. The domino effect of Lewiston dam eventually resulted in the reduction of the native salmon population.

One method used to alleviate issues that have arisen from the use of control structures are environmental flows. When meticulously planned and assessed, environmental flows have provided appreciable ecological benefits (Postel & Richter, 2003). Environmental flows can be used to mimic part of a river's natural flow regime or to achieve a particular outcome. If a channel has become entrenched because of the geomorphic outcome of installing a dam or the banks of the river have become hardened due to vegetative establishment, greater flows than are experienced with dam operations may be required to achieve a new state of dynamic equilibrium that supports a healthy ecosystem.

At the most basic level, it is important to understand the flows required to initiate incipient motion of the in situ grain size distribution. The establishment of incipient motion further allows for the study of sediment transport and dynamic equilibrium.

The purpose of this research was to gain knowledge on the effects that implementation of environmental flows would have on sediment mobility within different reaches of river and the river as a whole. The research was performed at two sites, Archuleta and Cebolla, on the Rio Chama. The Rio Chama is being assessed for implementation of environmental flows to support the brown trout fishery, riparian areas and overall health of the river system. As alluded to, the sediment that makes up the stream bed and supply of a river are of high importance to the ecosystem.

Sediment and River Hydraulics Two-Dimensional Model (SRH-2D) was used to numerically evaluate hydraulic conditions for a range of flows. Resulting boundary shear stresses were used to calculate the median particle size, D_{50}, at which incipient motion

would occur for each flow interval using Shields equation and the Shields-Rouse equation (Guo, 2002).

State of Knowledge

Shields

In 1936, the empirical Shields equation was developed with the aid of flume studies of non-cohesive sediments that related entrainment to hydraulic conditions, particle shape, and particle weight (Shields, 1936). Shields equation is implicitly expressed as a relationship between Shields parameter, τ_{*c}, (includes D_{50} particle size and critical shear stress) and the friction velocity, μ_*. The friction velocity in conjunction with particle size and kinematic viscosity make up the Boundary Reynolds Number (R_*) and describe the effects of the protrusion of particle size at the boundary (channel bed). As can be seen in Figure 1, Shields Diagram follows a log-log distribution. The line describes the point at which incipient motion begins, where points plotting in the field above the line denote movement and those below the line indicate static conditions. Beginning at the left axis, R_* is low (< 2) and τ_{*c} has been extrapolated for large values (Graf, 1971)- this area is laminar. The curve then enters what can be described as a saddle (Chien & Wan, 1999), where R_* is described as transitional. When R_*>400, motion occurs in hydraulically turbulent conditions and the line defining entrainment asymptotically approaches a constant critical shear parameter (Graf, 1971) of 0.045 (Chien & Wan, 1999; Yalin & da Silva, 2001). The relationship between particle size, critical shear stress and friction velocity in Shields equation is intuitive. However, in reviewing the experiments completed, concerns have remained throughout the years.

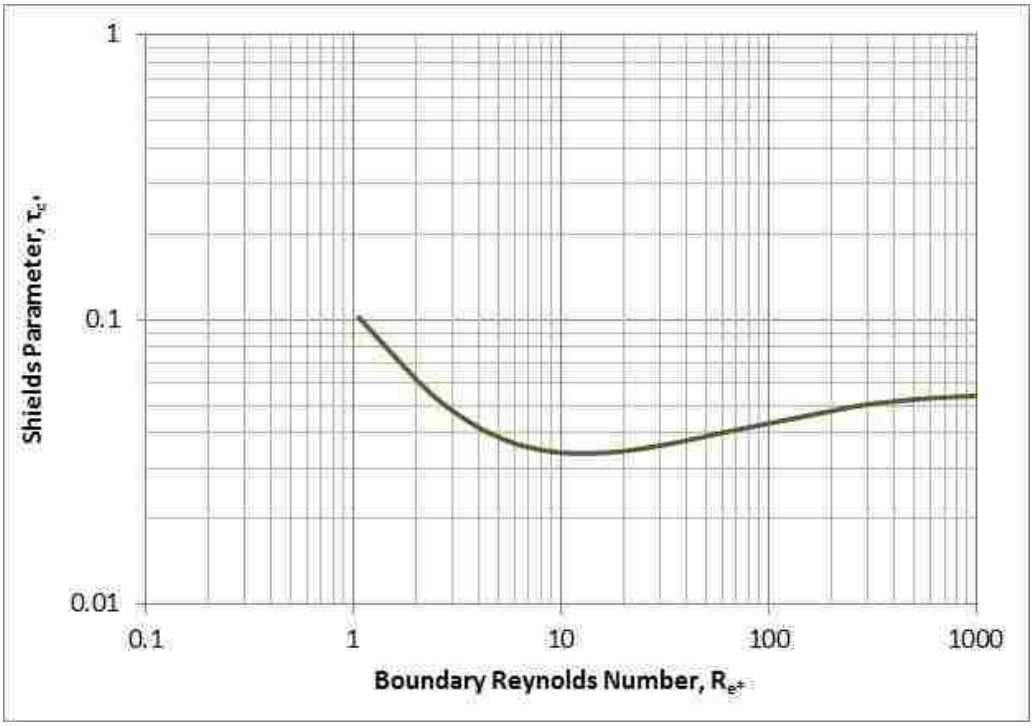

Figure 1: Shields Diagram Reproduced After Shields (1936)

Buffington (1999) and Kennedy (1995) have both studied Shields' work and have noted that Shields did not clearly state whether incipient motion was said to begin when partial or full bed movement occurred. Other criticisms include the use of mixed grain sizes, and unaccounted form drag as issues affecting the validity of his work. In addition, practitioners have found that the implicit nature of Shields equations make it difficult to calculate the critical shear stress at which motion begins for a particular condition (Guo, 2002). Nonetheless, his work has remained at the core of sediment transport work and critical tractive force studies (Cao et al., 2006).

To relieve the complexity of Shields parameters, numerous assumptions and explicit equations have been developed. In 1981, Brownlie proposed a curve similar to Shields for uniform surface gravels. Brownlie's research supported Neill's 1968 findings that for uniform gravels collected on the streambed surface, $\tau_{*c} = 0.03$. Neill's method is

practical for situations where pebble counts have been taken (Wilcock et al., 2009). The limitation of Neill's findings are that they are appropriate only when gravel size varies by one order of magnitude (Wilcock et al., 2009). To determine the relationship between the D_{50} particle size, shear stress, and incipient motion additional equations would be needed to determine the point of entrainment. Expression of Shields equation has been made easier with the help of Rouse's Reynolds Number, Guo's expression of Shields parameter as a function of the boundary Reynold's number, and Bonnefille and Gessler's dimensionless diameter (Raudkivi, 1998; Guo, 2002).

Equal Mobility vs. Selective Mobility

The oversimplification of incipient motion as a function of particle size led researchers to propose two opposing hypotheses regarding incipient motion. The concept of equal mobility was introduced by Parker et al. (1982) and Andrews (1983). Equal mobility refers to the movement of different size classes at the same shear stress (Knighton, 1998). Later research showed that equal mobility does not occur (Ashworth and Ferguson, 1989; Komar and Shih, 1992). However, the incipient motion of larger sediments in mixed sediments does occur at lower values of shear stress than initially represented by Shields equation. The movement of one particle size is known as selective mobility.

The concepts of selective mobility and equal mobility are important when considering sediment transport for environmental flows because they can aid in the determination of extent of mobilization (partial or full) in channel.

Site Description

The Rio Chama originates in southern Colorado's San Juan and Cumbres Mountains and flows south through northern New Mexico. The Rio Chama watershed is 8,300 square kilometers and the Rio Chama has historically contributed more flow to the Rio Grande in New Mexico than any other tributary (Swanson, Meyer, & Coonrod, 2012). Over time it has been modified to include several dams and transport interbasin flow from the San Juan River watershed. Unlike many rivers with dams, the Rio Chama below El Vado Reservoir has inflow of sediments from several tributaries and active erosion of the banks that maintain the sediment supply. In comparison to other systems that are more susceptible to sorting and armoring in the channel bed, the Rio Chama is fairly well off due to the positioning of these tributaries that contribute large amounts of sediment. In terms of water, the introduction of interbasin flows has caused mean annual flow to increase from 347 cfs to 432 cfs (Morrison, 2013). However, the frequency of maximum flows has been reduced and has caused channel narrowing and downcutting (Swanson et al., 2012). The lack of high flows within this reach of river is the driving force for evaluating sediment transport for environmental flows. An example of a typical year on the Rio Chama in terms of flow is shown in . The hydrograph shows flows prior to the introduction of San Juan water to the Rio Chama in 1971. Another note regarding the daily hydrograph is that two different gages were used to compare flows. The La Puente gage is located 13 miles upstream of El Vado reservoir and is unaffected by a control structure. As can be seen, the maximum flows in spring are reduced and flows are increased in the summer months when little flow would be available if no control

structure was in place.

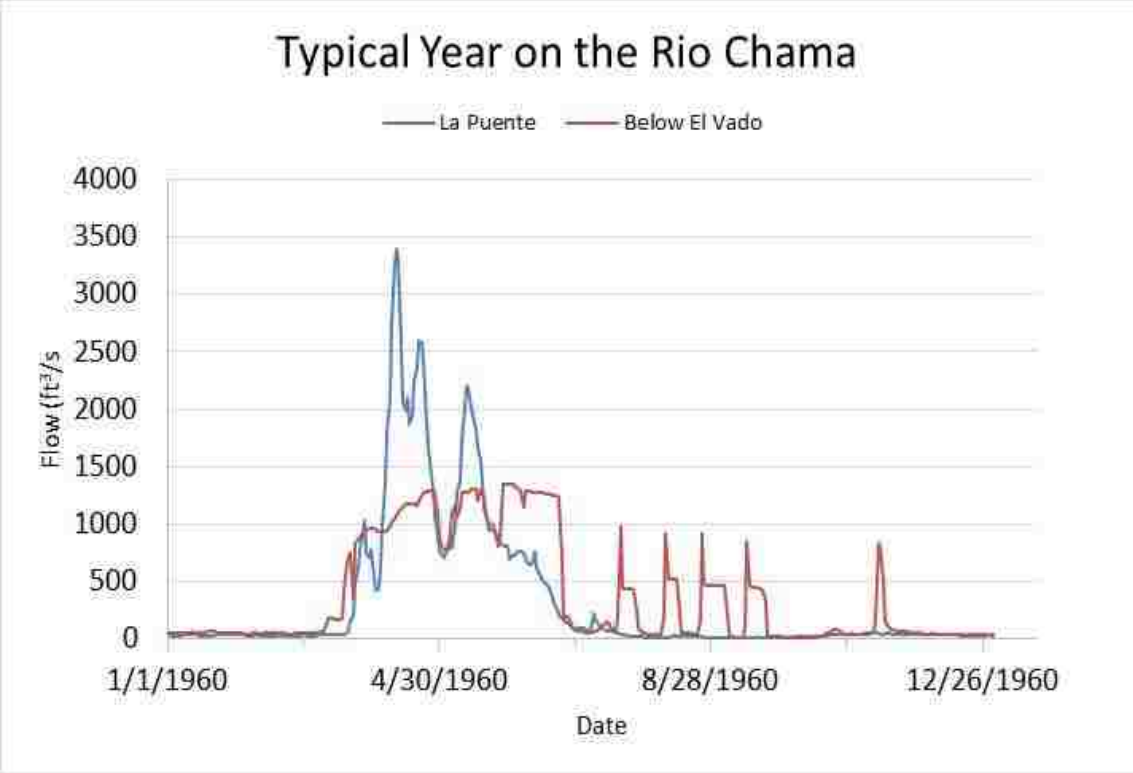

Figure 2: Daily Average Flow on the Rio Chama, 1960

Located between El Vado and Abiquiui Reservoirs, the Archuleta site, 36°32' N, -106°44'W, and Cebolla site, 36°27'N, -106°42', (see Figure 3) were identified as places of interest for the purposes of this study.

Archuleta is located 11.7 kilometers downstream of El Vado Dam. The reach is approximately 875 meters in length and has an overall slope of 0.002. The Rio Nutrias flows in just upstream of the site and Arroyo del Puerto Chiquito (Chiquito) comes in from the west. This reach has numerous vegetated bars and the channel is braided. The D_{50} particles size ranged between 40 mm and 90 mm, see Appendix D for more information. From observation, the channel primarily consisted of gravels with sand deposits located at the inlet of the Chiquito and at the heads and tails of vegetated bars.

Cebolla is located 12.6 kilometers downstream of Archuleta and sediments are delivered from the Rio Cebolla from the east. The reach is 970 meters in length and has a slope of 0.003. Cebolla is more entrenched than Archuleta and is surrounded by canyon walls. In addition, the channel has fewer vegetated bars, is narrower and less sinuous. The D_{50} particle size ranged between 50 mm and 70 mm. Similar to Archuleta, the channel is predominantly gravel materials with sand deposits located in the vicinity of vegetated bars and at the confluence of the Rio Cebolla.

Figure 3: Location Map of Archuleta Site and Cebolla Site

Method

This research was completed in several phases. First topographic data and pebble count data were collected at Archuleta and Cebolla. A mesh was then developed using SMS and was used in completing model runs in SRH-2D for a range of flows. Boundary shear stress was interpreted as critical shear stress and the critical D_{50} was then calculated. Each of these phases is discussed in depth in the proceeding sections.

Tetra Tech, Inc. collected topographical information from the Archuleta and Cebolla sites. In order to provide data that would be most useful for two dimensional hydraulic modeling, linear interpolation was completed between each of the cross-sections in channel. Some areas were not included in the interpolation due to the complicated topography and number of survey points, see Appendix E for more details. The topographical data can be seen in Figure 4 and Figure 5.

Once interpolation was completed for both sites, the survey points were brought into SMS, a graphical user interface that allows individuals to develop a numerical mesh. Each channel was split into three primary sections: floodplain left, channel and floodplain right. From there, polygons that could be used to define mesh elements were developed and further divided so that channel features such as vegetated gravel bars could be identified. The polygons were made up of vertices that were equally spaced at 1.5 m apart. Once all of the polygons were composed, each was defined by material type, mesh type, and interpolation (linear) and extrapolation methods (inverse distance weighted).

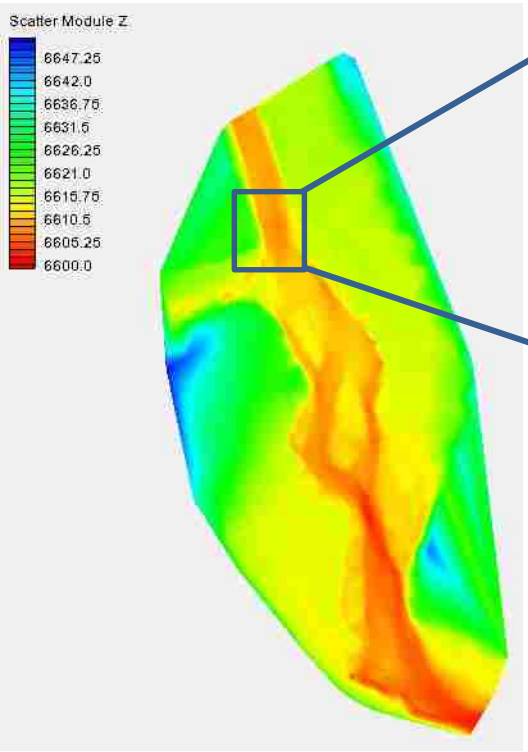

Figure 4a: Archuleta Site Topography

Figure 4b: Inset of Topography in Figure 4a at Archuleta

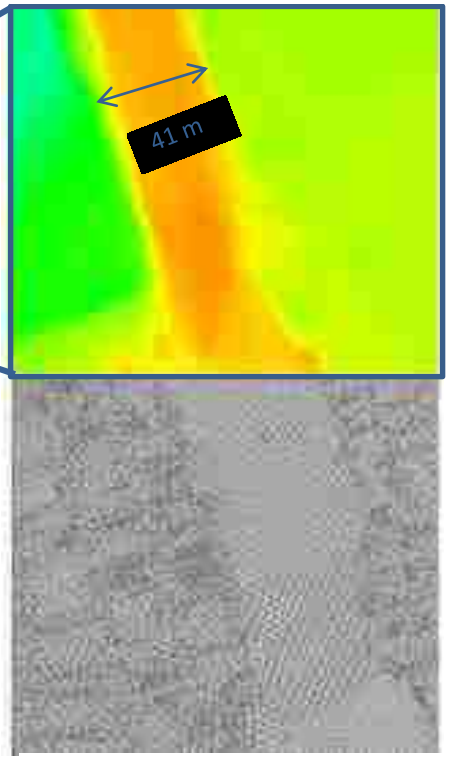

Figure 4c: Mesh Elements (1.5 m.) at Archuleta for Inset in Figure 4b

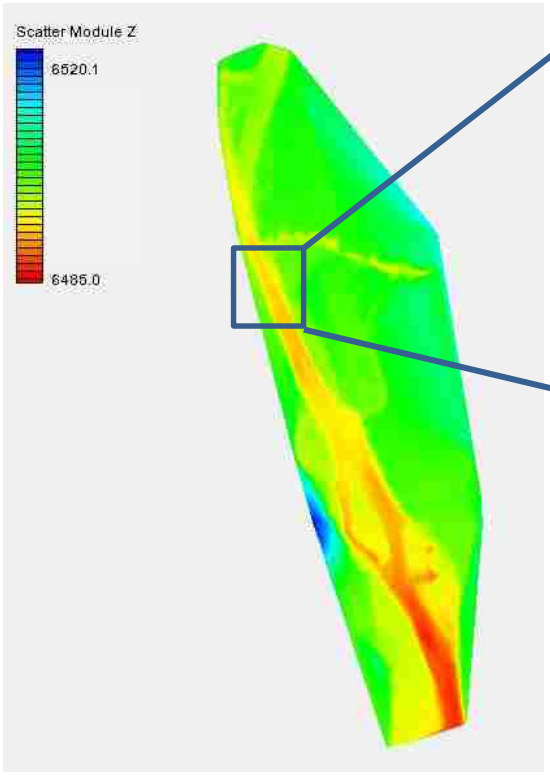

Figure 5a: Cebolla Site Topography

Figure 5b: Inset of Topography in Figure 5a at Cebolla

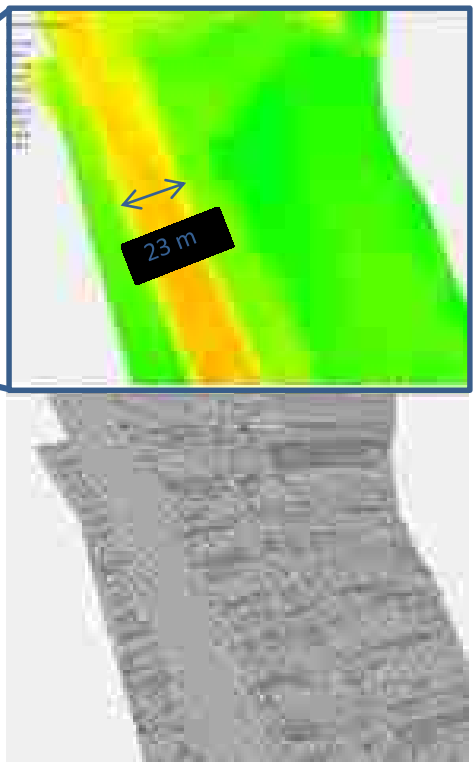

Figure 5c: Mesh Elements (1.5 m) at Cebolla for Inset in Figure 5b

Researchers have recognized that hybrid meshes can provide the most benefit when considering numerical hydraulic models (Bernard & Berger, 1999). Lai noted that triangular mesh elements should be used in the floodplain and quadrilateral elements should be used within the river to ease the rigidity of the mesh. Polygons located in the floodplain were labeled, "paving," which is the equivalent of triangular meshing. Polygons located within the Rio Chama were defined as "patch-" the equivalent of quadrilateral meshing.

Each site was then divided into four different material types: floodplain, gravels, gravels with fines, and fines. As observed in situ, the reaches of concern are predominantly gravel bed channel with fine sediment being found in pockets within gravel bars and in deposits located at the mouth of the inflowing tributary. Primary sources of fine and gravel sediments are the Rio Cebolla and the Rio Nutrias. To characterize the particle size distribution for the channel bed surfaces at each site, the Wolman Pebble Count method (Wolman, 1954) was used in riffles as defined by Bunte & Abt (2001). Each riffle was divided into sections of ten, longitudinally, and samples were hand-picked in equally spaced increments. A total of five pebble counts were taken each at Archuleta and Cebolla. For the purposes of this study, the D_{50} at Archuleta and Cebolla are set to 50 mm and 60 mm respectively.

The data collected was used to define the Manning's *n* for material types "Gravels" and "Gravels with fines." Areas with higher fine sediment content were used to characterize the Manning's *n* for sites defined as having material type "Gravels with fines," and sites with lower contents were used for "Gravels." The pebble count data was

plotted against the percent passing and the D_{50} and D_{90} were identified. The Manning's-Strickler equation, see Equation 1, was then used to determine the Manning's *n* values. Values of Manning's n are presented in Table 1. Manning's –Strickler Equation is a fixed-bed friction factor developed using data from gravel-bed rivers and fixed bed channels (Brownlie, 1983; Strickler, 1923).

Equation 1: Manning's-Strickler Equation

$$n = \frac{D_{90}^{1/6}}{21.1}$$

Table 1: Range of Strickler's n Values for Collected Pebble Counts

Site	Archuleta	Cebolla
n-value	0.034-0.036	0.032-0.034

Areas located in the floodplain and in areas where fines were deposited were separately defined using values from Chow (1959) as can be seen in Table 2. A sensitivity analysis was completed based on varying floodplain *n-values*. No other n-values were changed in the sensitivity analysis due to their small range of variability.

Table 2: *n*-values for Floodplain and Fines

Material Type	Floodplain	Fines
n-value	0.045 or 0.060	0.030

Upon finishing the definitions for each polygon, the mesh was generated, see Appendix F. Boundary conditions were set at the inlet and outlet of the Rio Chama at each site within SMS. The mesh was then entered into SRH-2D and individual boundary conditions were set for each model run. The inlet boundary condition was set to known

inflow and varied in 14 m^3/s increments up to 170 m^3/s. The outlet boundary conditions were set to known water surface elevation for each flow increment and were based on a HEC-RAS model completed by Tetra Tech, Inc. Iterative calculations for each site were set for 10 second time steps starting at time 0 hours and ended at 24 hours. Steady conditions were generally reached between hour 3 and hour 4, for each model run at each site. All results presented are from the 12 hour time step.

SRH-2D runs were completed for each flow increment at each site. SRH-2D is a two-dimensional hydraulic model developed by the Bureau of Reclamation that relies on St. Venant's equations, see Equation 2. St. Venant's equations were derived from the three dimensional Navier-Stokes equation with the assumption that for shallow channels vertical motion is minute (Lai, 2010).

Equation 2: St. Venant's Equations

$$\frac{\partial h}{\partial t} + \frac{\partial hU}{\partial x} + \frac{\partial hV}{\partial y} = 0$$

$$\frac{\partial hU}{\partial t} + \frac{\partial hUU}{\partial x} + \frac{\partial hVU}{\partial y} = \frac{\partial hT_{xx}}{\partial x} + \frac{\partial hT_{xy}}{\partial y} - gh\frac{\partial z}{\partial x} - \frac{\tau_{bx}}{\rho}$$

$$\frac{\partial hV}{\partial t} + \frac{\partial hUV}{\partial x} + \frac{\partial hVV}{\partial y} = \frac{\partial hT_{xy}}{\partial x} + \frac{\partial hT_{yy}}{\partial y} - gh\frac{\partial z}{\partial y} - \frac{\tau_{by}}{\rho}$$

where x and y are Cartesian coordinates, U and V are directional velocities, g is gravity, t is time, ρ is density of water, h is water depth, T_{xx}, T_{xy}, and T_{yx} are effective shear stresses, and τ_{bx} and τ_{by} are boundary shear stresses.

Boundary shear stresses were calculated using Manning's Resistance Equation, see Equation 3.

Equation 3: Manning's Resistance Equation

$$(\tau_{bx}, \tau_{by} = \rho U_*^2 \frac{(U,V)}{\sqrt{U^2+V^2}} = \rho C_f \sqrt{U^2+V^2}(U,V)$$

where,

$$C_f = \frac{gn^2}{h^{1/3}},$$

U_* is the friction velocity and *n* is the Manning's roughness coefficient (Lai, 2010). Boundary shear stress is then used to calculate the critical D_{50} at which incipient motion begins. Two methods were used to calculate the D_{50}: Neill's method (1968) and the Shields-Rouse Equation (Guo, 2002). Neill's method is shown in Equation 4,

Equation 4: Neill's Method

$$\tau_c^* = 0.03 = \frac{\tau_c}{(s-1)\rho g D_{50}},$$

where, τ_C^* equals Shields Parameter and s is the specific gravity of the sediment. For calculation of particle size related to entrainment, the specific gravity was set equal to 2.65.

The D_{50} at which entrainment occurred was also calculated using Shields equation and the Shields-Rouse equation (Guo, 2002) for dimensionless diameter as seen in Equation 5.

Equation 5: Shields-Rouse Equations for Dimensionless Diameter

$$d_* = \left[\frac{(s-1)g}{\upsilon^2}\right]^{1/3} D_{50}$$

$$\tau_c^* = \frac{0.23}{d_*} + 0.054\left[1 - exp\left(-\frac{d_*^{0.85}}{23}\right)\right],$$

where, d_* is the dimensionless diameter, and υ is the kinematic viscosity. The boundary shear stress was set equal to critical shear stress in Shields equation and the D_{50} was

solved for implicitly by calculating the error between the Shields Parameters for each iteration within a Matlab script.

Results

Boundary shear stress and the particle size of entrainment were evaluated with SRH-2D. Model runs were completed at each site for flows ranging from 14 m^3/s to 170 m^3/s. Flows of 85 m^3/s and 170 m^3/s were of particular importance for this study. Based on Tetra Tech's prior HEC-RAS modeling efforts, it is expected that bankfull stage occurs at Archuleta and Cebolla at 85 m^3/s. In unregulated systems, bankfull flow is defined as the channel-forming flow or the flow that is most responsible for shaping the channel (Leopold & Wolman, 1957). At 170 m^3/s, it is speculated that enough disturbance would occur to allow the river to migrate laterally across the floodplain. This is based on observations following a release in 2008 that enabled the river to laterally adjust. It also corresponds to the maximum discharge allowed under current infrastructure constraints on the Rio Chama – particularly the outlet works at El Vado dam.

Water Depth

At Archuleta, water depths varied from 0.0 m. to 3.4 m. overall and the results of individual runs. As can be seen Figures 5-7, maximum water depths are generally observed along the top of the reach and below the second vegetated bar. The flow characteristics are heavily influenced by bedrock that confines the channel.

At 28 m^3/s, the vegetated bars are not flooded and overbanking does not occur (Figure 6). Also, very little backwater is seen in the Chiquito that comes in on the left

side of the river. For comparison, the water depths associated with larger flows begin to increase and encroach on the floodplain.

In Figure 7, the SRH-2D results are shown for flows at 85 m^3/s. The increased stage is just enough to cover most of the vegetated islands. In addition, flow begins to overtop the banks and backs water into the Chiquito approximately 75 meters. At this flow, floodwater begins to approach a secondary terrace which is seen in Figure 6 as a tree line along the lower left side of the channel.

Last, we see the effects of flows of 170 m^3/s in Figure 8. With flows doubled from 85 m^3/s, the entire channel is submerged. The backwater area into the Chiquito is approximately 150 meters. The second floodplain terrace has been overtopped and much of the floodplain on the right side of the river is flooded. It appears that the floodwaters

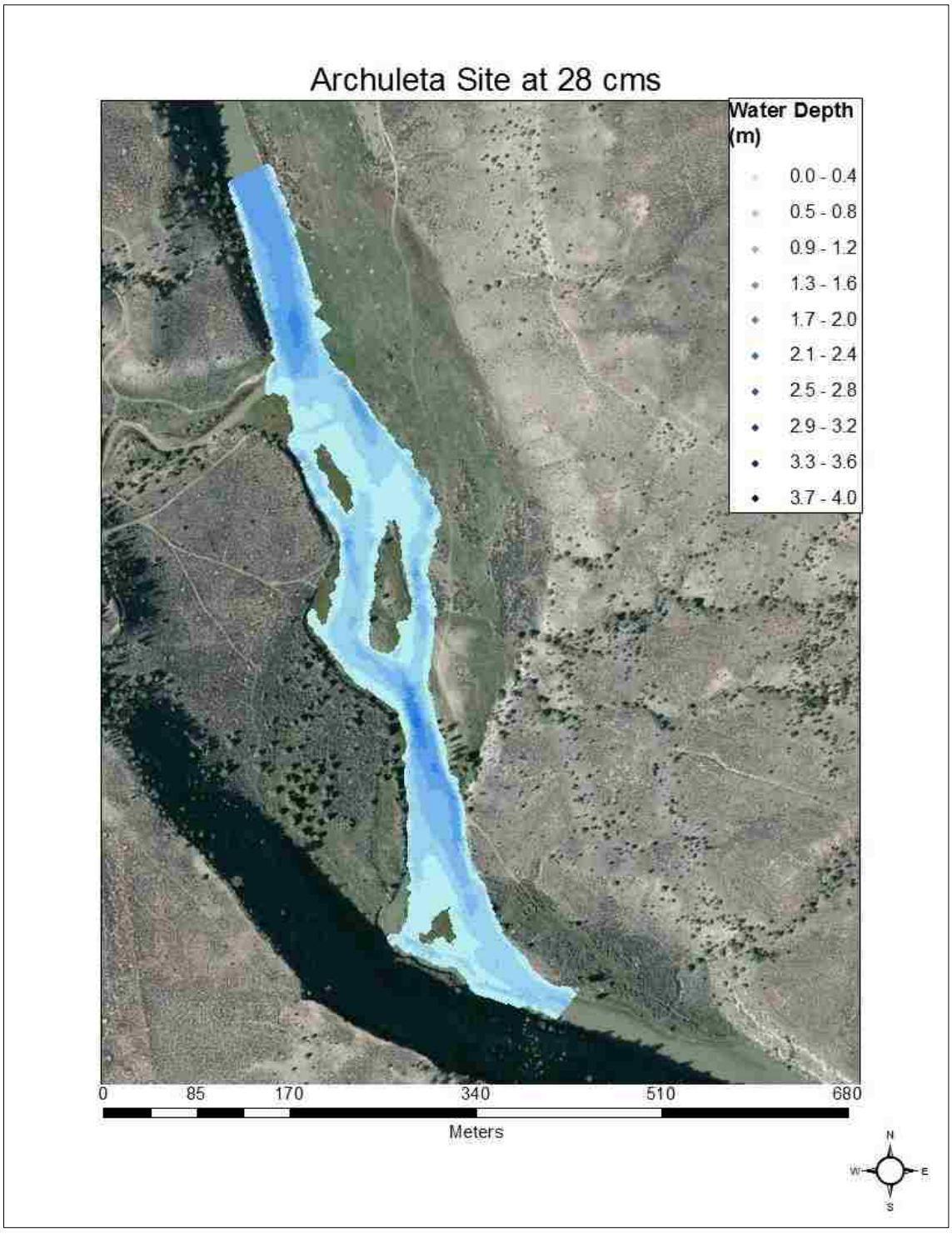

Figure 6: Archuleta Site Map of Water Depths at 28 m^3/s (1000 ft^3/s)

on the right side of the river reach the lower canyon wall. Any larger flows would likely cover most if not all of the floodplain.

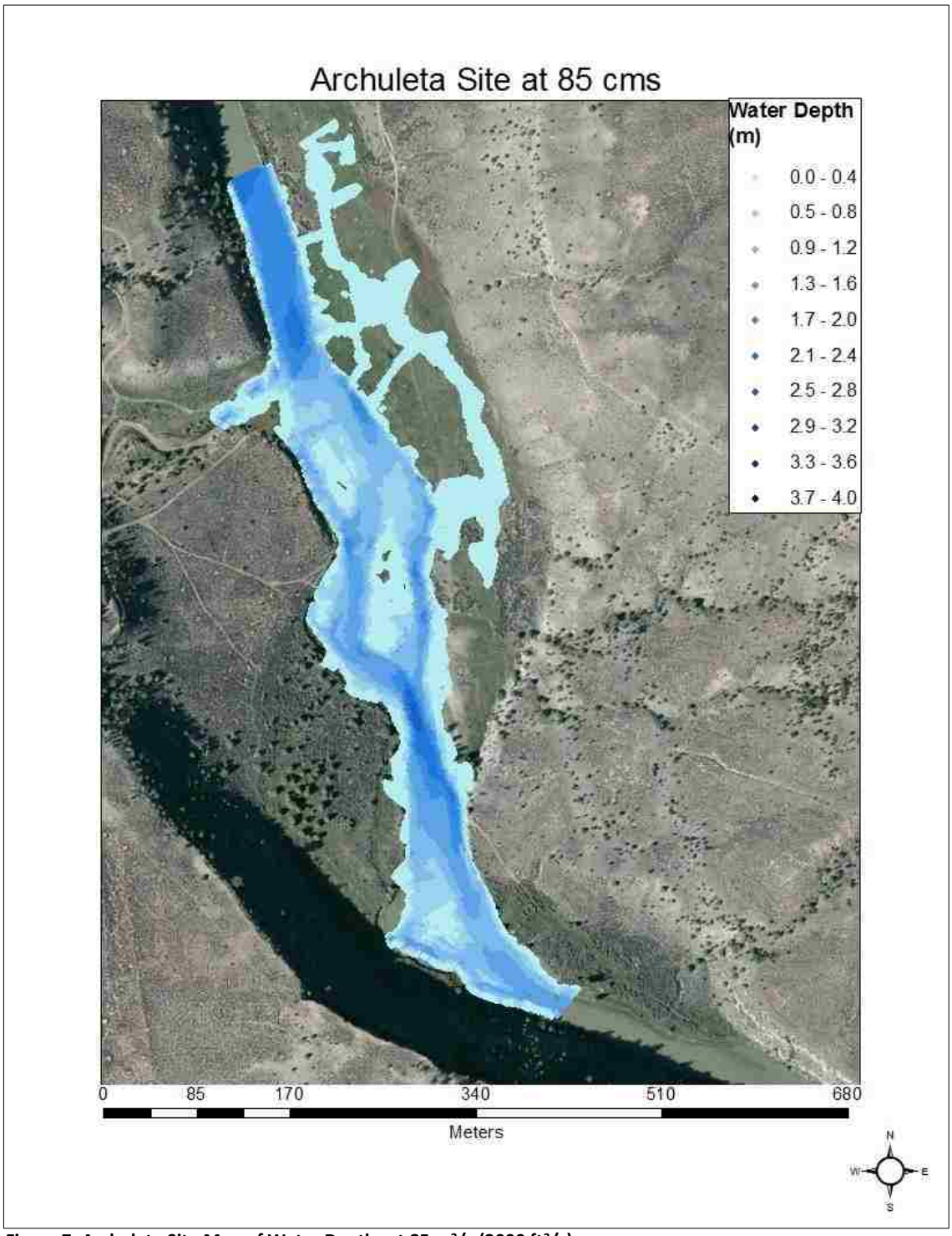

Figure 7: Archuleta Site Map of Water Depths at 85 m^3/s (3000 ft^3/s)

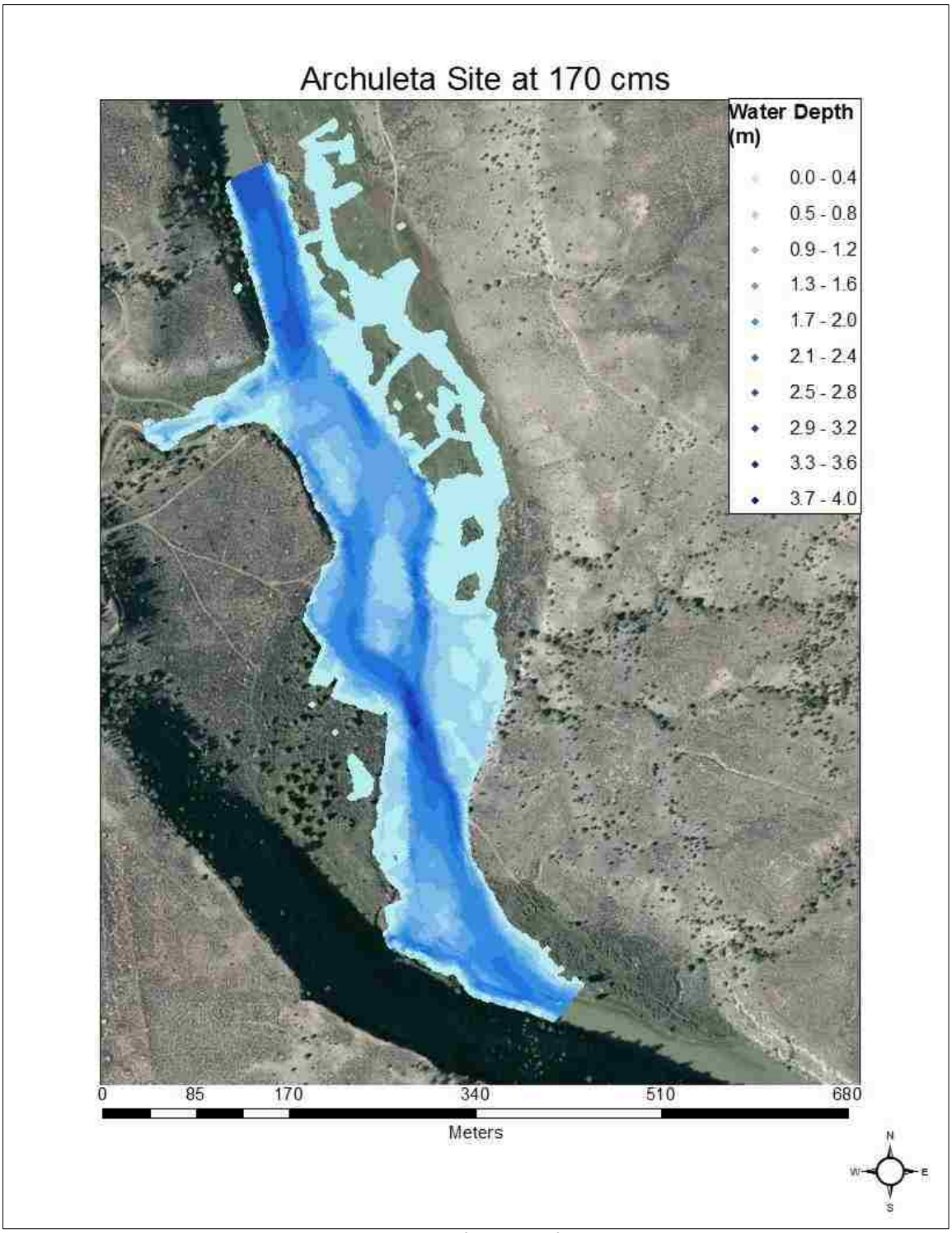

Figure 8: Archuleta Site Map of Water Depths at 170 m^3/s (6000 ft^3/s)

At Cebolla, water depth varies more greatly due to the physical features of the site. As flows increased, so did the variation in water depths, particularly above 85 m^3/s.

When Cebolla experiences flows of 28 m^3/s, see Figure 9, little flooding occurs with the exception of the upstream portion of the Rio Chama above the confluence of the Rio Cebolla. The deepest flows are observed below the Rio Cebolla with maximum depths reaching 1.8 meters, and at the lower end of the reach where flows reach a maximum depth of 1.7 meters. It is apparent that not all of the topography was well accounted for. In particular the side channel on the lower right side of the Rio Chama does not contain flow. The side channel does become wetted at higher flow rates within SRH-2D, however, this is inaccurate and from observation it does receive flow at 14 m^3/s. This discrepancy between the mesh and real physical conditions could be alleviated with more topographic data.

At 85 m^3/s, see Figure 10, Cebolla's vegetated islands are almost completely submerged and backwater into the Rio Cebolla extends nearly 100 meters upstream. Also, minor flooding occurs in the riparian areas. Above 85 m^3/s the Rio Chama is able to flood all riparian areas.

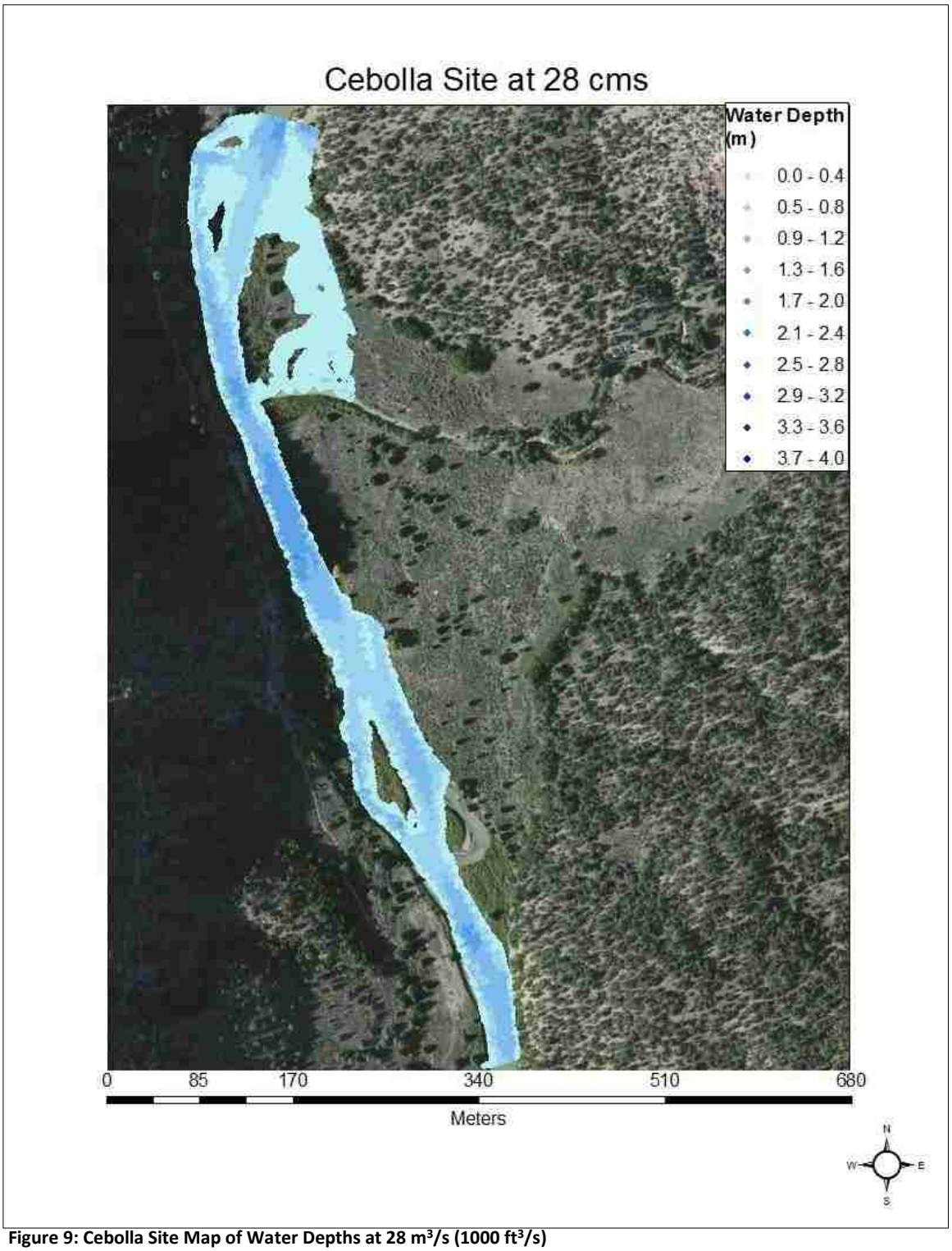

Figure 9: Cebolla Site Map of Water Depths at 28 m^3/s (1000 ft^3/s)

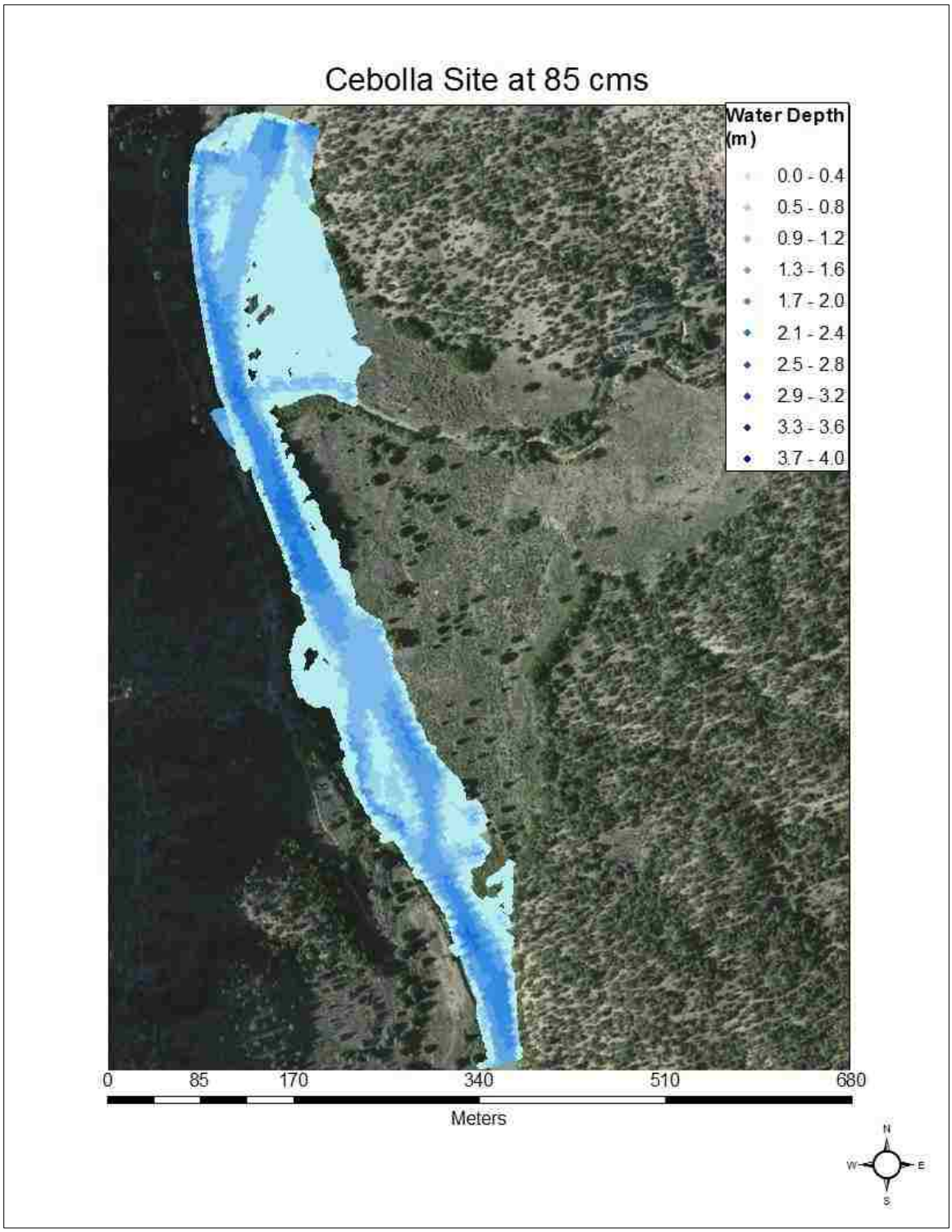

Figure 10: Cebolla Site Map of Water Depths at 85 m^3/s(3000 ft^3/s)

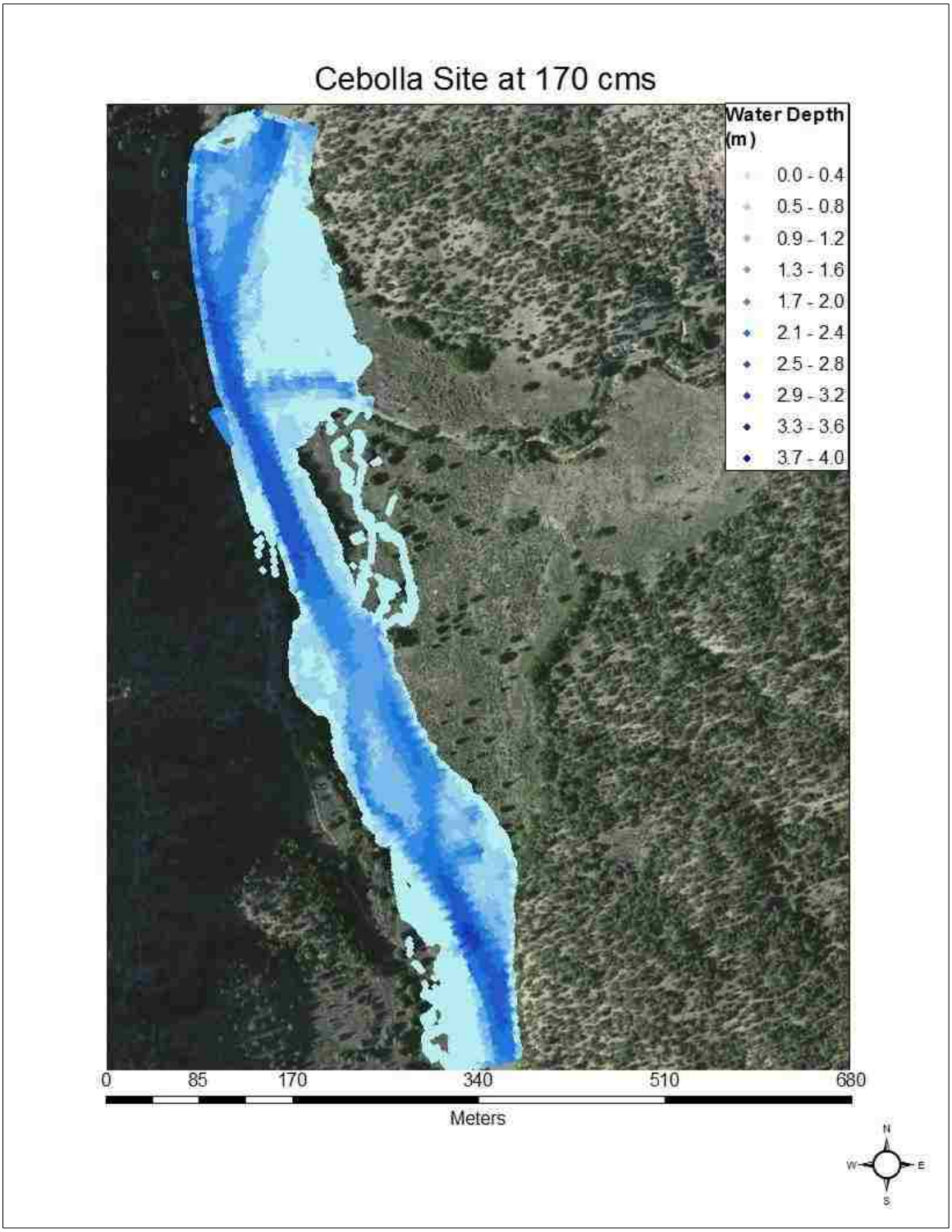

Figure 11: Cebolla Site Map of Water Depths at 170 m^3/s (6000 ft^3/s)

In Figure 11, Cebolla is shown with flows of 170 m^3/s. The riparian areas are nearly all submerged and backwater into the Rio Cebolla extends 125 meters upstream.

Incipient Motion and Particle Size

The median particle size (D_{50}) at which motion begins was calculated using Neill's method, the Shields-Rouse Method and SRH-2D results. Values of the critical D_{50} ranged greatly and are presented for each site in Table 3 and Table 4. The largest particle size measured in the field at both sites during pebble counts did not exceed the 256 mm size class for gravels and therefore less emphasis is placed on those results when considering the mobility of sediments in the Rio Chama.

Table 3: Archuleta Site Range of Critical Particle Sizes for Incipient Motion

	Max. Critical Particle Size (mm) Floodplain *n*=0.045		Max. Critical Particle Size (mm) Floodplain *n*=0.060	
Flow (m^3/s)	Shields-Rouse	Neill's	Shields-Rouse	Neill's
28	91	164	91	164
85	364	655	364	652
170	641	1154	641	1185

Critical particle sizes for incipient motion at 28 m^3/s at Archuleta are shown in Figure 12. The results show that the mean particle size of incipient motion is 26 mm using Neill's method. This is not large enough to transport the in situ D_{50} of 50 mm. Larger particle sizes appear to move in portions of the channel surrounding the vegetated island in the center of the reach and at the lower segment of the reach where the Rio Chama enters a narrow canyon. These areas were observed to be predominantly gravels with sands at the outer edges of the vegetated bar and will hence see at least partial movement for the full spectrum of particle sizes. Some motion is predicted to occur

below the confluence of the Chiquito where channel flow is concentrated on the bank opposite of the entrance. The Chiquito deposits fine materials, less than 2 mm in diameter, at its mouth and the movement of fine deposited sediments appears possible at low flows relative to this study. As flows increase movement of the fines layer appears more likely and flushing of fines can be achieved.

At 85 m^3/s, the mean critical particle size is 47 mm for Neill's method. The extent of entrainment has increased with the flow and the lowest portion of the reach continues to have the movement of the largest particle class, see Figure 13. This is in part due to the boundary condition at the bottom of the reach being set to normal depth and the changing channel features as the Rio Chama enters a more narrow reach of canyon. The degree to which either affects the critical D_{50} is unclear and further investigation would be needed to distinguish both components. Overall, the results correlate with the wide spread movement of the in situ D_{50} and smaller grain sizes below the Chiquito. The results also show the movement of larger particle sizes, although that is limited to a few areas in the lower portion of the reach.

When Archuleta experiences flows of 170 m^3/s the average critical particle size remains at 67 mm (Neill's Method). However, the decrease in mean particle size experiencing entrainment is a function of the banks being overtopped and hypothetical movement of small particles in the floodplain. Within the channel a significant portion of the channel could hypothetically see motion of particles with intermediate axis sizes of greater than 100 mm (Figure 14). The movement of particles greater than 100 mm would align with movement of at least 70% of the sediments, depending on spatial variation of particle size distribution.

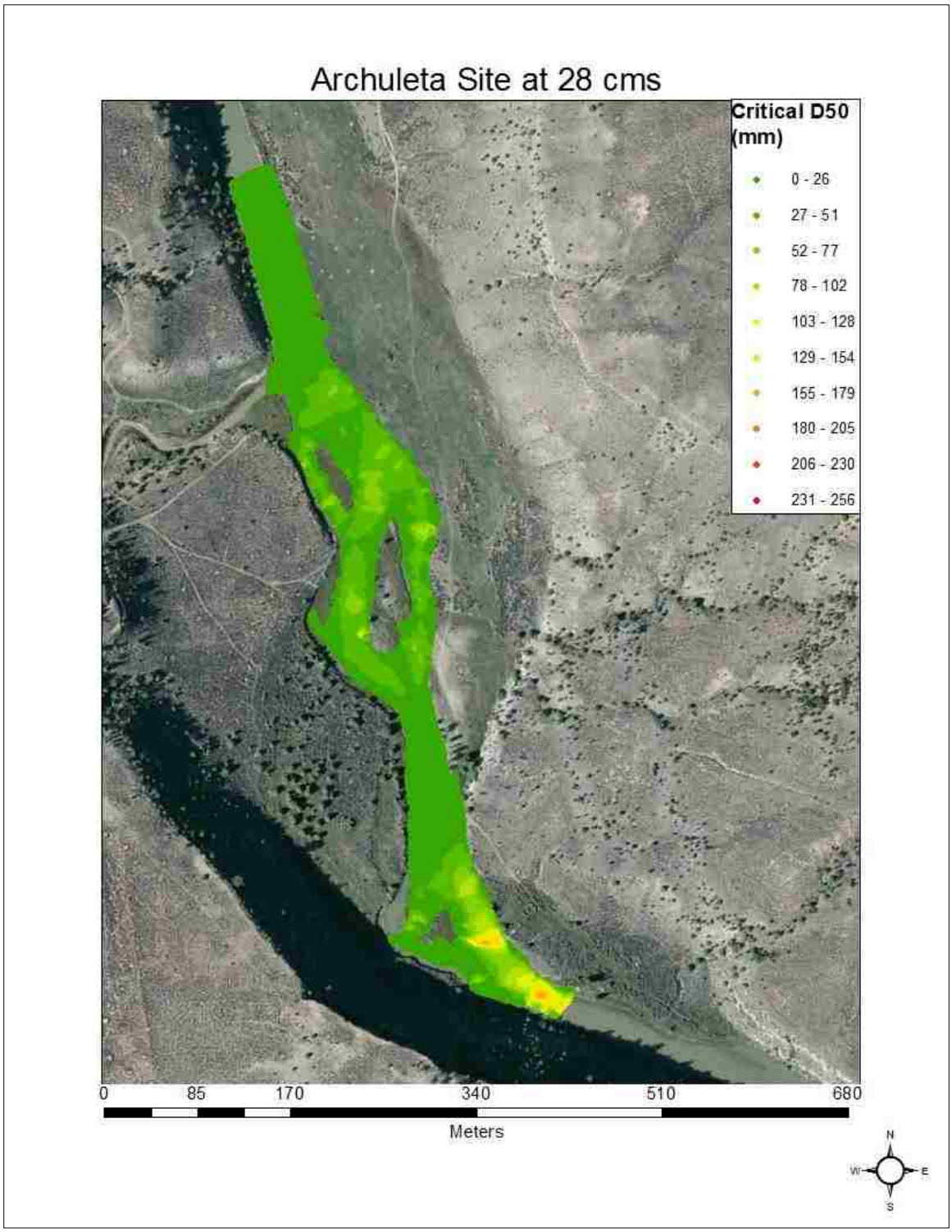

Figure 12: Archuleta Site Map of Critical D_{50} for Incipient Motion at 28 m^3/s (1000 ft^3/s)

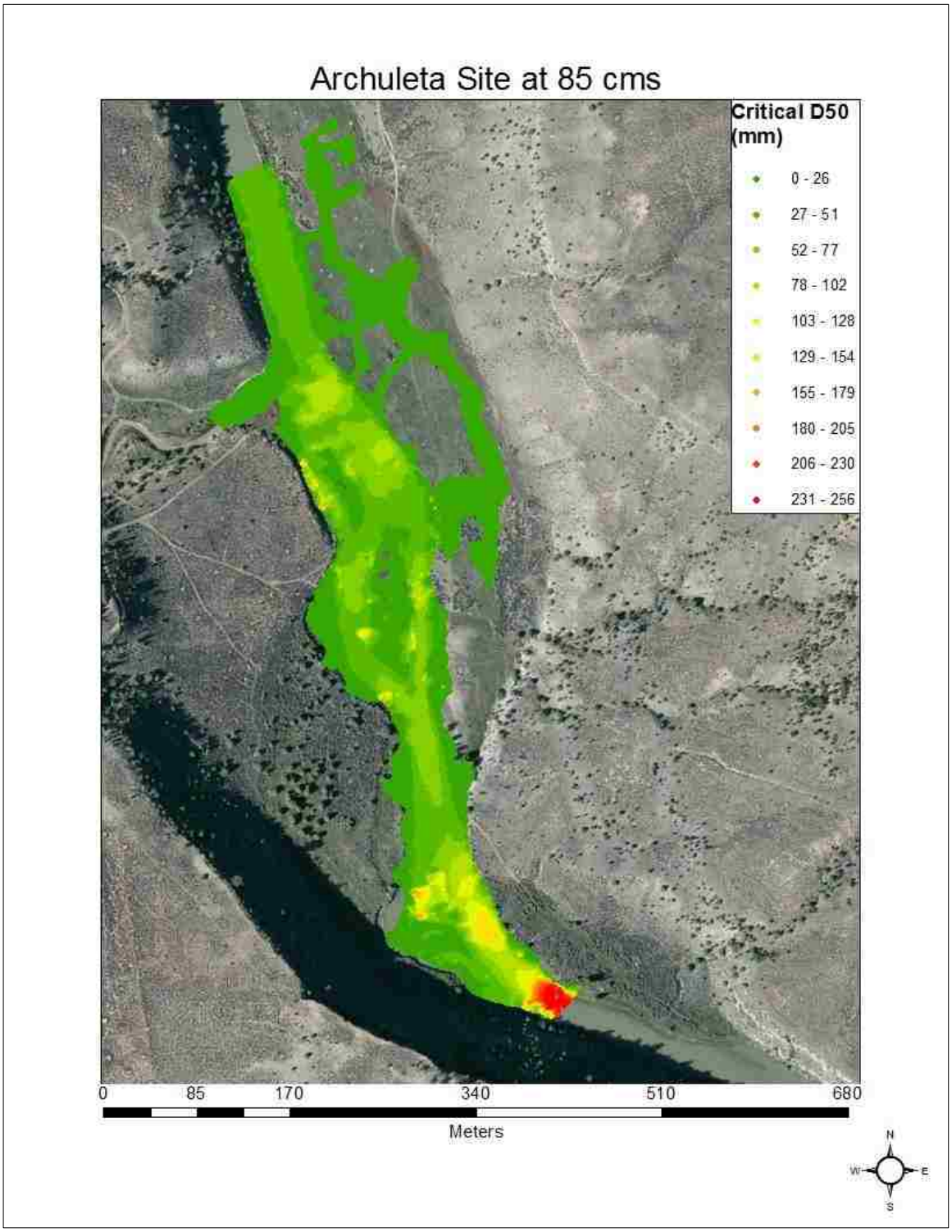

Figure 13: Archuleta Site Map of Critical D_{50} for Incipient Motion at 85 m³/s (3000 ft³/s)

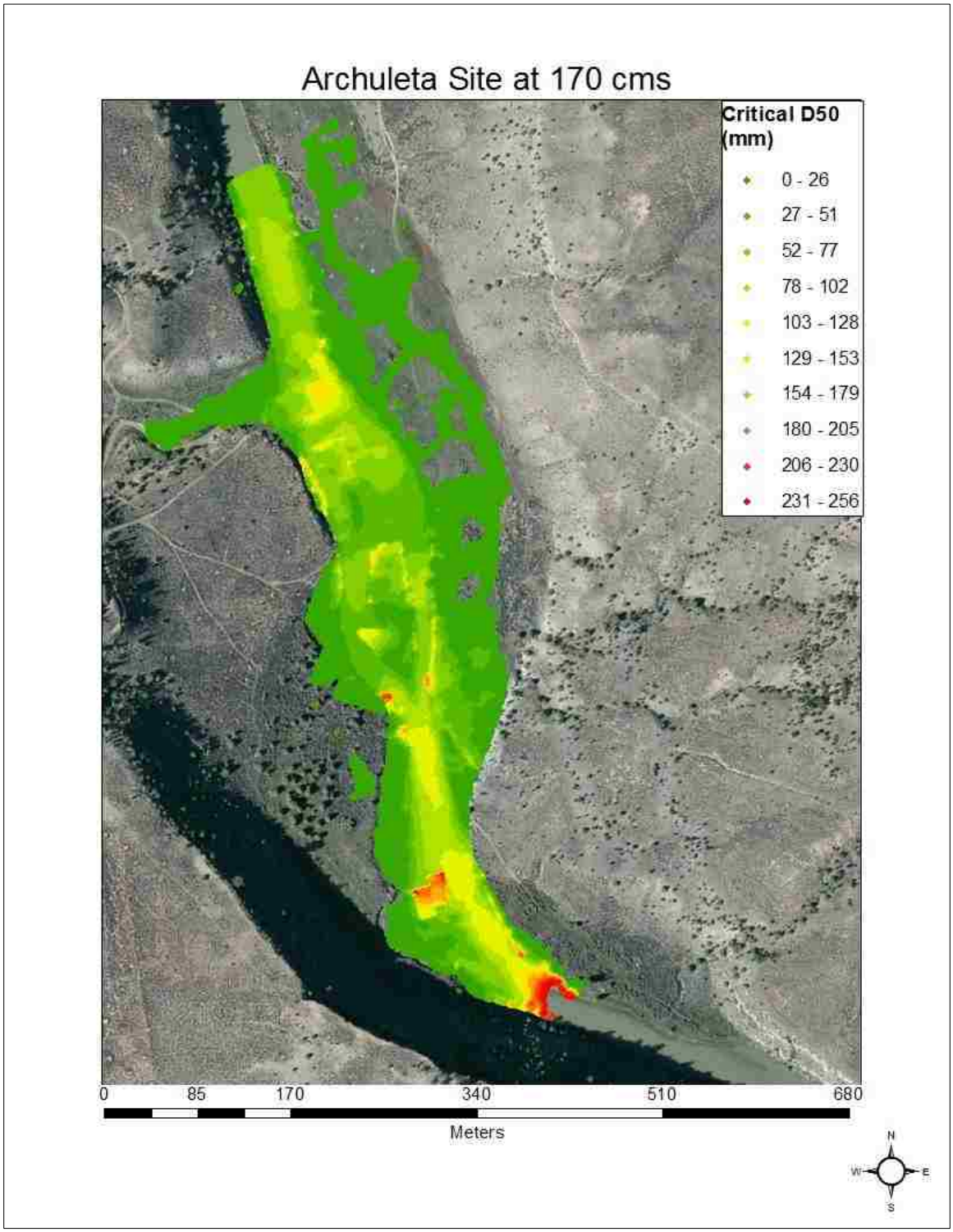

Figure 14: Archuleta Site Map of Critical D_{50} for Incipient Motion at 170 m^3/s **(6000** ft^3/s**)**

The Rio Chama at Cebolla is capable of moving much larger particle sizes than at Archuleta. The range of critical particle sizes at which entrainment occurs can be seen in Table 4. Of special interest, is the significant variability of the D_{50} at this site when reviewing the results between the two different models.

Table 4: Cebolla Site Range of Critical Particle Sizes for Incipient Motion

Flow (m^3/s)	Max. Critical Particle Size (mm) Floodplain n=0.045		Max. Critical Particle Size (mm) Floodplain n=0.060	
	Shields-Rouse	Neill's	Shields-Rouse	Neill's
28	458	824	641	1153
85	674	1212	897	1614
170	760	1365	1288	2317

The largest critical particle sizes are concentrated in the upper right side of the reach for all flows. Even when a maximum particle size is established as 256 mm, this region still maintains the largest particle sizes as can be seen in Figure 15. This is due to the limited amount of topographic data, slope between the banks and channel and the assignment of the inlet boundary condition. It is unlikely that the maximum particle sizes would be moved if they were in present at Cebolla.

The average particle size experiencing entrainment is 33 mm (Neill's Method) for flows of 28 m^3/s at Cebolla. This relates to the movement of 10% to 30% of the channel bed overall. Movement of larger particle sizes were predicted above the inlet of the Rio Cebolla and below the vegetated island located mid-reach. These areas were observed to be riffles during field visits. Most of the reach is incapable of transporting the D_{50} particle size for this event.

When flows of 85 m^3/s were modeled, the average particle size at which incipient motion occurs is 47 mm (Neill's Method). This is relatively low when considering the distributed data seen in Figure 16. The likely cause of this is the flooded area just above the Cebolla and other areas experiencing shallow flooding in the floodplain offsetting the average. A significant portion of the particles that would experience motion on the Rio Chama at Cebolla are larger than 75 mm along their intermediate axis. Movement of this particle size relates to movement of particles larger than the D_{50}. Areas that are moving particles that are greater than 100 mm have increased in size and move approximately 90% of the sediments in the channel.

For flows of 170 m^3/s, see Figure 17, it is apparent that particles larger than 100 mm are capable of moving through a majority of the channel although the average is 55 mm. Several areas in this reach of channel are capable of moving the maximum particle size as well, especially below the confluence of the Rio Chama.

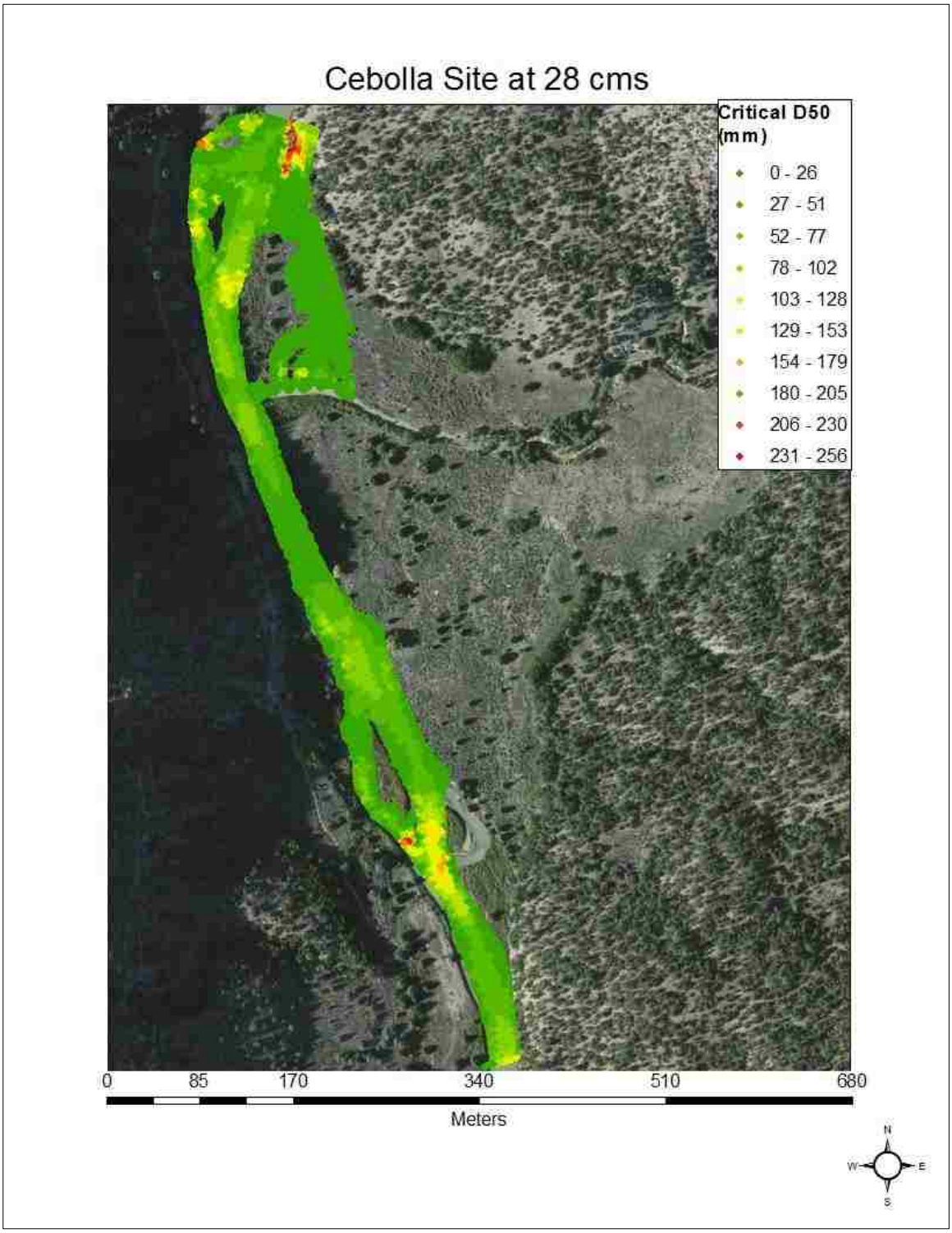

Figure 15: Cebolla Site Map of Critical D_{50} for Incipient Motion at 28 m^3/s (1000 ft^3/s)

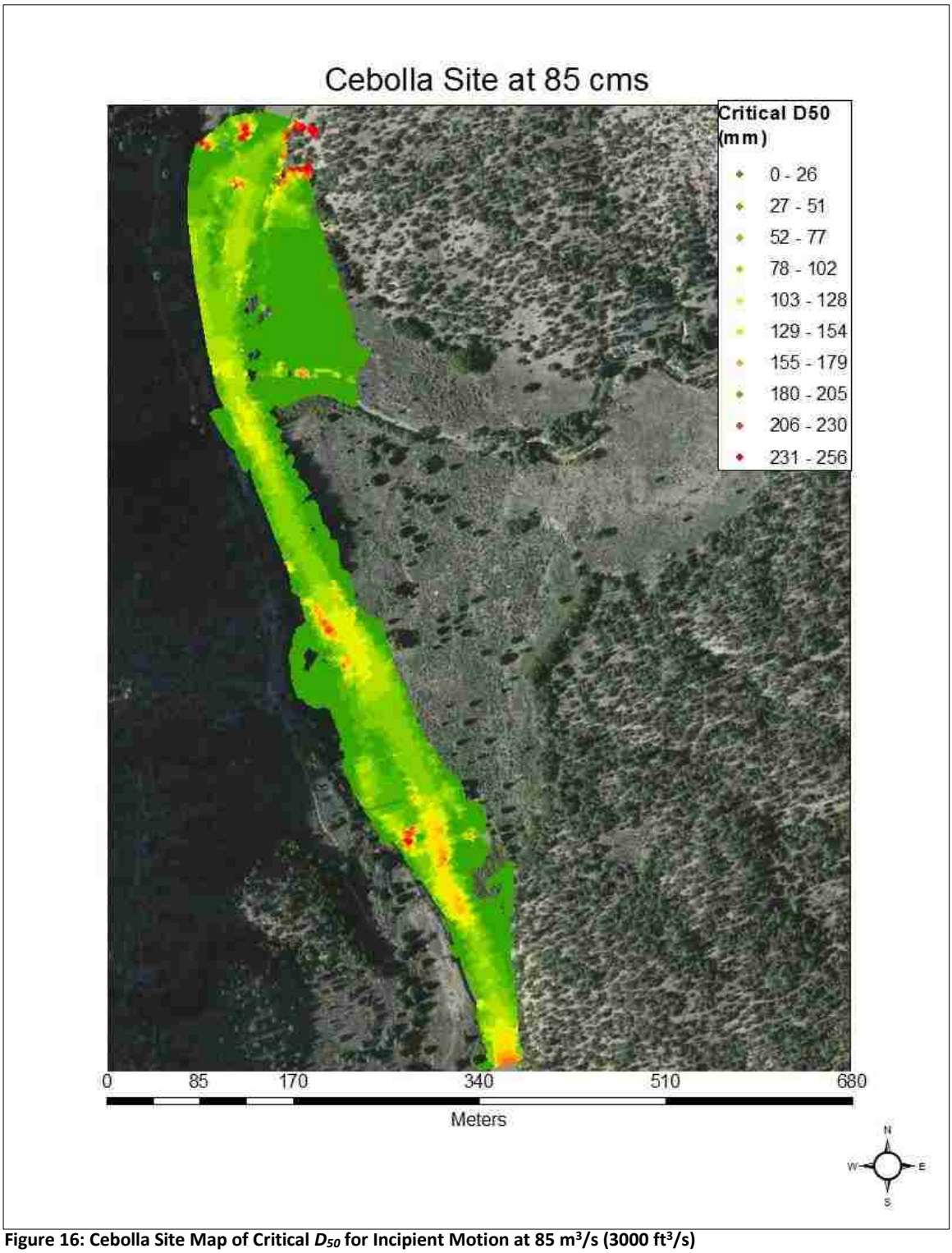

Figure 16: Cebolla Site Map of Critical D_{50} for Incipient Motion at 85 m^3/s (3000 ft^3/s)

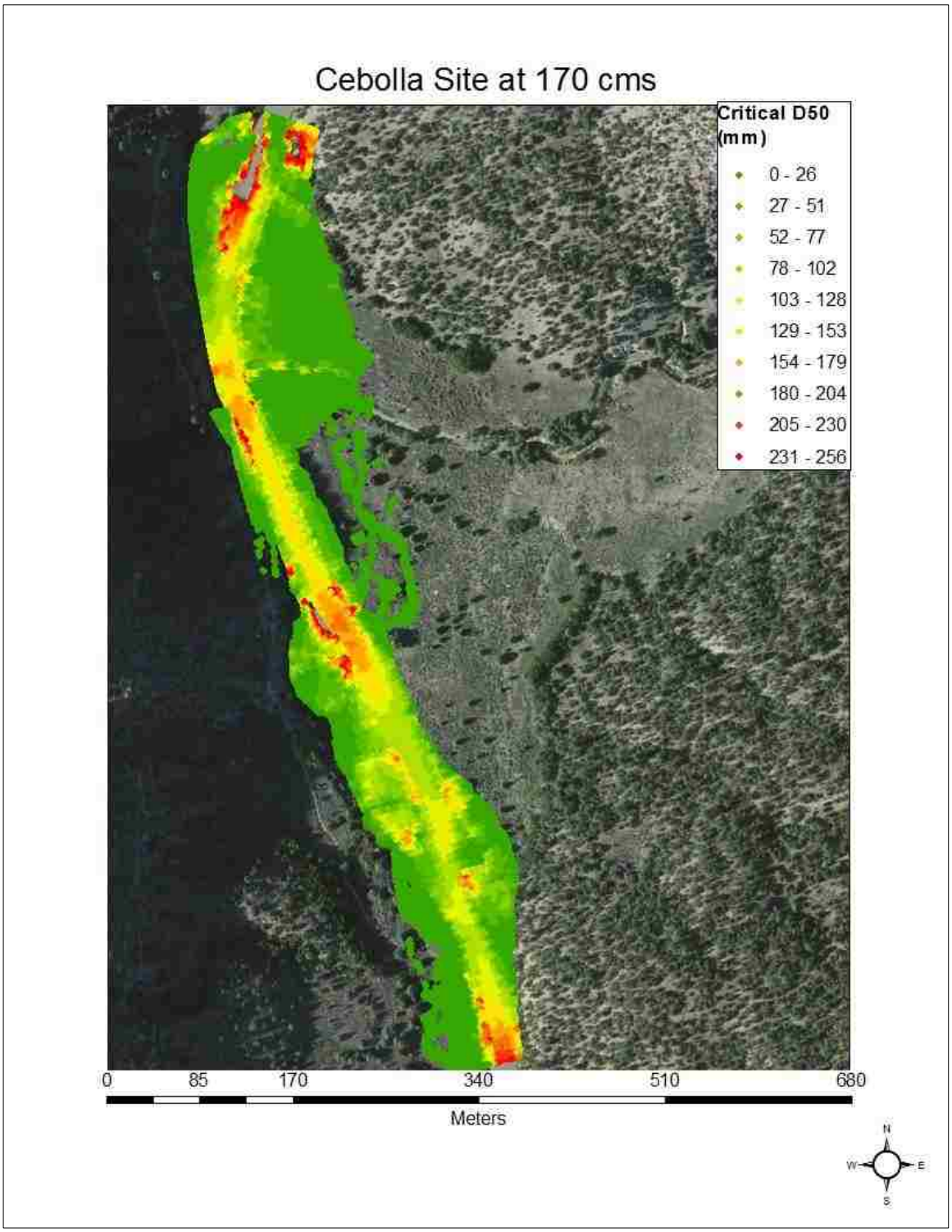

Figure 17: Cebolla Site Map of Critical D_{50} for Incipient Motion at 170 m³/s (6000 ft³/s)

Overall Archuleta and Cebolla experience increasing critical particle size in channel with increasing flows. A percent exceedance graph shows the distribution of particle sizes from a range of 1% to 90% exceedance for each site. At Archuleta, see Figure 18, critical particle size follows a near linear trend with the exception of particle sizes that are larger than the 10% exceedance. The ability of the Rio Chama to transport large particles appears to change with flows of greater than 57 m^3/s. Once 10% exceedance is approached for 57 m^3/s, the slope of the line increases and overlaps the critical particle size for all larger flows. At 85 m^3/s a maximum critical particle size is reached for the percentiles that were evaluated. Between 10% and 40% exceedance, critical particle size increases with flow. This range of exceedance intersects the observed median particle size range at Archuleta. For particle sizes less than 40% exceedance, the effects of overbank flow are seen at flows of greater than 85 m^3/s. The exceedance curves of high flows crossing those of low flows can be related to lower critical particle size movement in the shallow water of the floodplain constituting a larger percent of the critical particle size data as a whole.

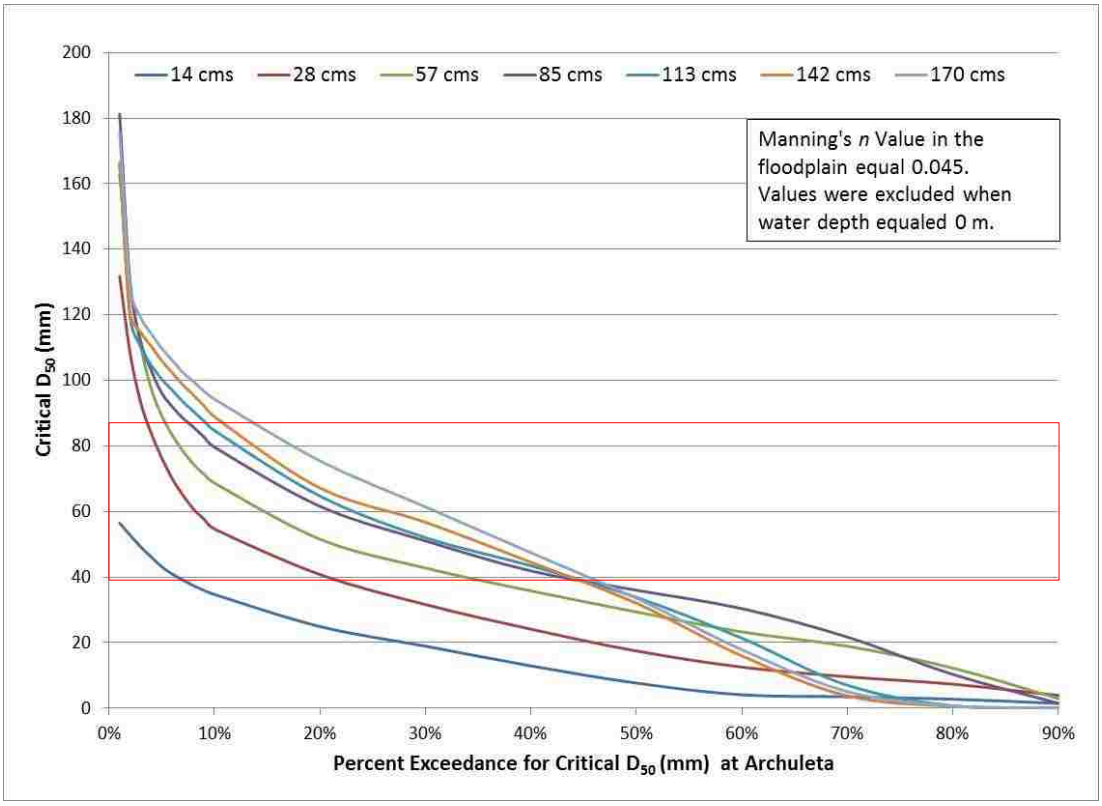

Figure 18: Critical Particle Size at Archuleta as Percent Exceedance for a Range of Flows

Similar to the percent exceedance graph, a histogram for 85 m^3/s was completed for Archuleta, see Figure 19. On the y-axis, the frequency at which a particular particle size was moved within the mesh is shown. On the x-axism the associated particle size is shown in 10 mm increments. The histogram shows that the most frequently moved particle size is between 45 and 55 mm with particle size of entrainment then tapering off to 150 mm. When considering the median particle size range, the ability to transport larger particles is lower at the high end of the range than for smaller median particle sizes. Interestingly, for a discharge of 170 m^3/s the distribution of particle sizes moved is less variable, see Figure 20. The most frequent occurring particle size of incipient motion

is between 35 and 45 mm. The mean critical particle size was 67 mm. 170 m^3/s appears to much more capable of moving larger median particles than a flow 85 m^3/s.

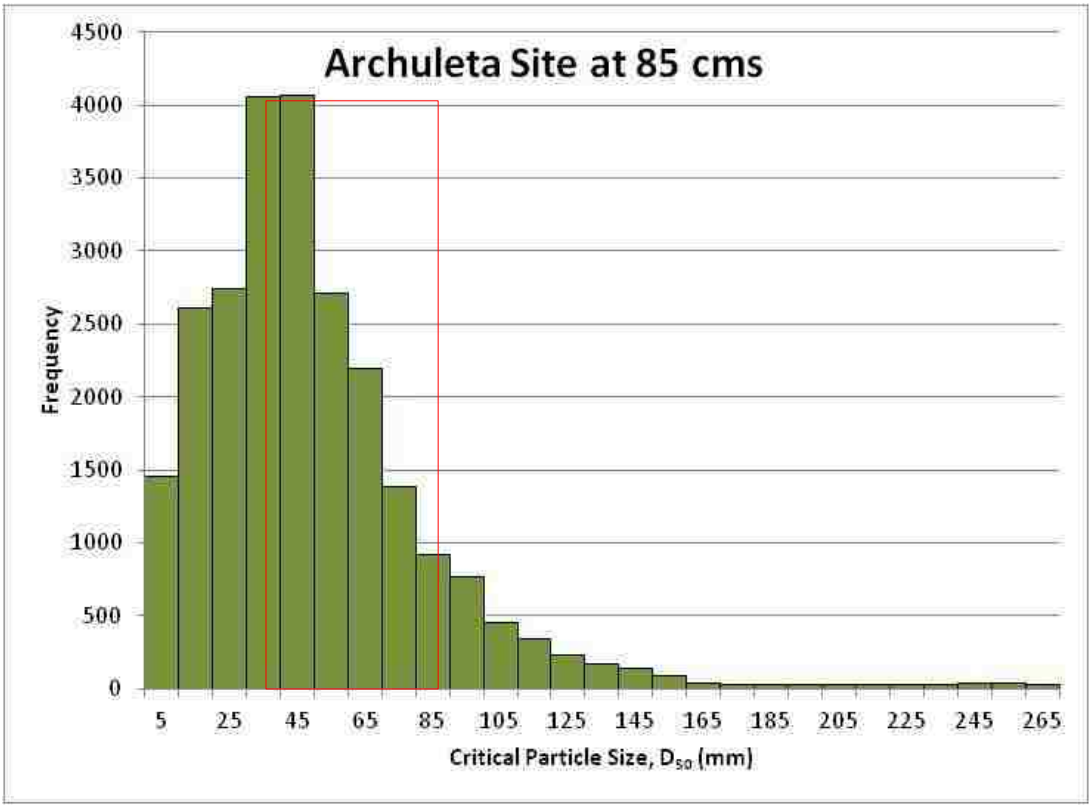

Figure 19: Histogram of D_{50} particle sizes for Archuleta at 85 m^3/s

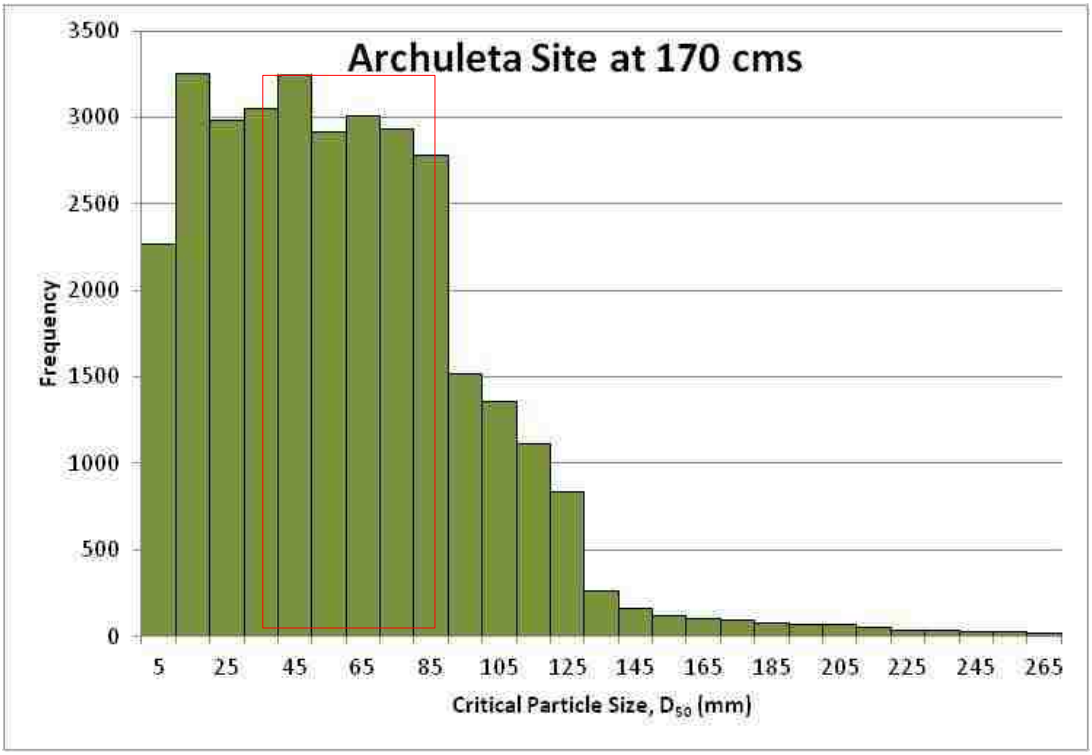

Figure 20: Histogram of D_{50} particle sizes for Archuleta at 170 m^3/s

For comparison, the critical D_{50} calculated using Neill's Method was compared to the Shields-Rouse Method (Guo, 2002) at 85 m^3/s, results are shown in Figure 21. Shields-Rouse always produced smaller values of critical D_{50} than Neill's Method. At smaller boundary shear stresses, the difference between the calculated particle sizes are small. However, as the shear stress increases so does the margin between the critical particle size. When considering the range of median particle size in the field, a significant difference is seen between each method used to calculate the particle size of

incipient motion and shows the difference between transporting the median particle size range and not.

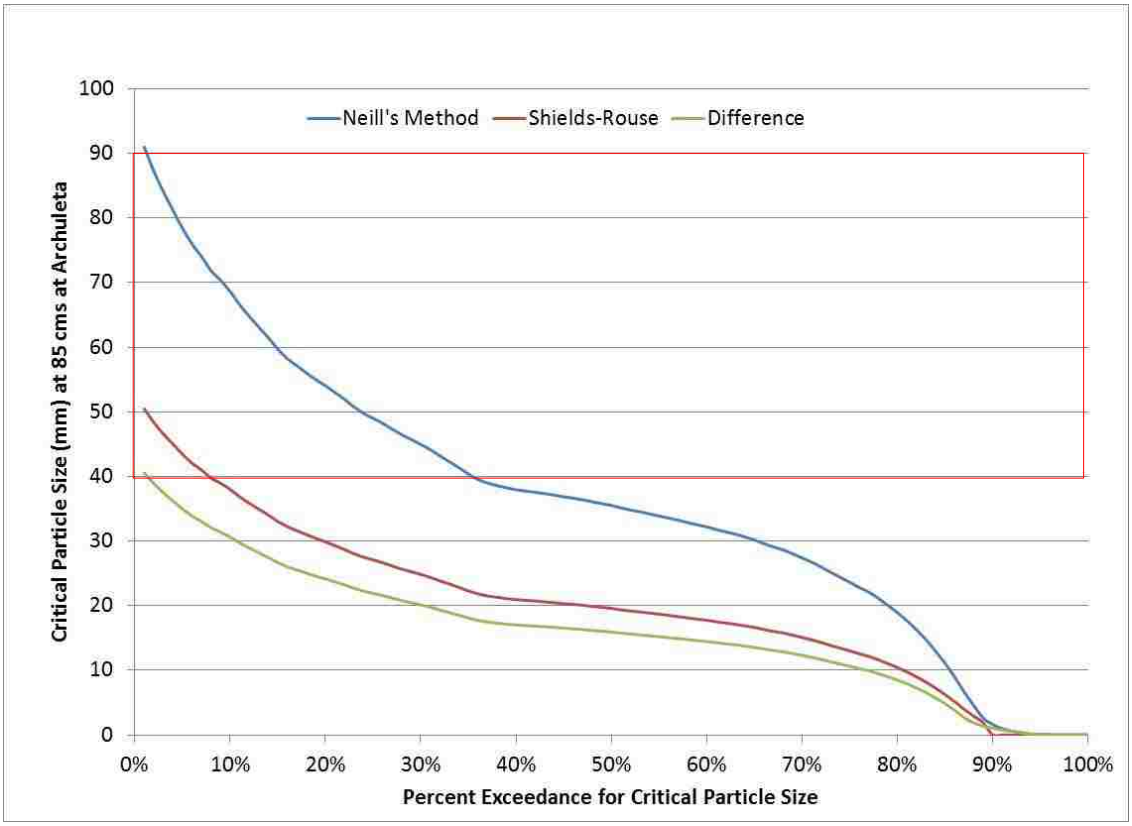

Figure 21: Comparison of Critical D_{50} at Archuleta for 85 m^3/s using Neill's Method and the Shields-Rouse Method

Cebolla, see Figure 22, follows similar trends as Archuleta, but to a much smaller extent. Below 5% exceedance each site is capable of moving particles larger than are present, although this is likely an artifact of the modeling challenges at the upper part of the reach. Linear relationships exist from approximately 5% exceedance to 40%, with particle size increasing with flow. Similar to Archuleta, this range of exceedance coincides with the median particle size for all flows. Above 40% exceedance, the critical

particle size at high flows begins to converge with those of lower flows. As mentioned earlier, this is due to the water flowing onto the floodplain.

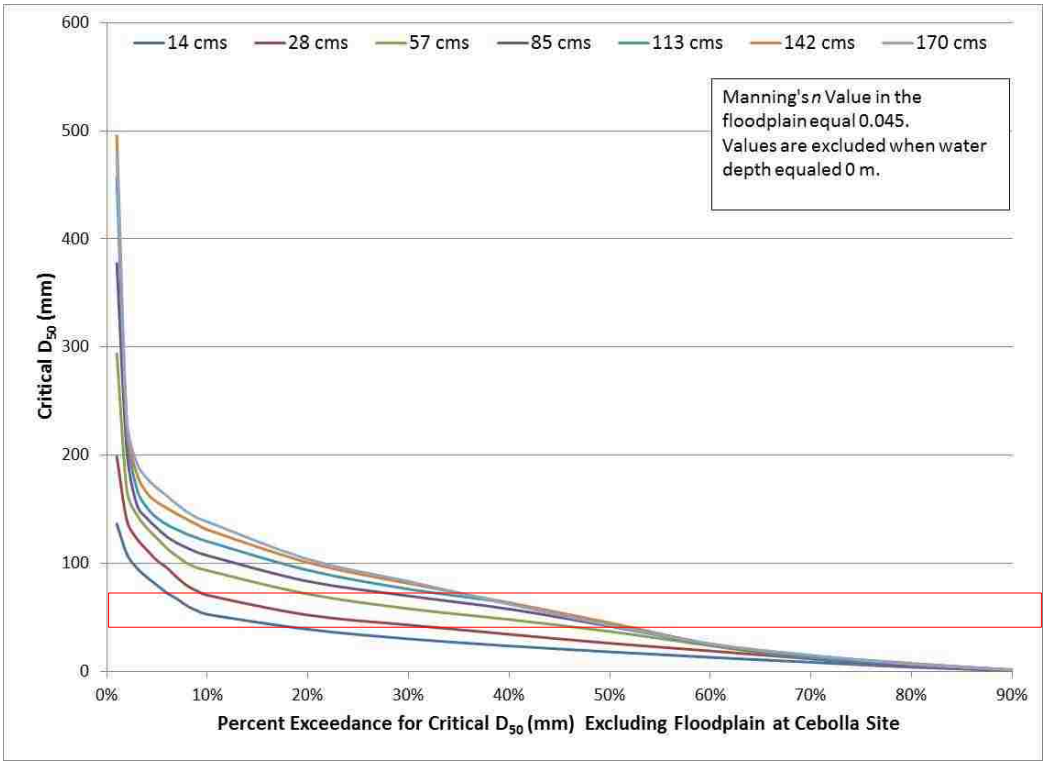

Figure 22: Critical Particle Size at Cebolla as Percent Exceedance for a Range of Flows

In Figure 23, the second largest particle size for incipient motion is between 55 and 65 mm with the frequency of incipient motion for larger particle sizes decreasing

thereafter. This range of particle sizes aligns with the observed D_{50}. The mean particle size for flows of 85 m^3/s was 58 mm (Neill's Method).

In comparison to the results calculated by using Neill's Method, Shields-Rouse produced much smaller values of critical particle size, see Figure 24. In fact, it produced values that were between 55% and 75% of those produced by Neill's Method.

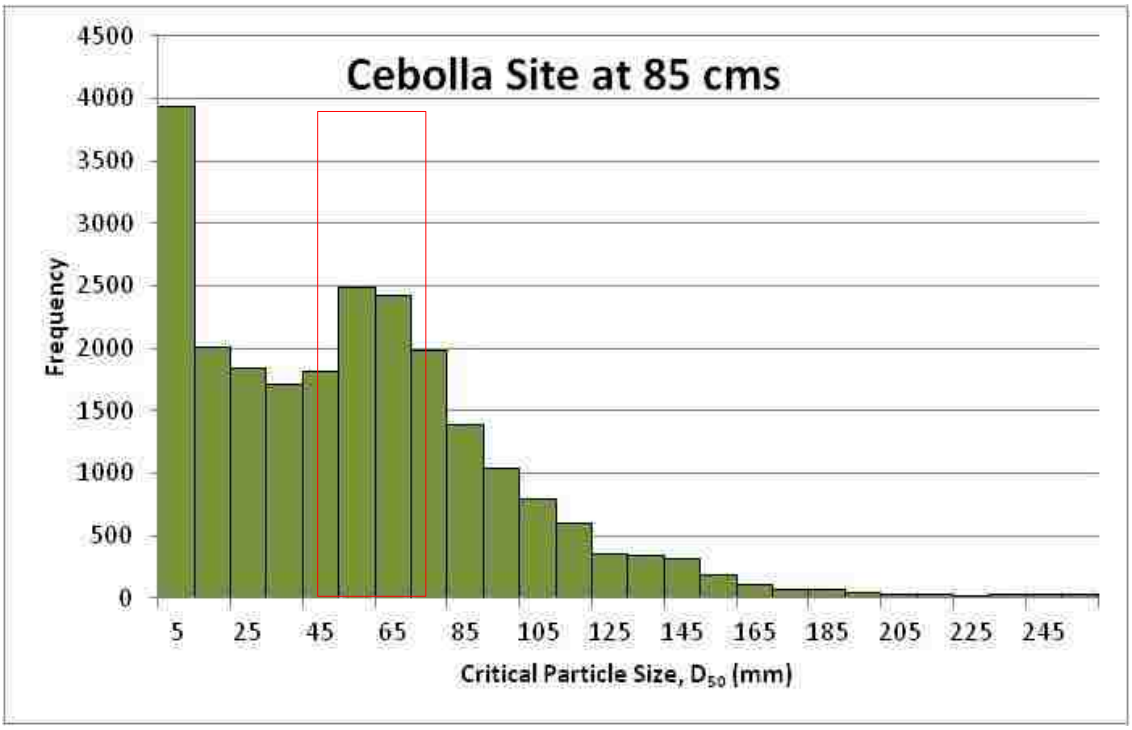

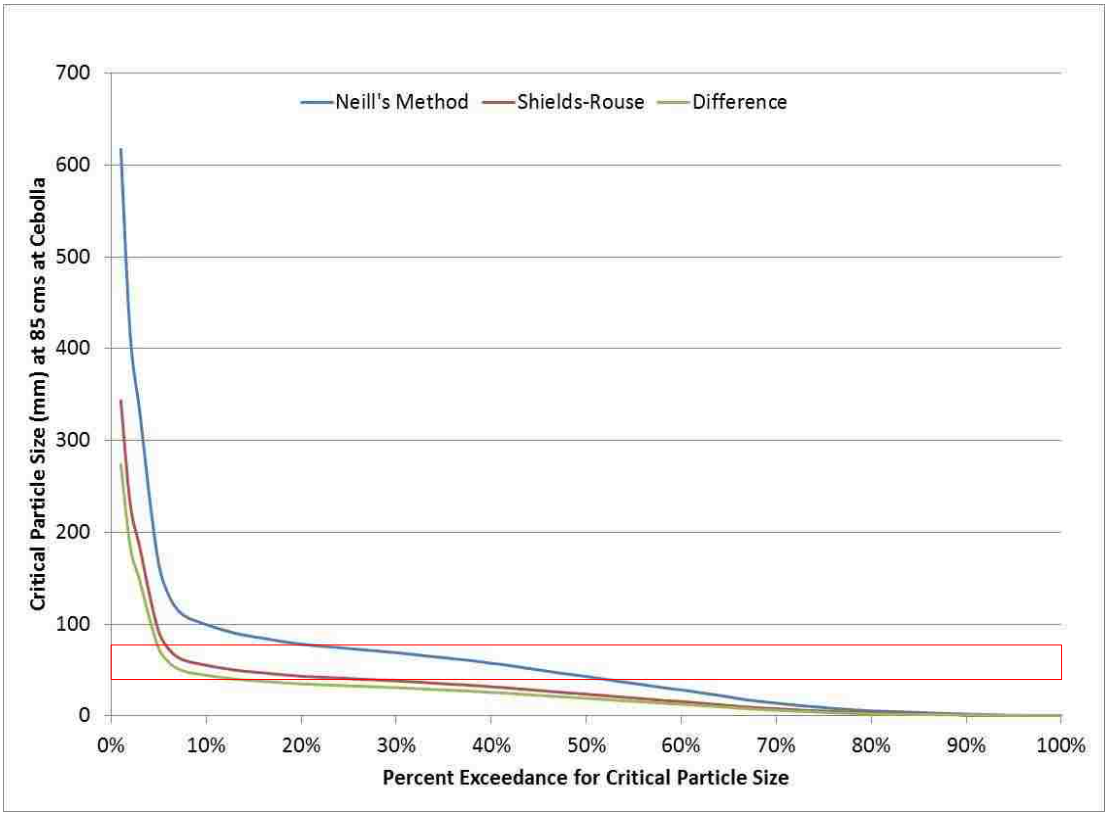

Figure 24: Comparison of Critical D_{50} at Cebolla for 85 m^3/s using Neill's Method and the Shields-Rouse Method

Discussion

The purpose of this research was to evaluate variations of critical particle size for incipient motion at a range of flows. This was accomplished by 1.) comparing the difference of SRH-2D model results when changing the Manning's *n* in the floodplain, 2.) reviewing the spatial variation of the critical D_{50} using Neill's Method, and 3.) comparing the critical D_{50} calculated using Neill's Method to the critical D_{50} calculated using the Shields-Rouse equations.

Sensitivity Analysis and Calibration

Sensitivity analysis at Archuleta and Cebolla showed that the difference between the maximum critical D_{50} calculated using Neill's Method was highly dependent on the topography and initial hydraulic conditions at the downstream boundary condition.

Where Archuleta varied to a small degree, Cebolla was much more sensitive to the changes in roughness. This is due to the fact that Cebolla is more confined to the channel and the gradient is steeper. Any changes in roughness play a major role in the ability of the Rio Chama to transport a set particle size at large flows. As the roughness in the floodplain increased, so did the water surface elevation and the ability to transport larger particle sizes within the channel. To calibrate the SRH-2D model, more data would need to be collected (ie. water surface elevations for flows, topographic data).

This research was conducted as a first step in the direction of environmental flows and therefore data was not yet available to calibrate models. Calibration could be completed for the SRH-2D models by developing a water surface elevation rating curve at the lower end of the reach and sediment discharge rating curve and modifying the Manning's *n* values within the models. Water surface elevation could be measured and graphed as a function of flow. This would require flow measurements for a range of flows at a specified cross-section that is unlikely to shift.

Sediment discharge would need to be evaluated by placing chains in the channel bed for a particular area and measuring the change in volume. From there, the change in sediment volume could be compared to flows and a sediment discharge rating curve could be developed. The sediment discharge curve would be particularly useful for evaluating changes in channel bed form features.

Spatial Variability

The pebble count data that was taken showed that the largest particle size was just under 256 mm along its intermediate axis. Based on the pebble count data and the results of the SRH-2D runs, when calculated using Neill's Method, entrainment for all particle

sizes is possible. At flows of 85 m^3/s, the 10 % percent exceedance at Archuleta and Cebolla are 80 mm and 107 mm, respectively. The 50% exceedance at Archuleta and Cebolla at 85 m^3/s using Neill's Method was 36 mm and 42 mm, respectively. Given that the D_{50} at Archuleta is 50 mm and at Cebolla is 60 mm, a flow of 85 m^3/s seems reasonable to transport both median particle sizes. Although the mean D_{50} is smaller than the in situ D_{50}, it is not necessarily a good indication of the actual size capable of incipient motion in the channel because of the inclusion of the floodplain. Also, due to the inverse relationship between critical shear stress and particle size, the averaging of time and depth, the interpolation of points between cross-sections, and small fluctuations in hydraulic conditions, it is expected that movement does not just occur for one particle size although the D_{50} has been established. For subsurface non-cohesive particles, sediments that are 0.3 times to 4.2 times the median particle size (Andrews, 1983), motion is possible. More variability is inherent when considering channel bed surface materials and Andrews (1983) work was disproved in terms of equal entrainment. However, this application is nonetheless important in defining entrainment for the largest particle size. With that being said, it is likely that for most flows evaluated the Rio Chama only experiences partial transport. Partial motion refers to the immobility of portions of a channel during a transport event (Wilcock & McArdell, 1993, 1997). As flows increase, it would be expected that transport moves from areas of large boundary shear stress to those with smaller boundary shear stresses (Haschenburger & Wilcock, 2003).

Comparing Methods

The Shields-Rouse method produced smaller critical D_{50} sizes than Neill's Method for the same flow conditions at both sites. The difference between the applications of these methods is typically the in situ grain size distribution where Shields-Rouse is applied to uniform grain sizes and Neill's method is applied to mixed media gravels. For mixed sands and gravels a hiding factor is applicable, where coarse particles entrain more easily than fine particles and fine particles are sheltered by coarse particles (Wu et al., 2000; Wiberg & Smith, 1987). This is why Neill's method uses a Shields Parameter that correlates with a R_* located in the transitional area of the Shields curve. Multiplying the Shields-Rouse D_{50} by a factor of 1.5 to 2 would produce nearly the same results as Neill's Method, with larger D_{50} having a larger multiplication factor. The increase in this factor is directly related to the particle sizes relationship to the BRN for turbulent conditions. For large particles that protrude into the boundary layer, the BRN is large and the Shields parameter ranges between 0.045 and 0.060. One issue that was noticed when reviewing the percent exceedance graphs was that once the critical median particle size was at least 100 mm, the trend was for particle entrainment size to substantially increase. Although most of the encountered particle sizes were smaller than 100 mm, the difference between the actual shear stress and critical shear stress aid in the understanding of bed form development. In areas where the shear stress would be associated with a critical D_{50} of greater than 100 mm, special care should be taken to address movement and any resulting changes in bed form shape.

Conclusion

The purpose of this research was to evaluate the impacts that environmental flows can have on critical particle size for incipient motion. This research was performed on the Rio Chama between El Vado and Abiquiu Reservoir and contributes to the knowledge of critical particle size sensitivity for environmental flow applications. It was determined that evaluation of not just the hydraulic conditions but also the geomorphology that contributes to the functionality of the river is of significant importance. In addition, mapping the critical particle size of incipient motion can be used to understand the potential extent of sediment mobilization within a reach. This was a valuable tool when trying to understand the ability of each site to transport the median particle sizes and the full range of particle size distribution at each site.

Based on the results, implementation of environmental flows should be multi-faceted to accommodate the differing spatial features along the river and optimize the health of the river and its aquatic species. Bankfull flows are enough to keep the river actively maintaining the floodplain (Leopold et al., 1964). However, bankfull varies by site due to differences in channel and landform geometry and therefore effects the ability to transport sediments within each reach. In the instance of the Rio Chama, where flood flows are captured but sediment is still available, use of peak flows should be varied annually to mimic the river's original hydrologic conditions within the constraints of the infrastructure limitations at El Vado Dam. In addition, the Rio Chama will benefit from adaptive management. At this time, flow in the Rio Chama is based on demand of water users only. During years of extreme drought, adaptive management can provide flexibility to water managers that would otherwise not be available if environmental

flows were mandatory on an annual basis. The adaptive management process could also be used as a tool to calibrate the SRH-2D models, so that a functioning process-based model would be developed that informs the outcome of sediment transport due to environmental flows. This would be a powerful tool in quantifying the positive outcomes that resulted from environmental flows. Specifically, quantifying the sediment transport by flow event could be related to the change in fish population or vegetation recruitment.

References

Andrews, E. (1983). Entrainment of gravel from naturally sorted riverbed material. *Geological Society of America Bulletin*, 1225-1231.

Bernard, R., & Berger, R. (1999). A parallel coupling scheme for disparate flow solvers. *Proceedings of 1999 Users Group Conferene.* Monterey, California: Department of Defense.

Biedenharn, D., Watson, C., & Thorne, C. (2008). Fundamentals of Fluvial Geomorphology. In ASCE, *Sedimentation Engineering; Processes, Measurements, Modeling and Practice* (pp. 355-386). Reston, VA: ASCE.

BLM. (1992). *Rio Chama Instream Flow Assessment.* Denver: BLM.

Brownlie, W. (1981). *Prediction of flow depth and sediment discharge in open channels. Report No. KH-R-43A.* Pasadena, California: W.M. Keck Laboratory of Hydraulics and Water Resources. California Institute of Technology.

Brownlie, W. (1983). Flow depth in sand-bed channels. *Journal of Hydraulic Engineering*, 959-990.

Buffington, J. (1999). The legend of A.F. Shields. *Journal of Hydraulic Engineering, Vol. 125(4)*, 376-387.

Bunte, K., & Abt, S. (2001). *Sampling surface and subsurface particlee-size distributions in wadable gravel- and cobble-bed streams for analyses in sediment transport, hydraulics, and streambed monitoring, General Technical Report RMRS-GTR-74.* Fort Collins, Colorado: USDA Forest Service.

Cao, Z., Pender, G., & Meng, J. (2006). Explicit Formulation of the Shields Diagram for Incipient Motion of Sediment. *Journal of Hydraulic Engineering*, 1097-1099.

Chang, H. (1988). *Fluvial Processes in River Engineering.* Malabar: Krieger Publishing Company.

Chapman, D. (1988). Critical Review of Variables Used to Define Effects of Fines in Redds or Large Salmonids. *Transactions of the American Fisheries Society 117*, pp. 1-21.

Chien, N., & Wan, Z. (1999). *Mechanics of Sediment Transport.* Reston, VA: ASCE.

Chow, V. (1959). *Open Channel Hydraulics.* New York, New York: McGraw-Hill.

Dietrich, W., Kirchner, J., Ikeda, H., & Iseya, F. (1989). Sediment Supply and the Development of the Coarse Surface Layer in Gravel-Bedded Rivers. *Nature, 340*, pp 215-217.

Einstein, H. (1950). *The bed-load function for sediment transportation in open channel flows, Technical Bulletin 1026.* Washington, D.C.: U.S. Department of the Army, USDA Soil Conservation Service.

Graf, W. (1971). *Hydraulics of Sediment Transport.* New York: McGraw-Hill.

Guo, J. (2002). Hunter Rouse and Shields Diagram. *Advances in Hydraulics and Water Engineering, 13th IAHR-APD Congress, Vol.2* (pp. 1096-1098). Singapore, China: World Scientific.

Hack, J. (1960). Interpretation of erosional topography in humid temperate regions. *American Journal of Science, Vol. 258-A*, 80-97.

Haschenburger, J., & Wilcock, P. (2003). Partial transport in a natural gravel bed river. *Water Resources Research, Vol. 39*, 1-9.

Heggenes, J. (1988b). Effect of Induced Short-Term Flow Fluctuations on Emigration and Habitat Choice of Brown Trout in Small Streams. *Transactions of American Fisheries Society 117*, pp336-344.

Hey, R., & Thorne, C. (1986). Stable channels with mobile gravel beds. *Journal of Hydraulic Engineering, Vol. 112*, 671-689.

Hynes, H. (1968). Further studies on the invertebrate fauna of a welsh mountain stream. *Archive fur Hydrobiologie, Vol. 65*, 360-379.

Kennedy, J. (1995). The Albert Shields Story. *Journal of Hydraulic Engineering*, 766-772.

Kondolf, M., & Minear, J. (2004). *Coarse sediment augmentation on the Trinity River below Lewiston Dam: Geomorphic perspectives and review of past projects.* Berkeley, California: UC Berkeley.

Lai, Y. (2010). Two-dimensional depth-averaged flow modeling with an unstructured hybrid mesh. *Journal of Hydraulic Engineeing*, 12-23.

Lane, E. (1955). The importance of fluvial morphology in hydraulic engineering. *Proc. ASCE, Vol. 81 (745)*, 1-17.

Leopold, L., Wolman, M., & Miller, J. (1964). *Fluvial Processes in Geomorphology.* New York: Dover Publications, Inc.

Neill, C. (1968). *A reexamination of the beginning of movement for coarse granular bed materials. Report INT 68 .* Wallingford, England: Hydraulics Research Station.

Pitlick, J., & Wilcock, P. (2001). Relations between streamflow, sediment transport, and aquatic habitat in regulated rivers. *Water Science and Application, Vol. 4*, 185-198.

Postel, S., & Richter, B. (2003). *Rivers for Life: managing water for people and nature.* Washington, D.C.: Island Press.

Raleigh, R., Zuckerman, L., & Nelson, P. (1986). *Habitat Sustainability Index Models and Instream Flow Sustainability Curves: Brown Trout, revised.* Washington, D.C.: Fish and Wildlife Service.

Raudkivi, A. (1998). *Loose Boundary Hydraulics.* Rotterdam, Netherlands: A.A. Balkema.

Richard, G., Julien, P., & Baird, D. (2005). Case Study: Modeling the Lateral Mobility of the Rio Grande below Cochiti Dam, New Mexico. *Journal of Hydraulic Engineering*, pp. 931-941.

Sarriquet, P., Bordenave, P., & Marmonier, P. (2007). Effects of bottom sediment restoration on interstitial habitat characteristics and benthic macroinvertebrate assemblages in a headwater stream. *River Research and Application, Vol. 23*, 815-828.

Schumm, S., & Lichty, R. (1965). Time, Space, and Causality in Geomorphology. *American Journal of Science, Vol. 263*, 110-119.

Sheldon, A. (1986). Species diversity and longitudinal succession in stream fishes. *Ecology, Vol.49*, 193-198.

Shields, I. (1936). Application of similarity principles and turbulence research to bed-load movement. *Mitteilungen der Preussischen Versuchsanstalt fur Wasserbau und Schiffbau*, 1-44.

Shin, Y., & Julien, P. P. (2011). Effect of Flow Pilses on Degradation Downstream of Hapcheon Dam, South Korea. *Journal of Hydraulic Engineering*, pp. 100-111.

Strickler, A. (1923). *Contributions to the question of a velocity formula and roughness data for streams.* Pasadena, California: W.M. Keck Laboratory Translation T-10, by T. Roesgen and W. Brownlie, California Institute of Technology.

Suttle, K., Power, M., Levine, J., & McNeely, C. (2004). How Fine Sediment in Riverbeds Impairs Growth and Survival of Juvenile Salmonids. *Ecological Society of America*, Vol. 14, No. 4, pp. 969-974.

Swanson, B., Meyer, G., & Coonrod, J. (2008). *Coupling of Hydrologic/Hydraulic Models and Aerial Photos Through Time: Relating Geomorphic Change Measured from Air Photos to Hydrology. Rio Chama, NM, 1935-2005.* Albuquerque: Unpublsihed Report to Army Corps of Engineers.

Swanson, B., Meyer, G., & Coonrod, J. (2012). *Coupling of Hydrologic/Hydraulic Models and Aerial Photos through Time Fluvial Geomorphologic Changes along the Rio Chama, New Mexico 1935 - 2005.* Albuquerque: University of New Mexico.

Townsend, C., & Hildrew, A. (1994). Species traits in relation to a habitat templet for river systems. *Freshwater Biology, Vol. 31*, 265-275.

Wiberg, P., & Smith, J. (1987). Calculations of the Critical Shear Stress for Motion of Uniform and Heterogenous Sediments. *Water Resources Research*, 1471-1479.

Wilcock, P., & McArdell, B. (1993). Surface-based fractional transport rates: Mobilization thresholds and partial transport of a sand-gravel sediment. *Water Resources Research, Vol. 29*, 1297-1312.

Wilcock, P., & McArdell, B. (1997). Partial transport of a sand/gravel sediment. *Water Resources Research, Vol. 33*, 235-245.

Wilcock, P., Pitlick, J., & Cui, Y. (2009). *Sediment transport primer. Estimating bed-material transport in gravel-bed rivers. General Technical Report RMRS-GTR-226.* Fort Collins, Colorado: USDA Forest Service.

Williams, G., & Wolman, M. (1984). Downstream effects of dams on alluvial rivers. *U.S. Geological Survey Professional Paper 1286*, 1-84.

Wolman, M. (1954). A method of sampling coarse bed material. *American Geophysical Union, Transactions, Vol. 35*, 951-956.

Wolman, M. (1967). A cycle of sedimentation and erosion in urban river channels. *Geogr. Ann.*, 385-395.

Wu, W., Wang, S., & Jia, Y. (2000). Nonuniform Sediment Transport in Alluvial Rivers. *Journal of Hydraulic Research*, 427-434.

Yalin, M., & da Silva, A. (2001). *Fluvial Processes.* Delft, Netherlands: IAHR.

Appendices

Appendix A: Background

In 1998, Congress identified the Rio Chama as a Wild & Scenic River between El Vado and Abiquiu Dam (BLM, 1992). However, like other basins with dams, the Rio Chama has seen a decrease in flood frequency and a reduction of sediment below El Vado Dam. Sources of sediment are now limited to tributaries that feed the Rio Chama below El Vado Reservoir. In addition, the New Mexico Game and Fish Department identified the brown trout (*salmo trutta*) as a target management species (BLM, 1992) below El Vado Dam and it is touted as a prized game fish by local fisherman.

Several studies on the Rio Chama have evaluated the geomorphological changes of the Rio Chama since the completion of the San Juan Chama project and construction Heron, El Vado and Abiquiu dams. Specifically work has been done to determine the amount of narrowing that has occurred in the reach of concern due to the construction of El Vado Dam and the inflow of San Juan Chama water. Between 1935 and 2000, the Rio Chama between El Vado and Abiquiu has narrowed on average 20 meters (Swanson, Meyer, & Coonrod, 2008).

Brown Trout and Macroinvertebrate Habitat

According to the Bureau of Land Management the brown trout was introduced to the Rio Chama in the 1946. Originally from Germany, it is a cold water fish with optimal temperatures of 12° - 19°C and a lethal limit of 27.2°C (Raleigh, Zuckerman, & Nelson, 1986). Flow requirements listed in the Rio Chama Instream Flow Assessment for brown trout and macroinvertebrates are shown in Table 5. In addition, it is important to mention that brown trout

do not appear to be effected by short term high flows (Heggenes, 1988b) which are useful in maintaining habitat.

Table 5: Flow Requirements (cfs) for Brown Trout and Macroinvertebrates

Juveniles and Adults (ft^3/s)	Fry (ft^3/s)	Spawning & Incubation (ft^3/s)	Minimum Flow for Macroinvertebrates (ft^3/s)
75 – 300	150 – 300	150 – 700	185

Brown trout are generally found in relatively clear rivers that have a significant amount of gravel sediments (Raleigh et al., 1986). The Rio Chama is not notably a clear river, although El Vado Reservoir likely helps to decrease the suspended sediments downstream of the dam. In addition, to maintain brown trout habitat flows must physically be large enough to transport both fine and gravel sediments. High flow events are limited to rare occasions and evidence of embedding of gravels is visible at Archuleta and Cebolla. The area below El Vado is composed of a combination of fine sediments and gravel throughout both reaches whose inflows are limited by sediment inflow from the Rio Nutrias and Rio Cebolla. Logically it seems that larger flows would be required to maintain brown trout habitat for three reasons: 1) to reduce fine sediments in gravel riffles where spawning occurs and 2) to introduce fresh gravels.

The deposition of fines has been directly linked with a decrease in cover, and a linear decrease in growth with increasing fine sediment concentration for steelhead trout, a variety of salmonid (Suttle, Power, Levine, & McNeely, 2004). Along with decreases in habitat, an increase in fine sediment is known to reduce survival of offspring from redds, due to the associated decrease in oxygen and limited water movement through interstitial spaces (Chapman, 1988). Other noted relationships include the decrease in macroinvertebrate abundance with increased fine sediments. A visible difference was seen between Archuleta and Cebolla, with Archuleta having significantly less macroinvertebrates than Cebolla.

Appendix B: Historical Flows

The Rio Chama is composed of three primary sections, although the primary focus of this research is between El Vado Dam and Abiquiu Dam at Archuleta and Cebolla. El Vado Dam and reservoir was completed in 1935 and Abiquiu Dam and reservoir was completed in 1963. Flows for the period of record (October 1935- October 2012) below El Vado have ranged from 0 cfs to 6,010 ft^3/s in 1985 and have exceeded 60 ft^3/s, 75% of the time as can be seen in Figure 25 below.

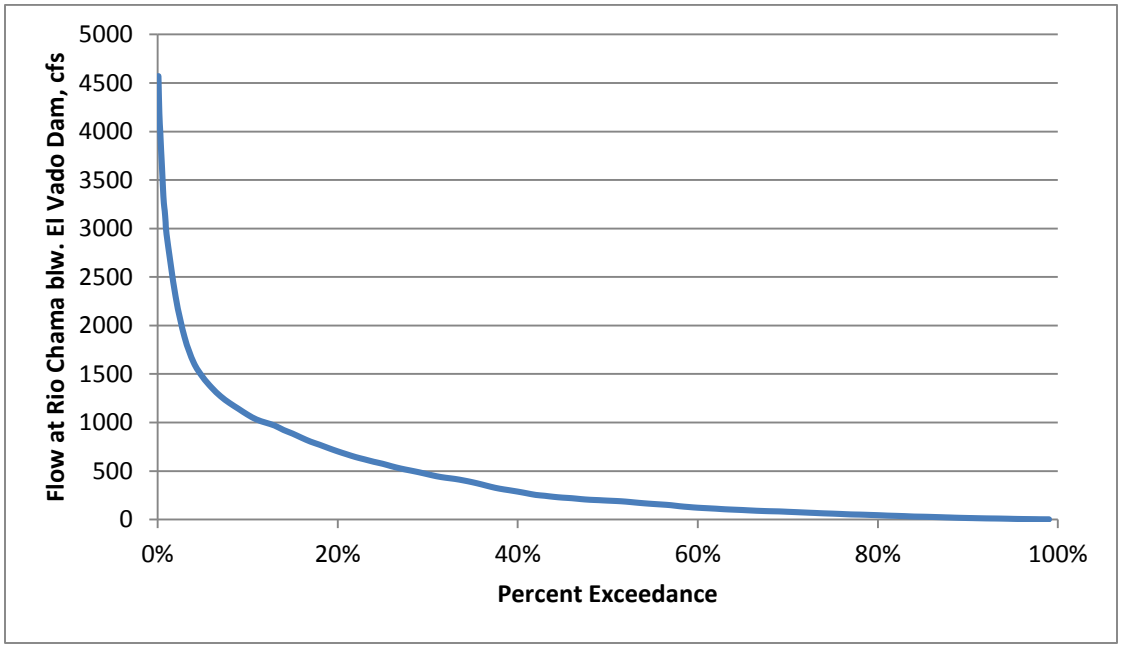

Figure 25: Flows below El Vado Dam, 1935-2012

Above El Vado Dam is the gage station Rio Chama nr. La Puente and Heron Dam. Heron was constructed from 1967 to 1971. Flows for Rio Chama nr La Puente for the period of 1955-1967, show that flows ranged between 4 ft^3/s and 5,760 ft^3/s and the percent exceedance curve can be seen in Figure 26. Flows below El Vado for the same period ranged from 0 ft^3/s to

3,620 ft^3/s. The reduced flow is related to the operation of El Vado dam for water rights holders by the Bureau of Reclamation.

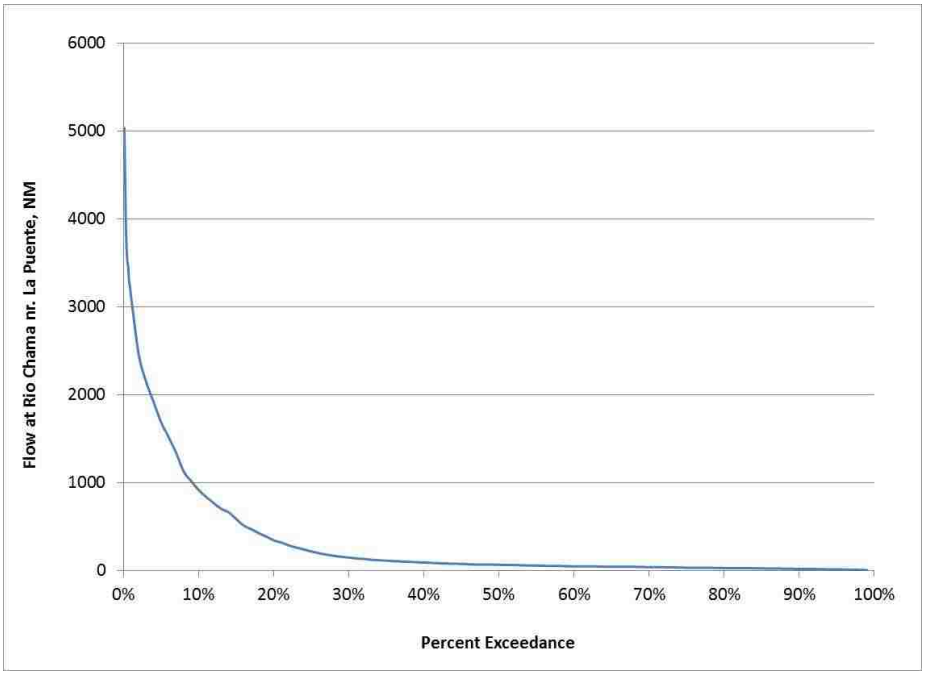

Figure 26: Flow Exceedance at Rio Chama nr. La Puente, NM 1955-1967

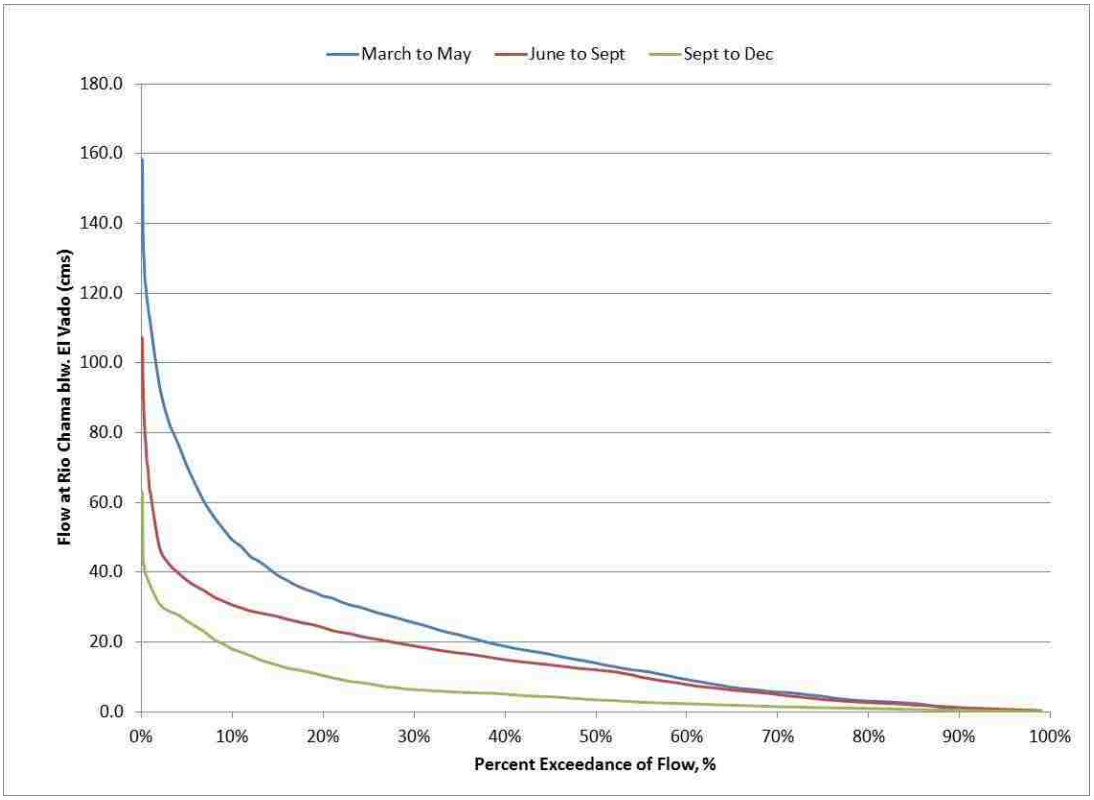

Figure 27: Percent Exceedance of Flow by Season, 10/1935 to 10/2012

Appendix C, Water Surface Elevations

Table 6: Archuleta Site Water Surface Elevations at Normal Depth (m)

Flow (m^3/s)	Water Surface Elevation (m)
14	2012.62
28	2012.83
42	2012.97
57	2013.09
71	2013.21
85	2013.33
99	2013.44
113	2013.54
127	2013.64
142	2013.73
156	2013.82
170	2013.91

Table 7: Cebolla Site Water Surface Elevations at Normal Depth (m)

Flow (m^3/s)	Water Surface Elevation (m)
14	1977.82
28	1978.04
42	1978.21
57	1978.35
71	1978.49
85	1978.61
99	1978.73
113	1978.85
127	1978.95
142	1979.05
156	1979.16
170	1979.26

Appendix D, Pebble Count Data

Pebble counts were taken on two separate occasions at each site to collect grain size distribution data. At Archuleta, 3 counts of 100 particles was completed during each visit. Data collected at Cebolla, included 2 pebble counts of 100 particles during each visit. In addition, pebble count data was collected on the Rio Cebolla in July of 2012, approximately 1500 feet from the inlet. Data collected on the Rio Cebolla included two collections of fine material found in the backwater pool at the inlet and 1 pebble count of 100 particles.

Table 8: Archuleta Pebble Count 1

Location	Archuleta			06/22/2012
ID	1			
Decription	River left at lower end of bar			
Size (mm)	No. of Particles Passing	Cumulative No. of Particles	% Passing	%Retained
<2			0.0%	100.0%
2.5			0.0%	100.0%
4			0.0%	100.0%
5.6			0.0%	100.0%
8			0.0%	100.0%
11	1	1	0.9%	99.1%
16	3	4	3.7%	96.3%
22.6	6	10	9.3%	90.7%
32	12	22	20.4%	79.6%
45	25	47	43.5%	56.5%
64	23	70	64.8%	35.2%
90	25	95	88.0%	12.0%
128	13	108	100.0%	0.0%
180		108	100.0%	0.0%
256		108	100.0%	0.0%
Total	108			

Table 9: Archuleta Pebble Count 2

Location	Archuleta			06/22/2012
ID	2			
Decription:	River left at upper end of bar, fines clogging bar			
Size (mm)	No. of Particles Passing	Cumulative No. of Particles	% Passing	%Retained
0				
<2	9	9	9.0%	91.0%
2.5		9	9.0%	91.0%
4		9	9.0%	91.0%
5.6		9	9.0%	91.0%
8	1	10	10.0%	90.0%
11	2	12	12.0%	88.0%
16	10	22	22.0%	78.0%
22.6	13	35	35.0%	65.0%
32	9	44	44.0%	56.0%
45	12	56	56.0%	44.0%
64	19	75	75.0%	25.0%
90	19	94	94.0%	6.0%
128	6	100	100.0%	0.0%
180		100	100.0%	0.0%
256		100	100.0%	0.0%
Total	100			

Table 10: Cebolla Pebble Count 1

Location	Rio Chama 1/4 mile below Cebolla Confluence			06/23/2012
ID	3			
Decription:	Top of bar			
Size (mm)	No. of Particles Passing	Cumulative No. of Particles	% Passing	%Retained
<2		0	0.0%	100.0%
2.5		0	0.0%	100.0%
4		0	0.0%	100.0%
5.6		0	0.0%	100.0%
8		0	0.0%	100.0%
11		0	0.0%	100.0%
16	1	1	0.9%	99.1%
22.6	8	9	8.3%	91.7%
32	8	17	15.6%	67.9%
45	18	35	32.1%	52.3%
64	17	52	47.7%	27.5%
90	27	79	72.5%	3.7%
128	26	105	96.3%	0.0%
180	4	109	100.0%	0.0%
256		109	100.0%	0.0%
Total	109			

Table 11: Cebolla Pebble Count 2

Location	Rio Chama 1/4 mile below Cebolla Confluence			06/23/2012
ID	4			
Decription:	mid bar			
Size (mm)	No. of Particles Passing	Cumulative No. of Particles	% Passing	%Retained
0			0.0%	100.0%
<2	1	1	1.0%	99.0%
2.5		1	1.0%	99.0%
4		1	1.0%	99.0%
5.6		1	1.0%	99.0%
8		1	1.0%	99.0%
11		1	1.0%	99.0%
16		1	1.0%	99.0%
22.6	5	6	6.0%	94.0%
32	6	12	12.0%	88.0%
45	12	24	24.0%	76.0%
64	26	50	50.0%	50.0%
90	24	74	74.0%	26.0%
128	20	94	94.0%	6.0%
180	6	100	100.0%	0.0%
256		100	100.0%	0.0%
Total	100			

Table 12: Cebolla Pebble Count 3

Location	Rio Chama 1/4 mile below Cebolla Confluence			06/23/2012
ID	5			
Decription:	mid bar			
Size (mm)	No. of Particles Passing	Cumulative No. of Particles	Percent Passing, %	%Retained
0				
<2		0	0.0%	100.0%
2.5		0	0.0%	100.0%
4		0	0.0%	100.0%
5.6		0	0.0%	100.0%
8		0	0.0%	100.0%
11		0	0.0%	100.0%
16	1	1	1.0%	99.0%
22.6	8	9	8.7%	91.3%
32	8	17	16.5%	83.5%
45	13	30	29.1%	70.9%
64	17	47	45.6%	54.4%
90	27	74	71.8%	28.2%
128	26	100	97.1%	2.9%
180	3	103	100.0%	0.0%
256		103	100.0%	0.0%
Total	103			

Table 13: Archuleta Pebble Count 3

Location	Archuleta			10/6/2012
ID	1			
Decription	River left at lower end of bar			
Size (mm)	No. of Particles Passing	Cumulative No. of Particles	% Passing	%Retained
<2	4	4	4%	96%
2.5	3	7	7%	93%
4	4	11	11%	89%
5.6	1	12	12%	88%
8	4	16	16%	84%
11	5	21	21%	79%
16	5	26	26%	74%
22.6	5	31	31%	69%
32	6	37	37%	63%
45	7	44	44%	56%
64	16	60	59%	41%
90	13	73	72%	28%
128	13	86	85%	15%
180	8	94	93%	7%
256	7	101	100%	0%
Total	101			

Table 14: Archuleta Pebble Count 4

Location	Archuleta			10/6/2012
ID	2			
Decription:	River left at upper end of bar, fines clogging bar			
Size (mm)	No. of Particles Passing	Cumulative No. of Particles	% Passing	%Retained
0				
<2		0	0.0%	100.0%
2.5		0	0.0%	100.0%
4		0	0.0%	100.0%
5.6		0	0.0%	100.0%
8		0	0.0%	100.0%
11		0	0.0%	100.0%
16		0	0.0%	100.0%
22.6		0	0.0%	100.0%
32	4	4	4.0%	96.0%
45	11	15	15.0%	85.0%
64	15	30	30.0%	70.0%
90	21	51	51.0%	49.0%
128	37	88	88.0%	12.0%
180	12	100	100.0%	0.0%
256		100	100.0%	0.0%
Total	100			

Table 15: Archuleta Pebble Count 5

Location	Archuleta			10/6/2012
ID	3			
Decription:	River left at upper end of bar, fines clogging bar			
Size (mm)	No. of Particles Passing	Cumulative No. of Particles	% Passing	%Retained
0				
<2		0	0.0%	100.0%
2.5		0	0.0%	100.0%
4		0	0.0%	100.0%
5.6		0	0.0%	100.0%
8		0	0.0%	100.0%
11		0	0.0%	100.0%
16	1	1	1.0%	99.0%
22.6	1	2	2.0%	98.0%
32	10	12	11.9%	88.1%
45	17	29	28.7%	71.3%
64	29	58	57.4%	42.6%
90	23	81	80.2%	19.8%
128	15	96	95.0%	5.0%
180	5	101	100.0%	0.0%
256		101	100.0%	0.0%
Total	101			

Table 16: Cebolla Pebble Count 4

Location	Rio Chama 1/4 mile below Cebolla Confluence			10/7/2012
ID	4			
Decription:	Top of bar			
Size (mm)	No. of Particles Passing	Cumulative No. of Particles	% Passing	%Retained
<2	11	11	11.0%	89.0%
2.5		11	11.0%	89.0%
4		11	11.0%	89.0%
5.6		11	11.0%	89.0%
8		11	11.0%	89.0%
11	2	13	13.0%	87.0%
16	2	15	15.0%	85.0%
22.6	6	21	21.0%	79.0%
32	9	30	30.0%	70.0%
45	15	45	45.0%	55.0%
64	17	62	62.0%	38.0%
90	23	85	85.0%	15.0%
128	11	96	96.0%	4.0%
180	4	100	100.0%	0.0%
256		100	100.0%	0.0%
Total	100			

Table 17: Cebolla Pebble Count 5

Location	Rio Chama 1/4 mile below Cebolla Confluence			10/7/2012
ID	5			
Decription:	mid bar			
Size (mm)	No. of Particles Passing	Cumulative No. of Particles	% Passing	%Retained
0			0.0%	100.0%
<2	2	2	2.0%	100.0%
2.5		2	2.0%	98.0%
4		2	2.0%	98.0%
5.6		2	2.0%	98.0%
8		2	2.0%	98.0%
11		2	2.0%	98.0%
16	2	4	4.0%	96.0%
22.6	4	8	8.0%	92.0%
32	17	25	25.0%	61.0%
45	14	39	39.0%	40.0%
64	21	60	60.0%	23.0%
90	17	77	77.0%	13.0%
128	10	87	87.0%	0.0%
180	13	100	100.0%	0.0%
256		100	100.0%	0.0%
Total	100			

Appendix E: Cross Section Interpolation and resulting mesh

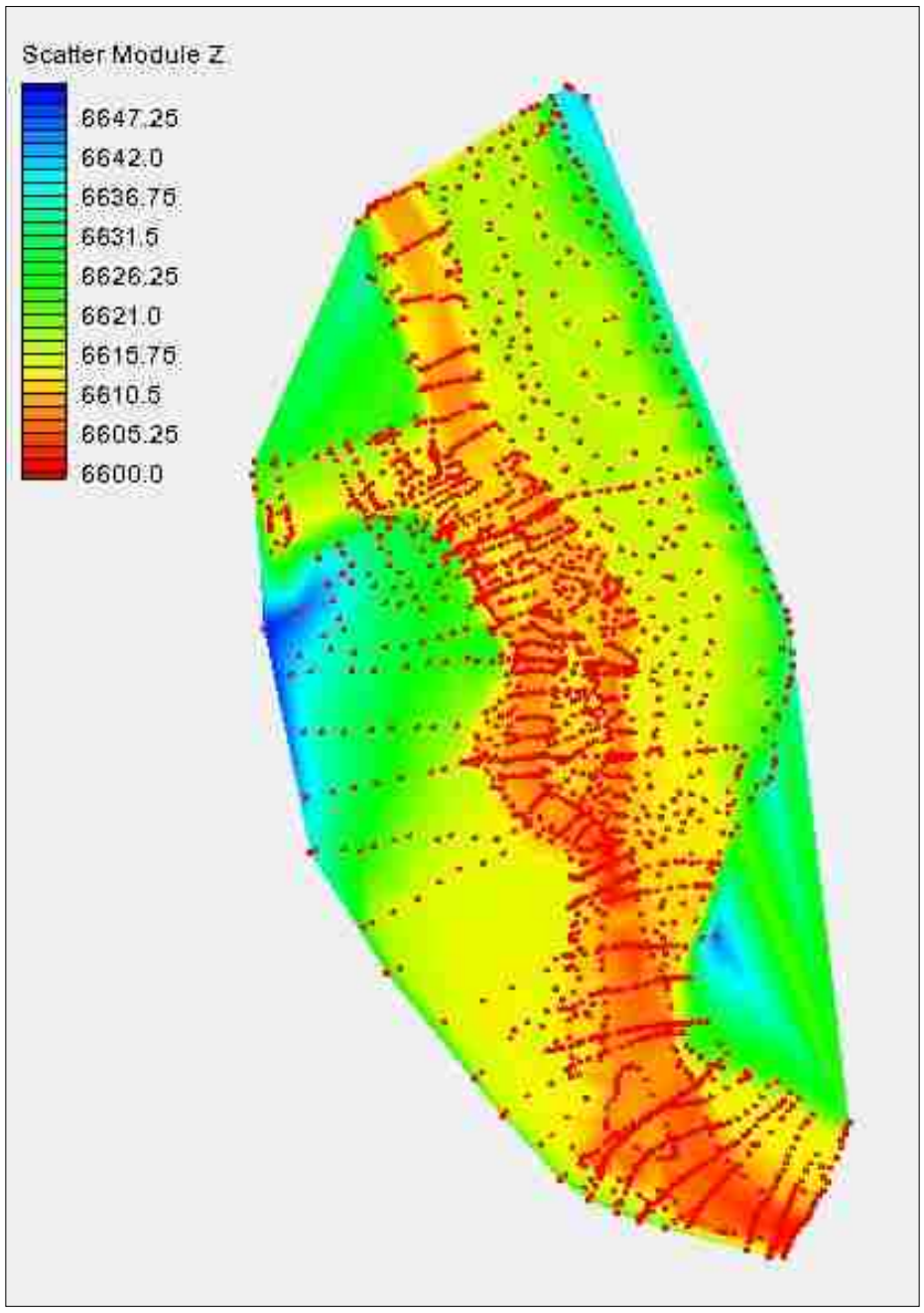

Figure 28: Archuleta Survey Points as Topography

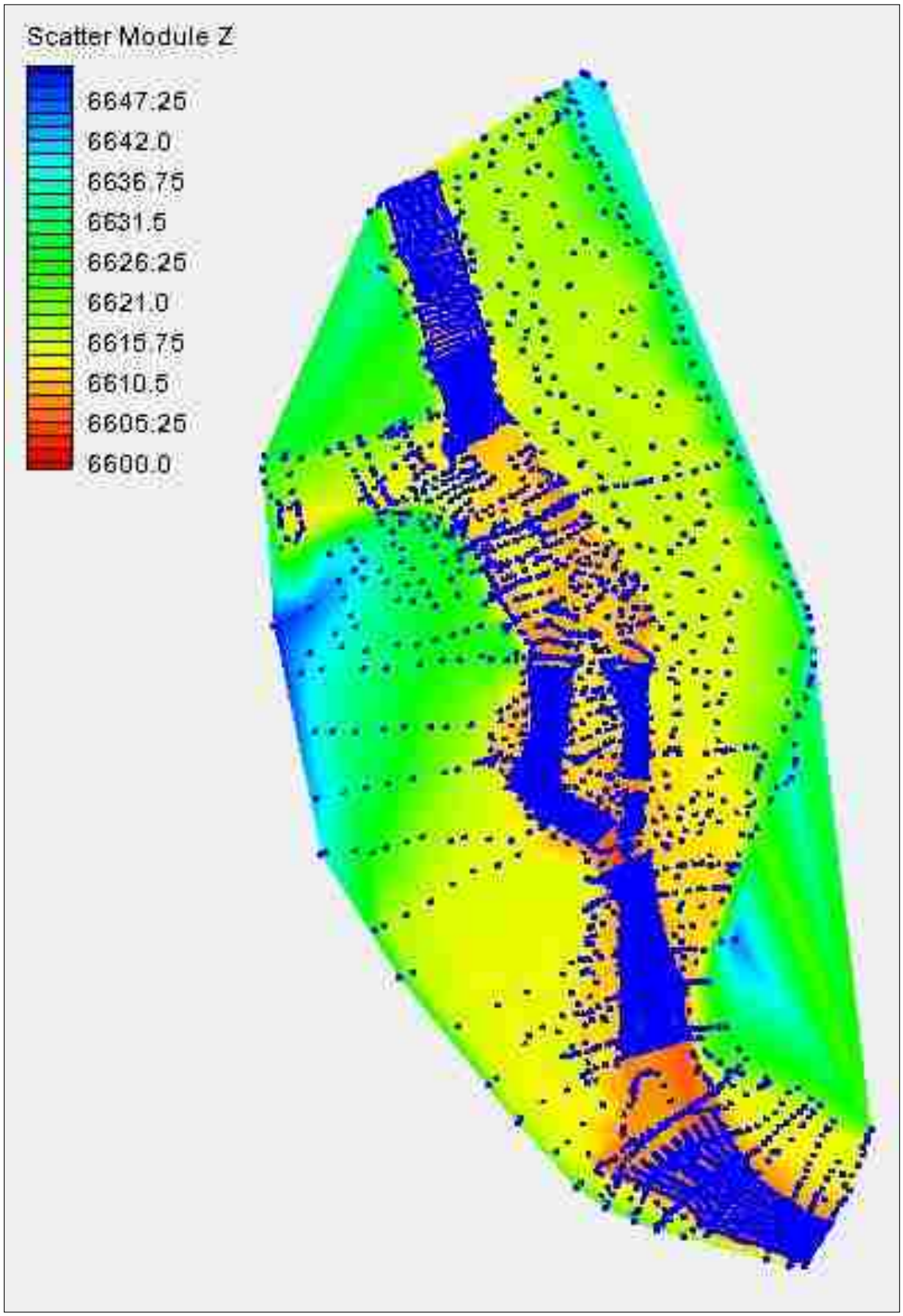

Figure 29: Archuleta Survey Data with Interpolated Points as Topography

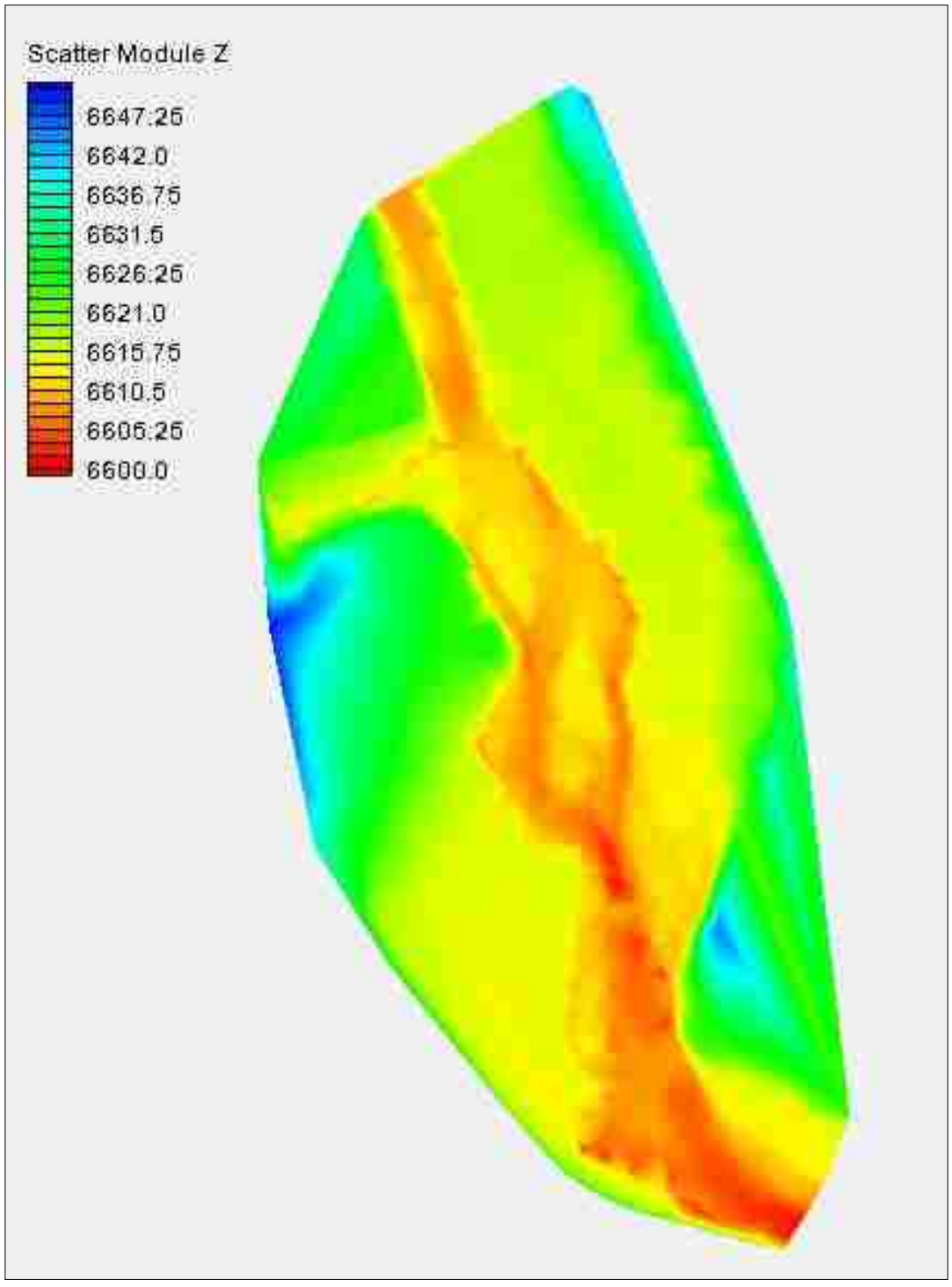

Figure 30: Archuleta Survey Data Triangulated to Mesh

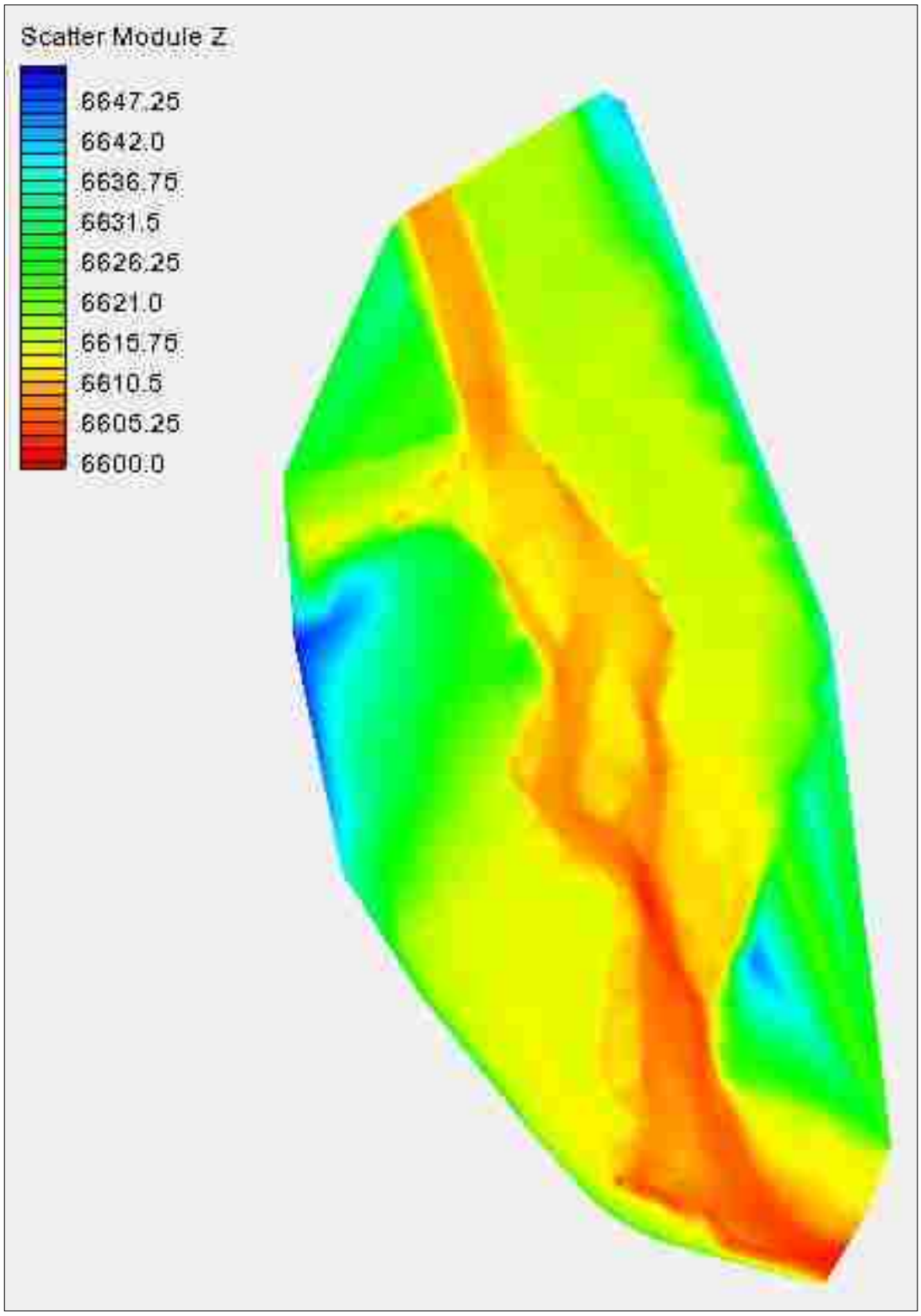

Figure 31: Archuleta Survey Data with Interpolated Points Triangulated to Mesh

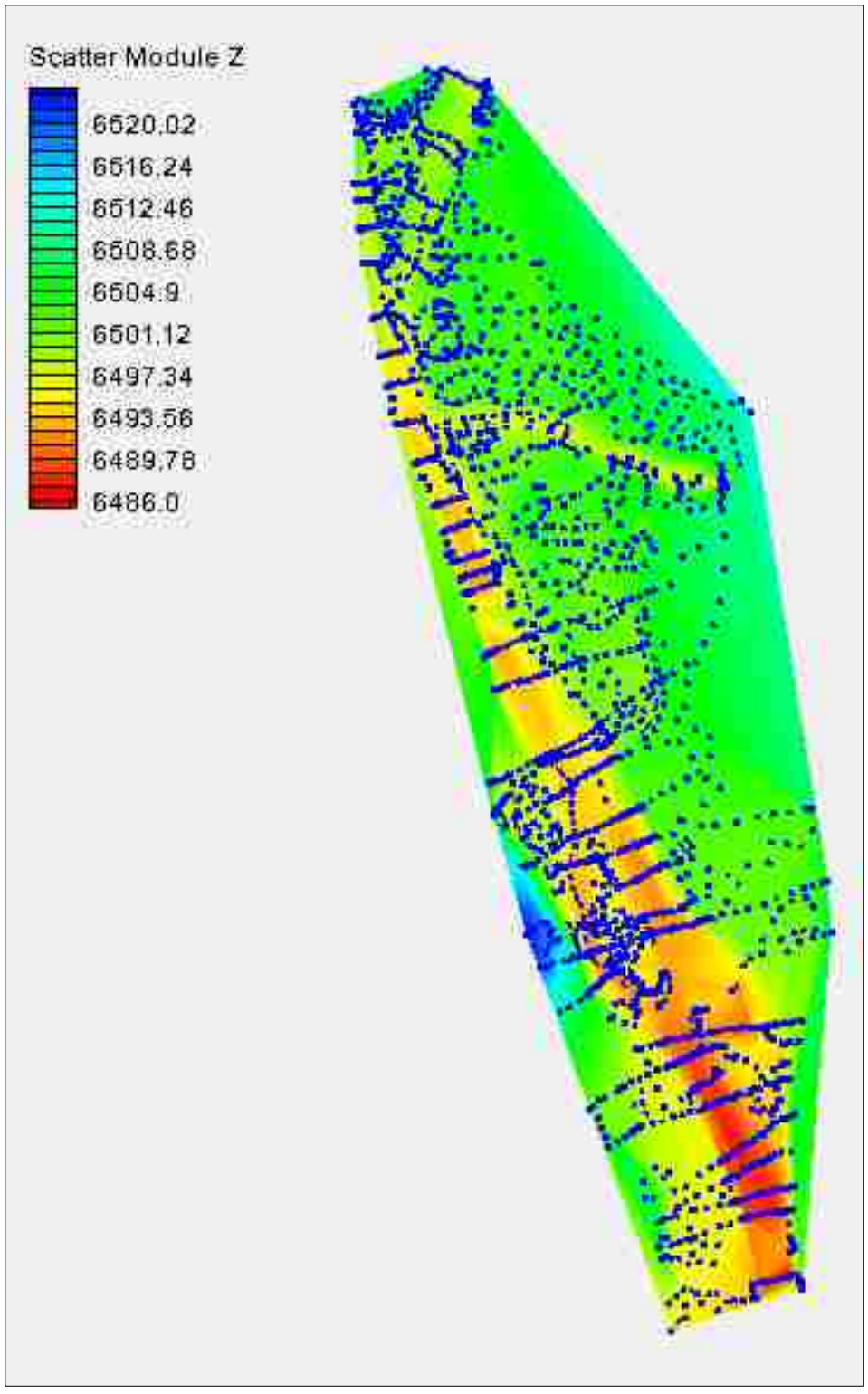

Figure 32: Cebolla Original Survey Data with Topography

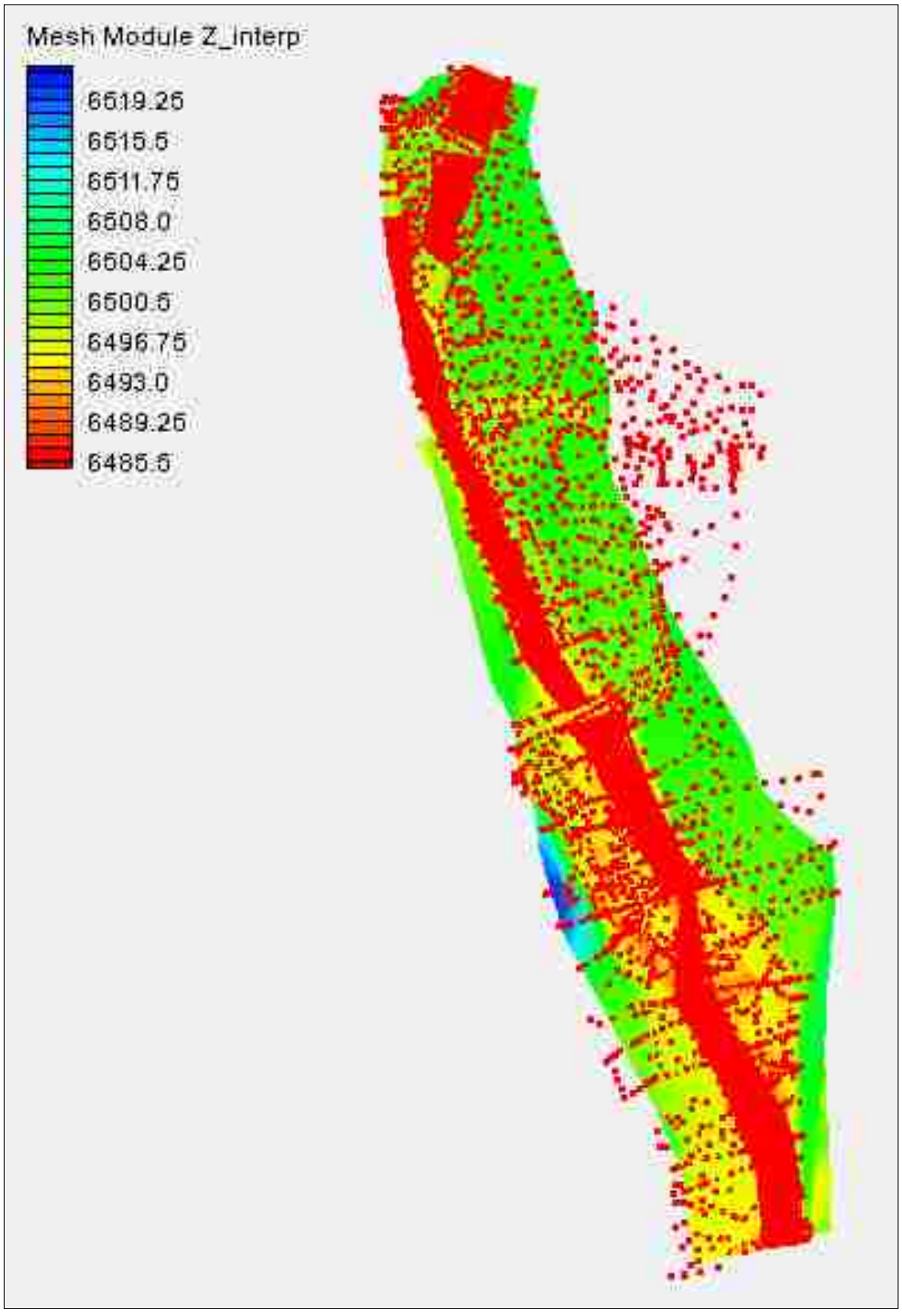

Figure 33: Cebolla Survey with Interpolated points and Topography

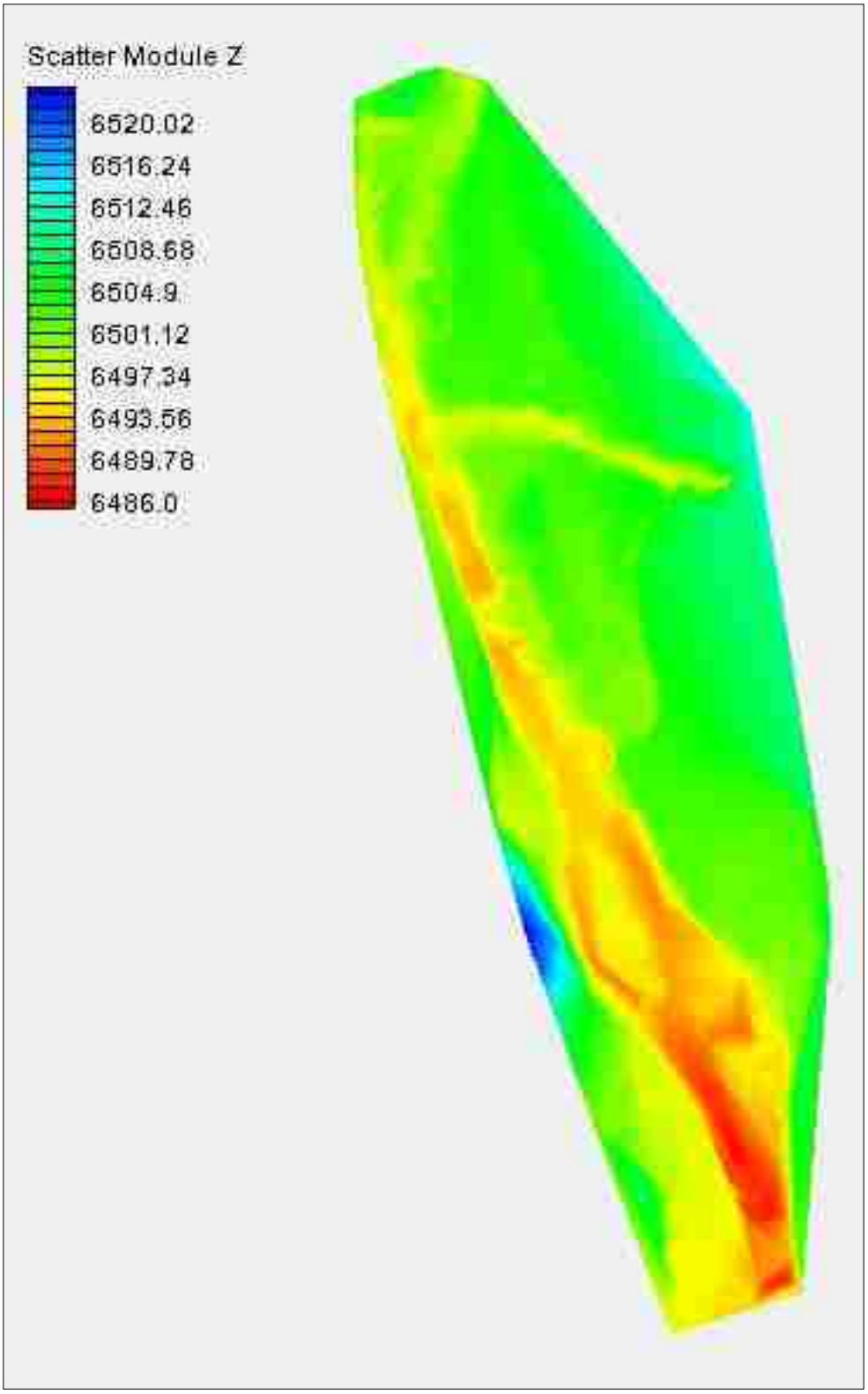

Figure 34: Cebolla Site Original Mesh

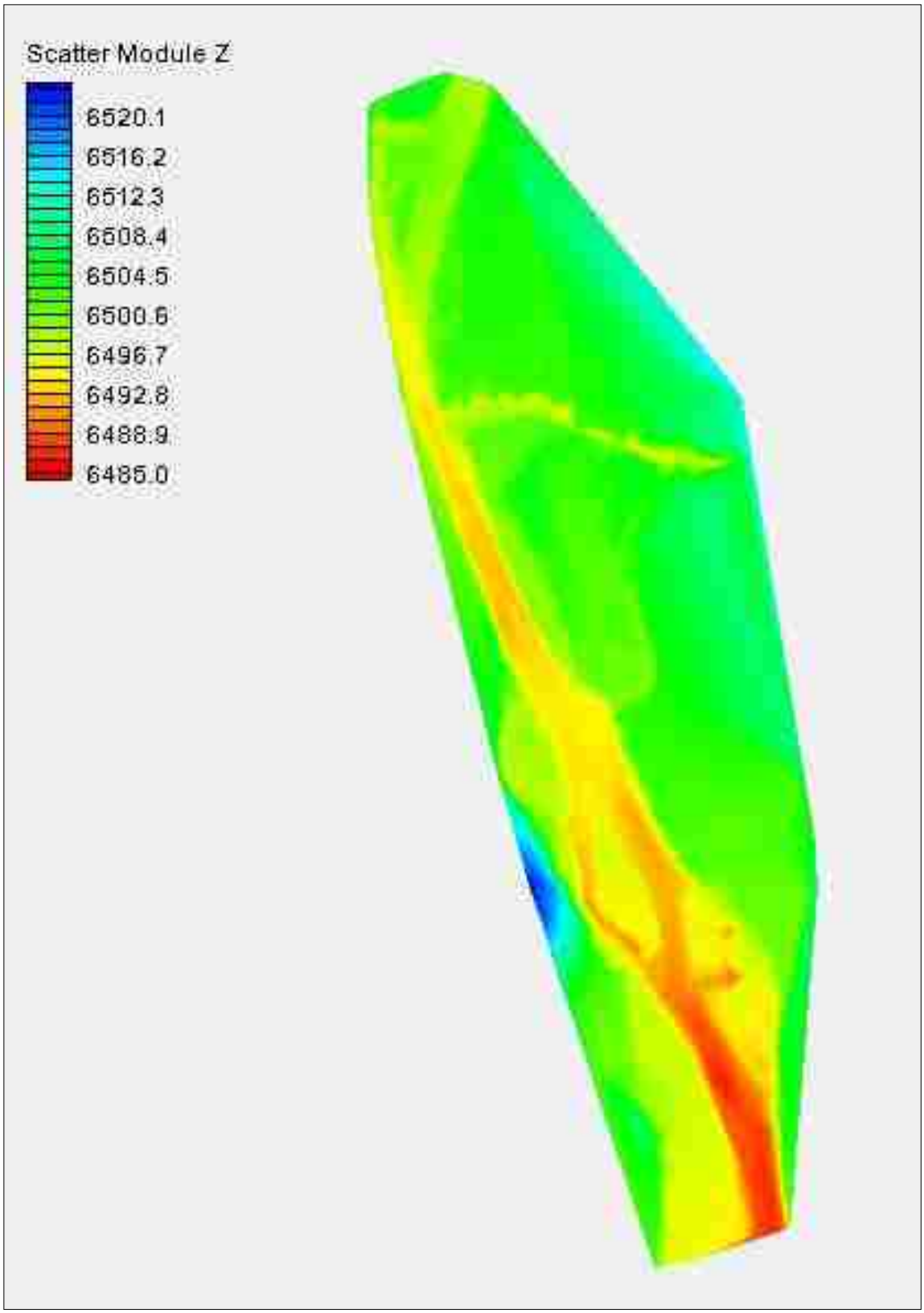

Figure 35: Cebolla Survey Data with Interpolated points as Mesh

Appendix F: Material type distribution in channel

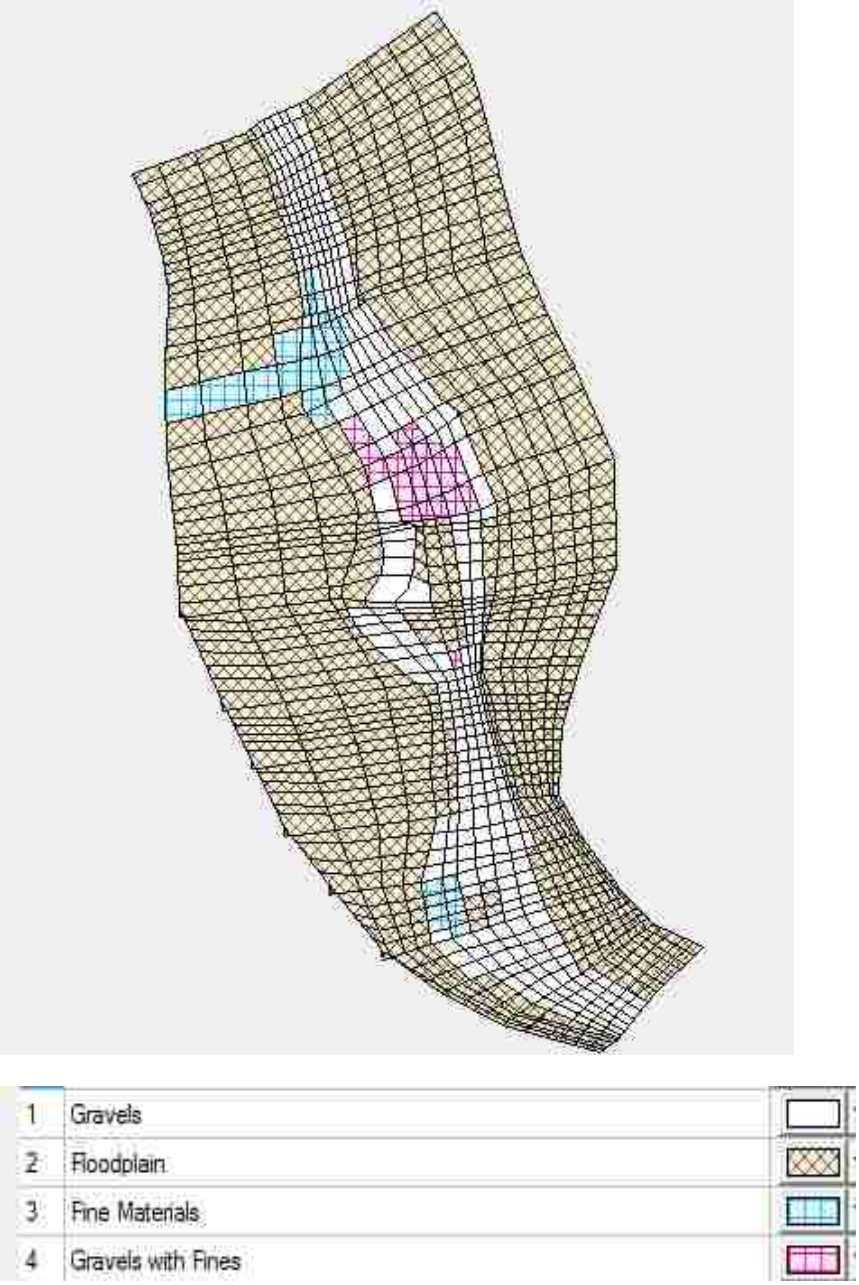

Figure 36: Material Type Map for Archuleta

Figure 37: Cebolla Material Type Map

Appendix G: Flow Results, Floodplain n=0.045

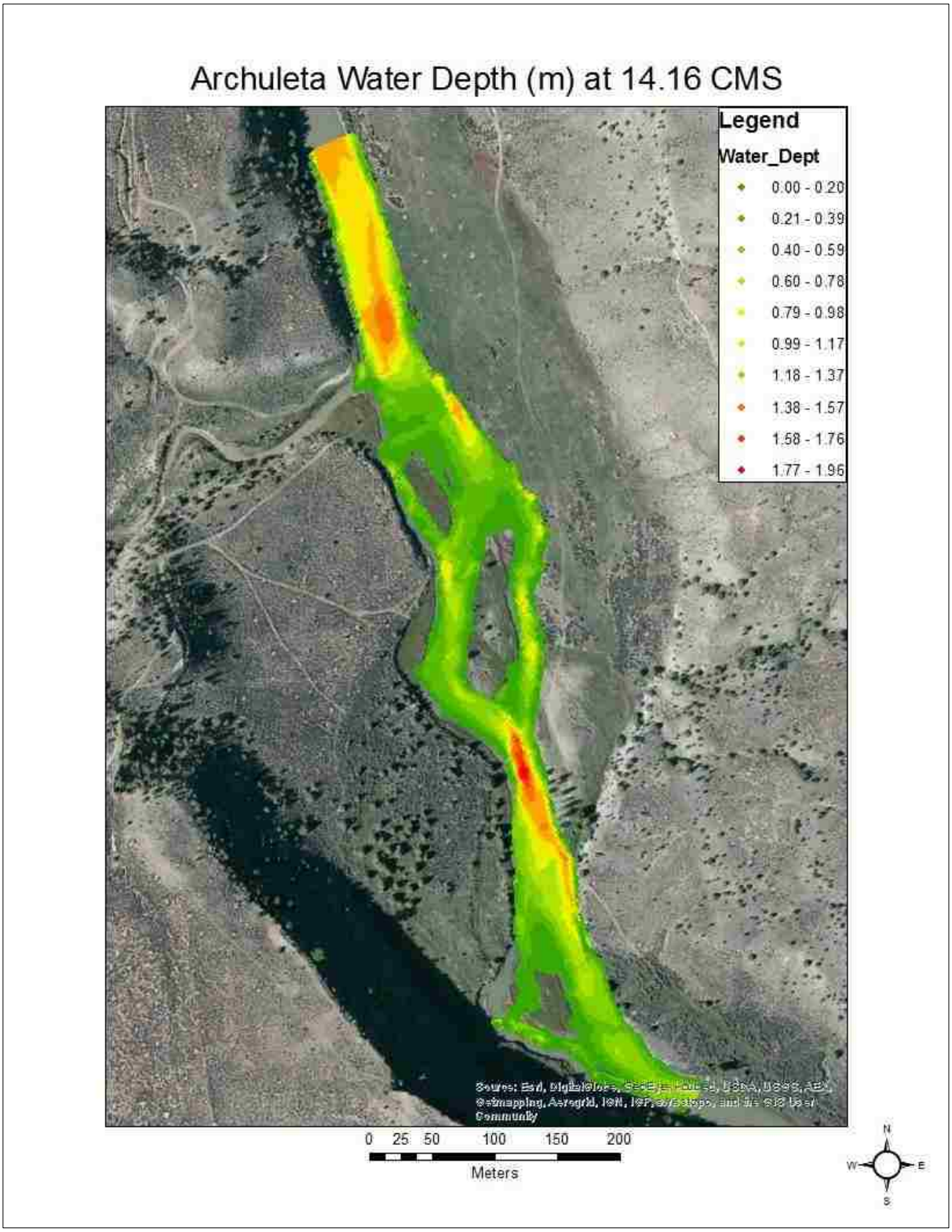

Figure 38: Archuleta Water Depth at 14 m^3/s

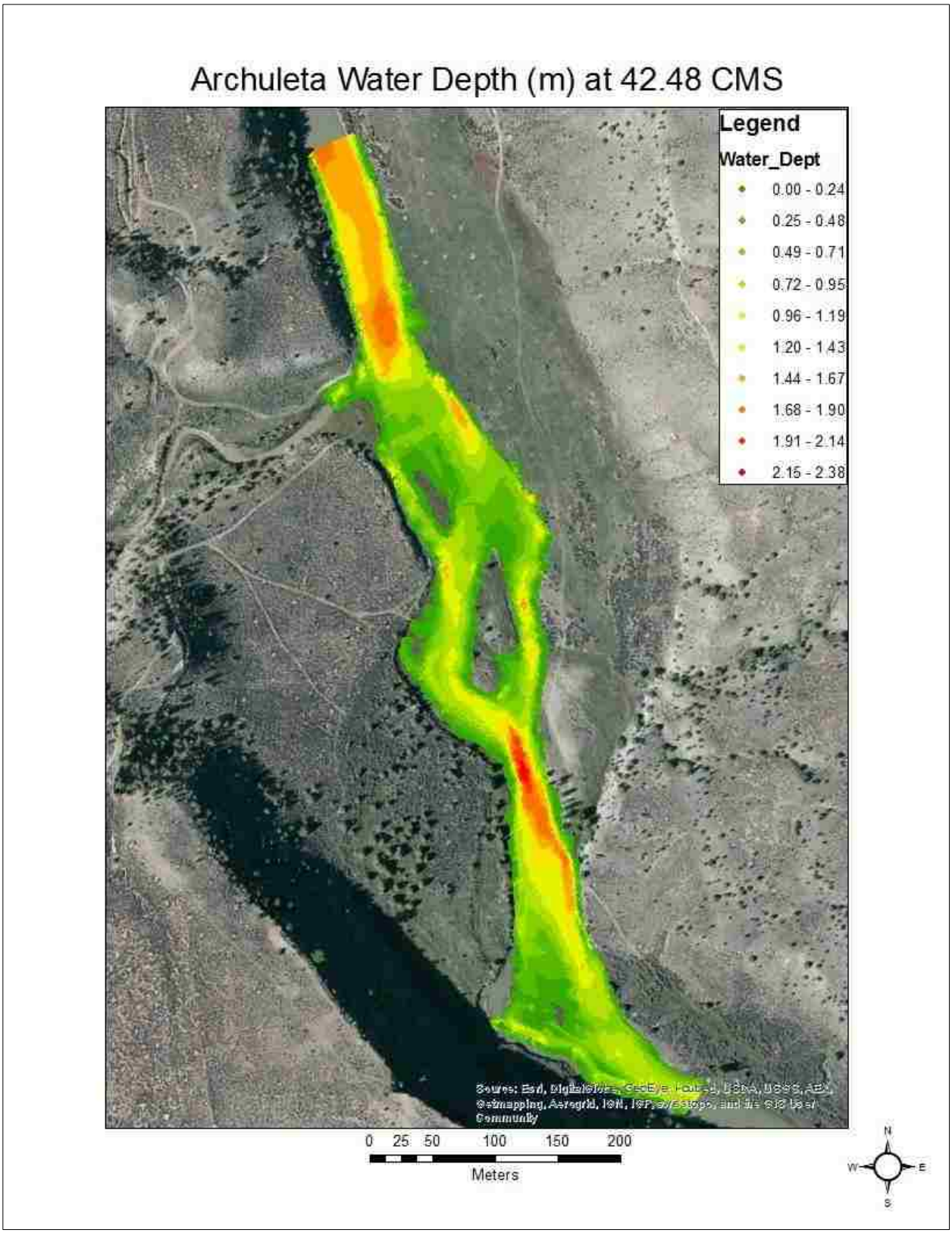

Figure 39: Archuleta Water Depth at 43 m³/s

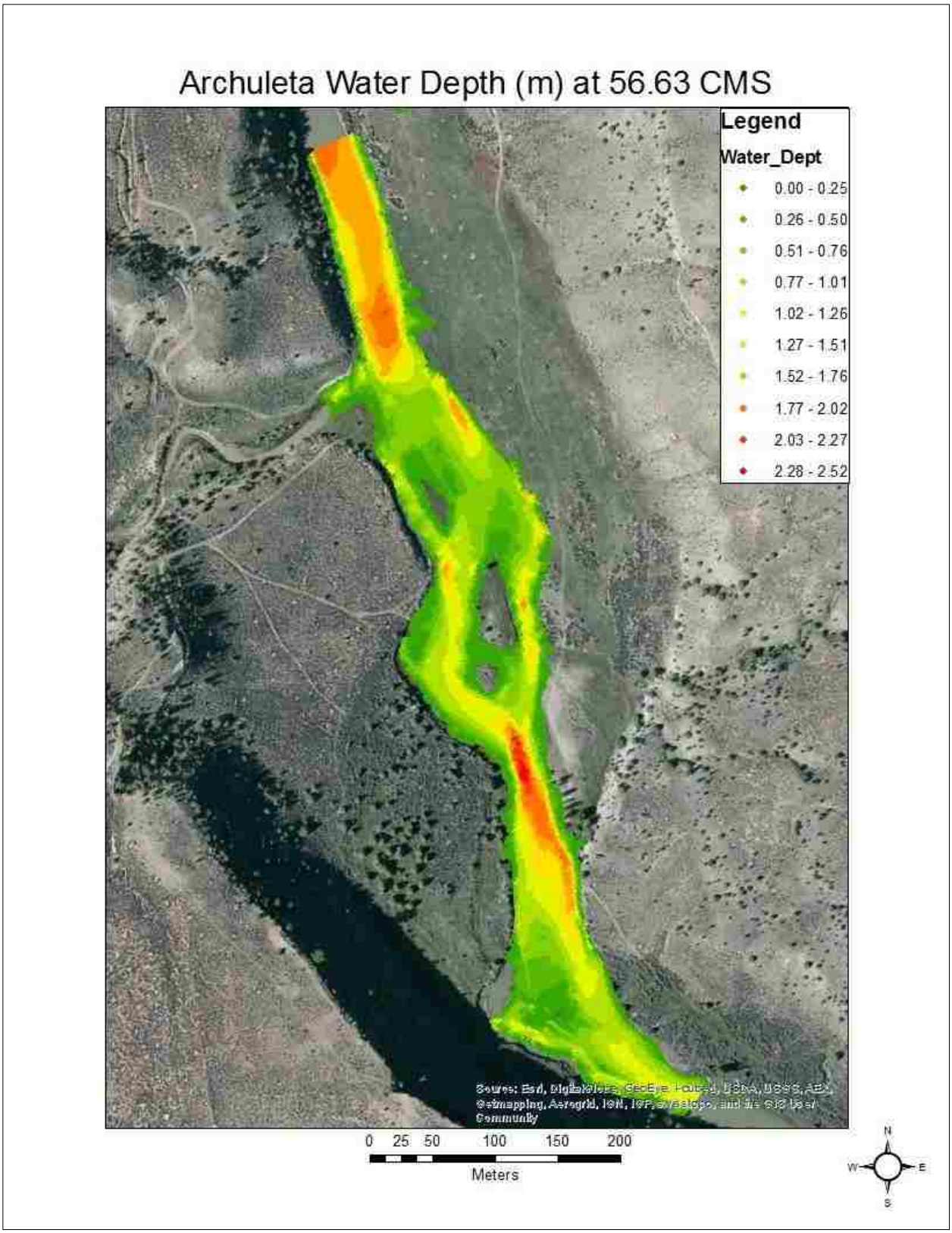

Figure 40: Archuleta Water Depth at 57 m³/s

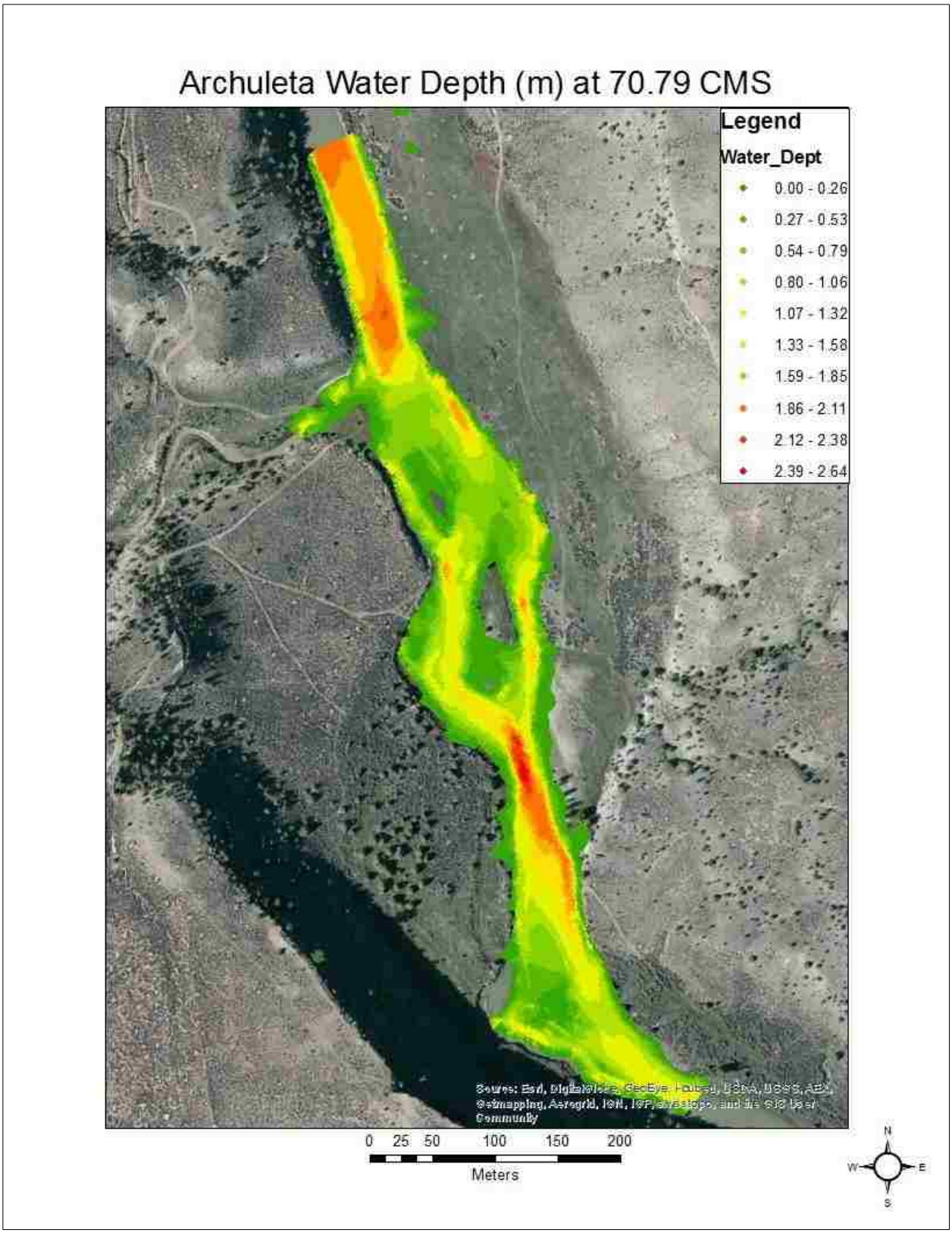

Figure 41: Archuleta Water Depth at 71 m³/s

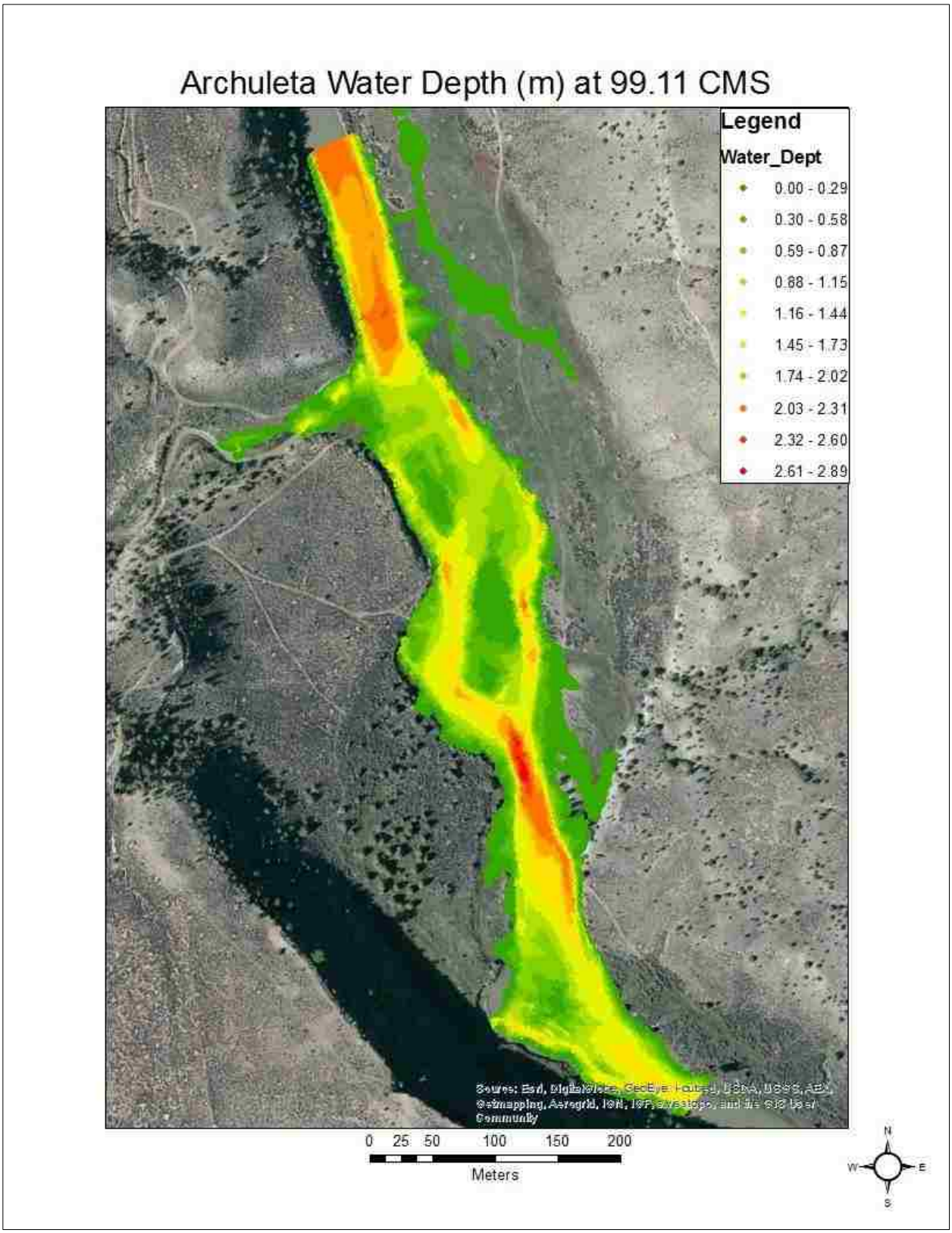

Figure 42: Archuleta Water Depth at 99 m^3/s

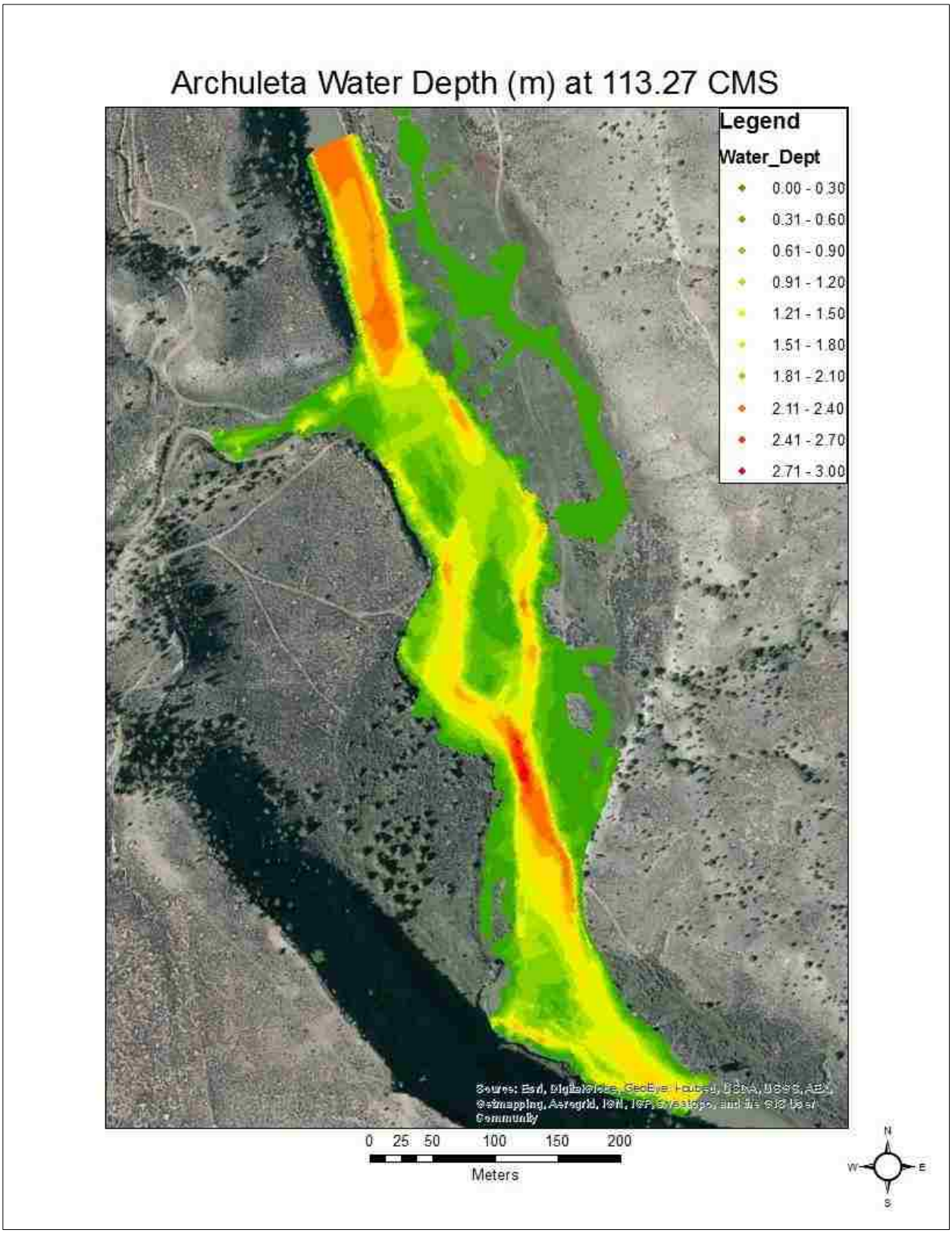

Figure 43: Archuleta Water Depth at 113 m³/s

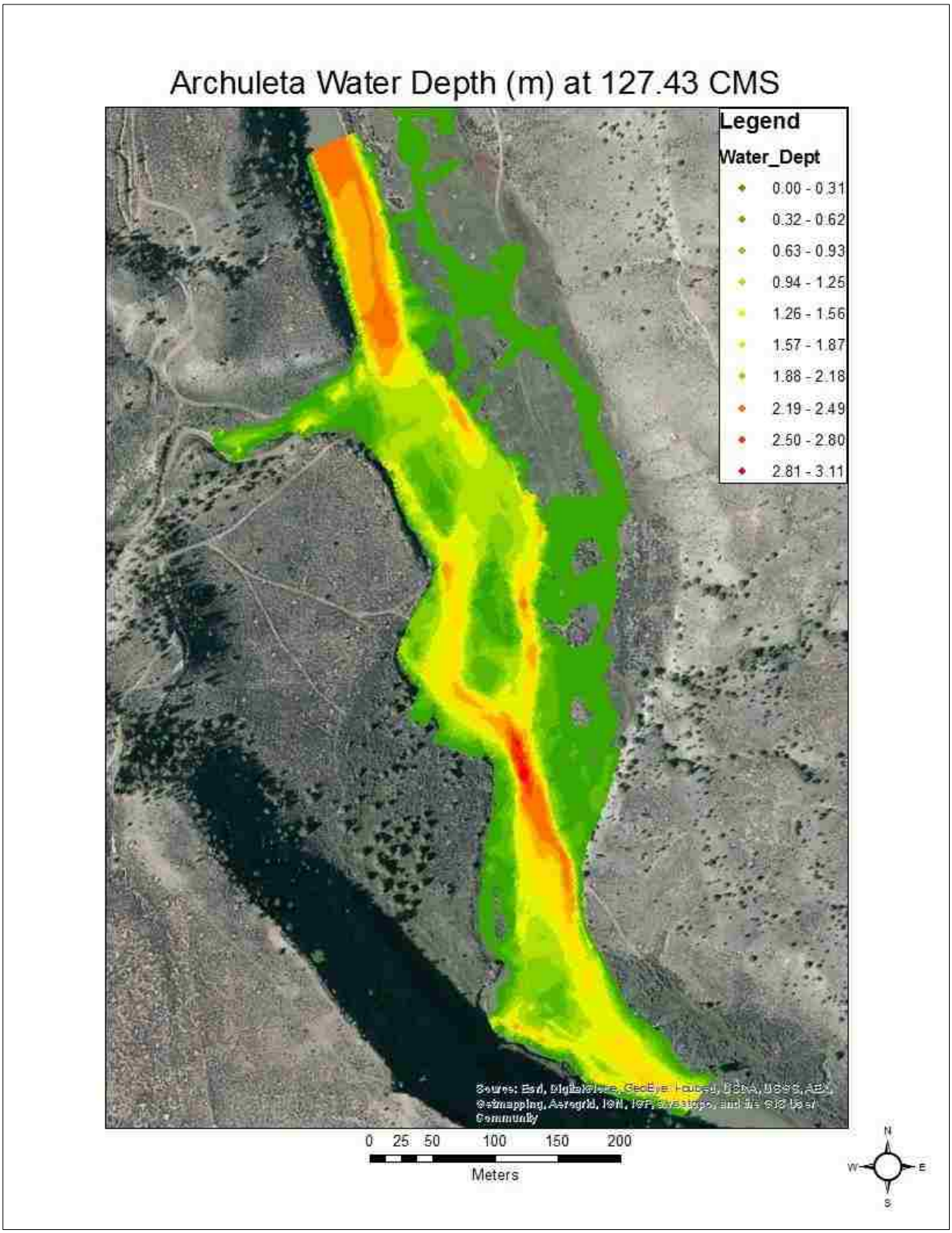

Figure 44: Archuleta Water Depth at 127 m^3/s

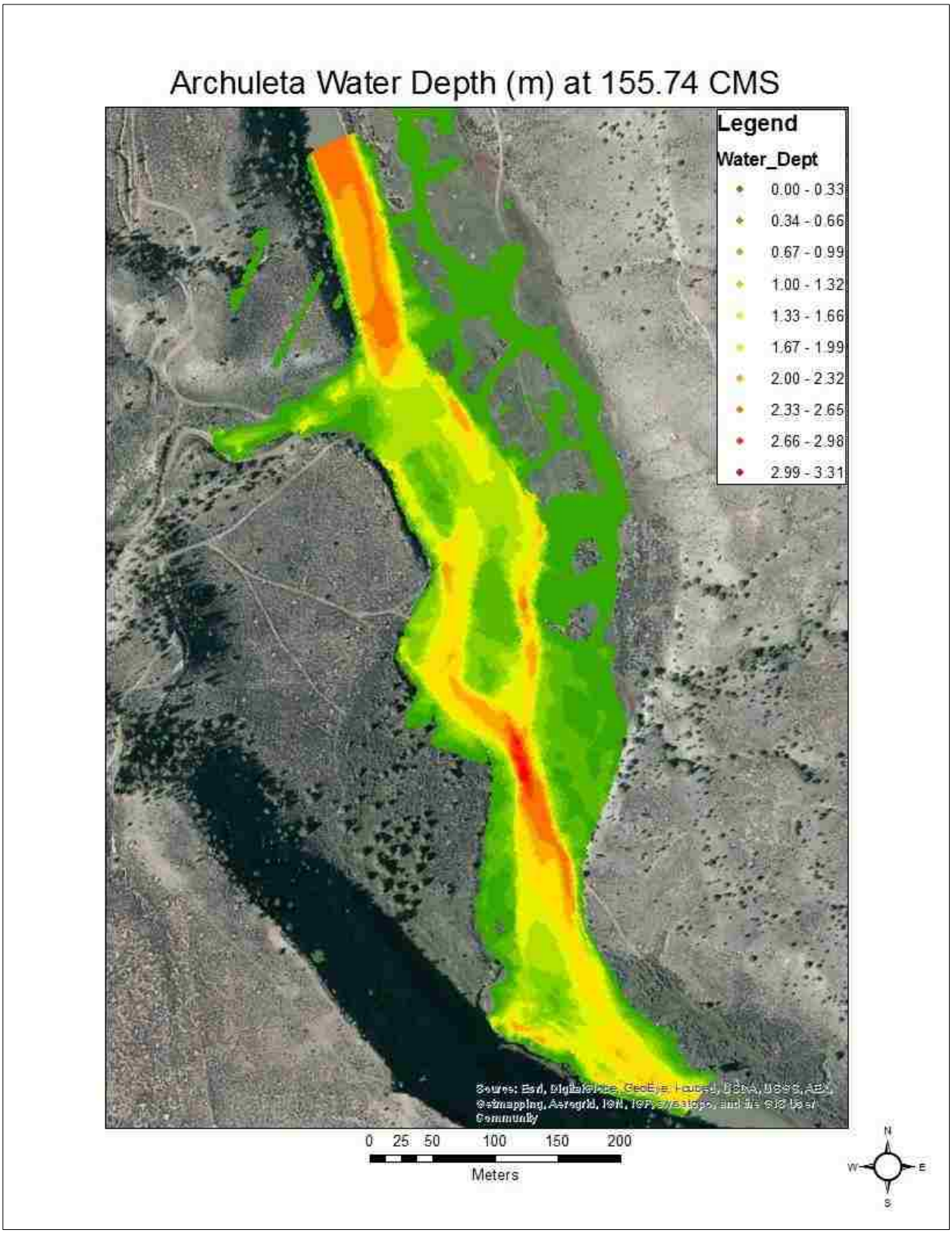

Figure 45: Archuleta Water Depth at 156 m^3/s

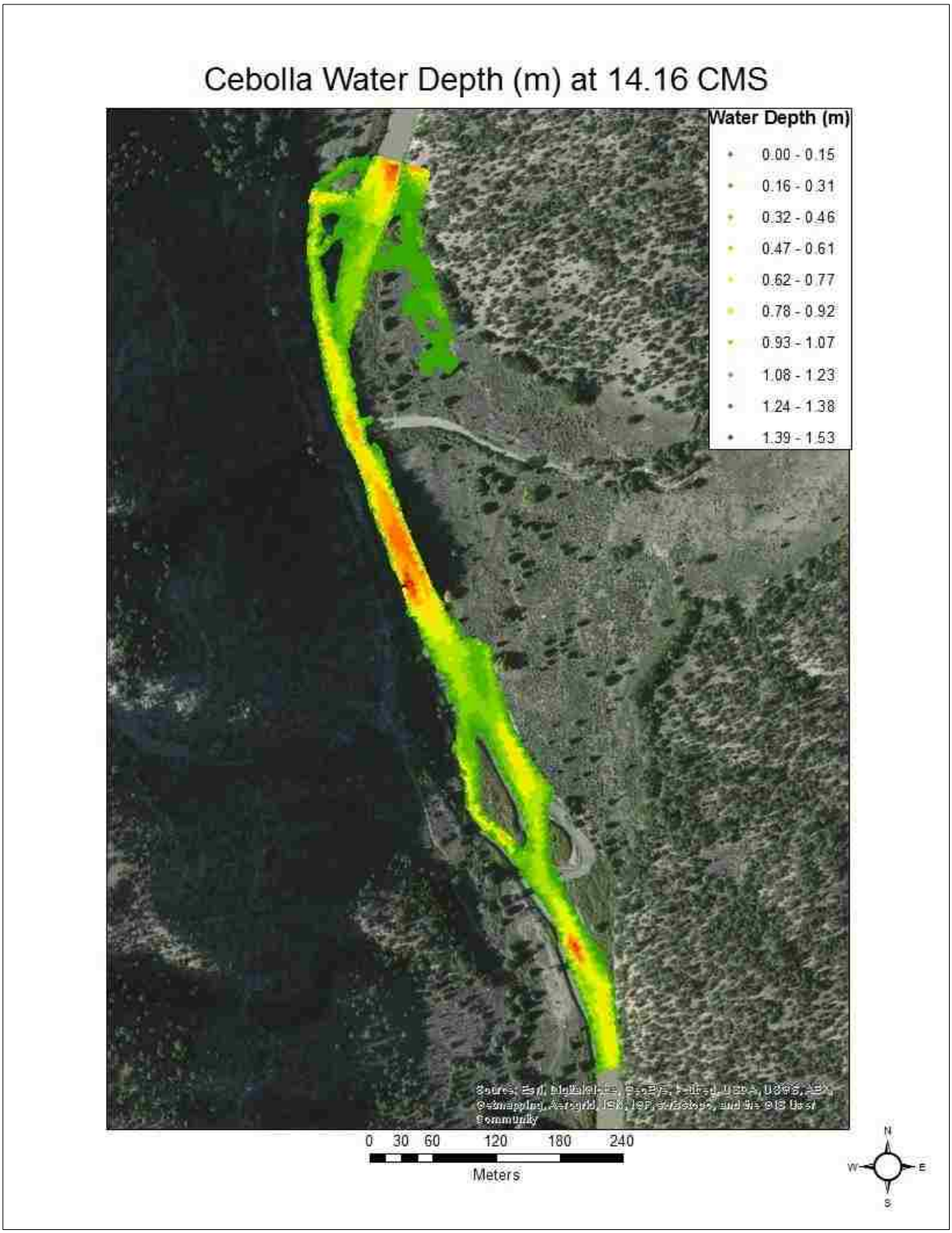

Figure 46: Cebolla Water Depth at 14 m^3/s

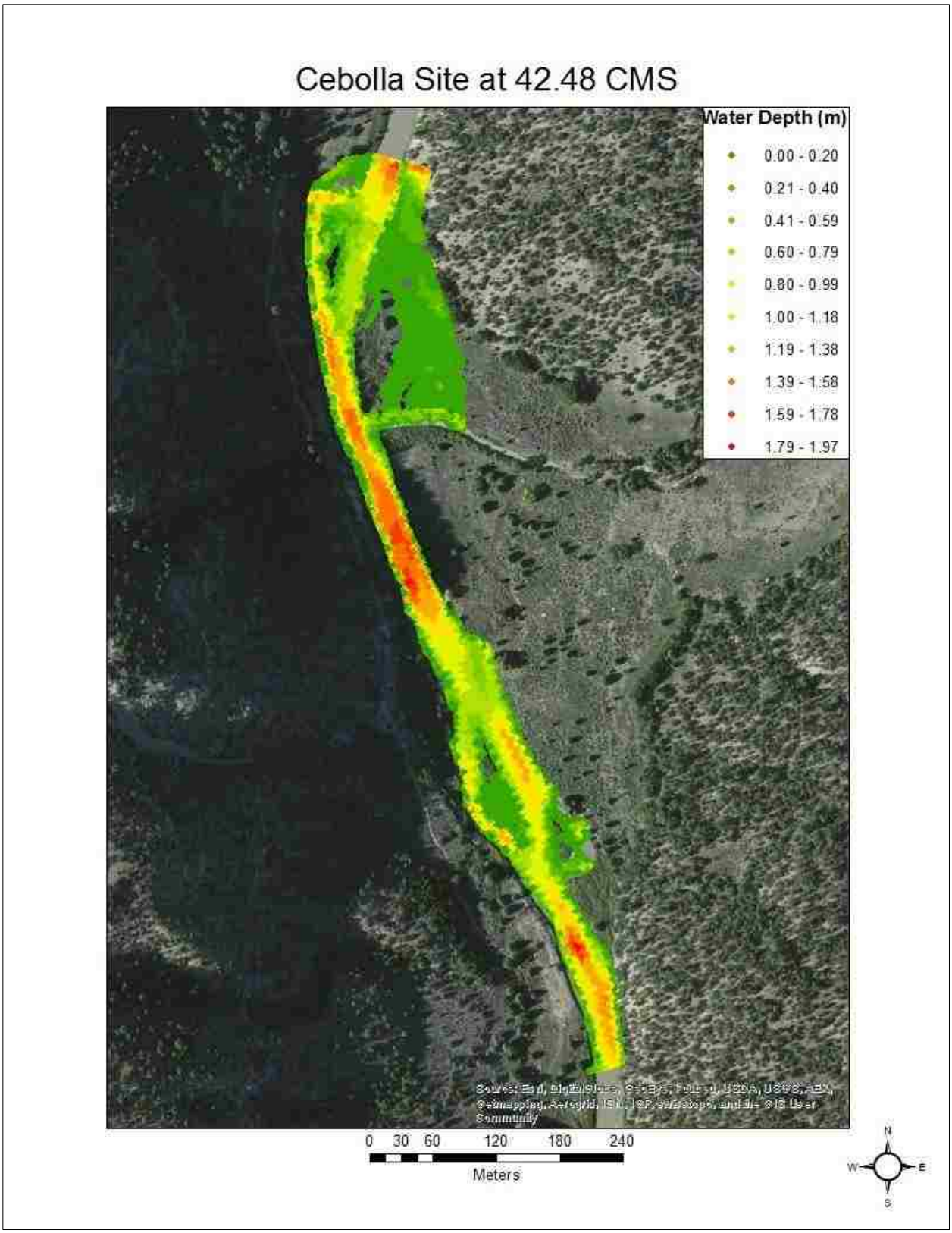

Figure 47: Cebolla Water Depth at 42 m^3/s

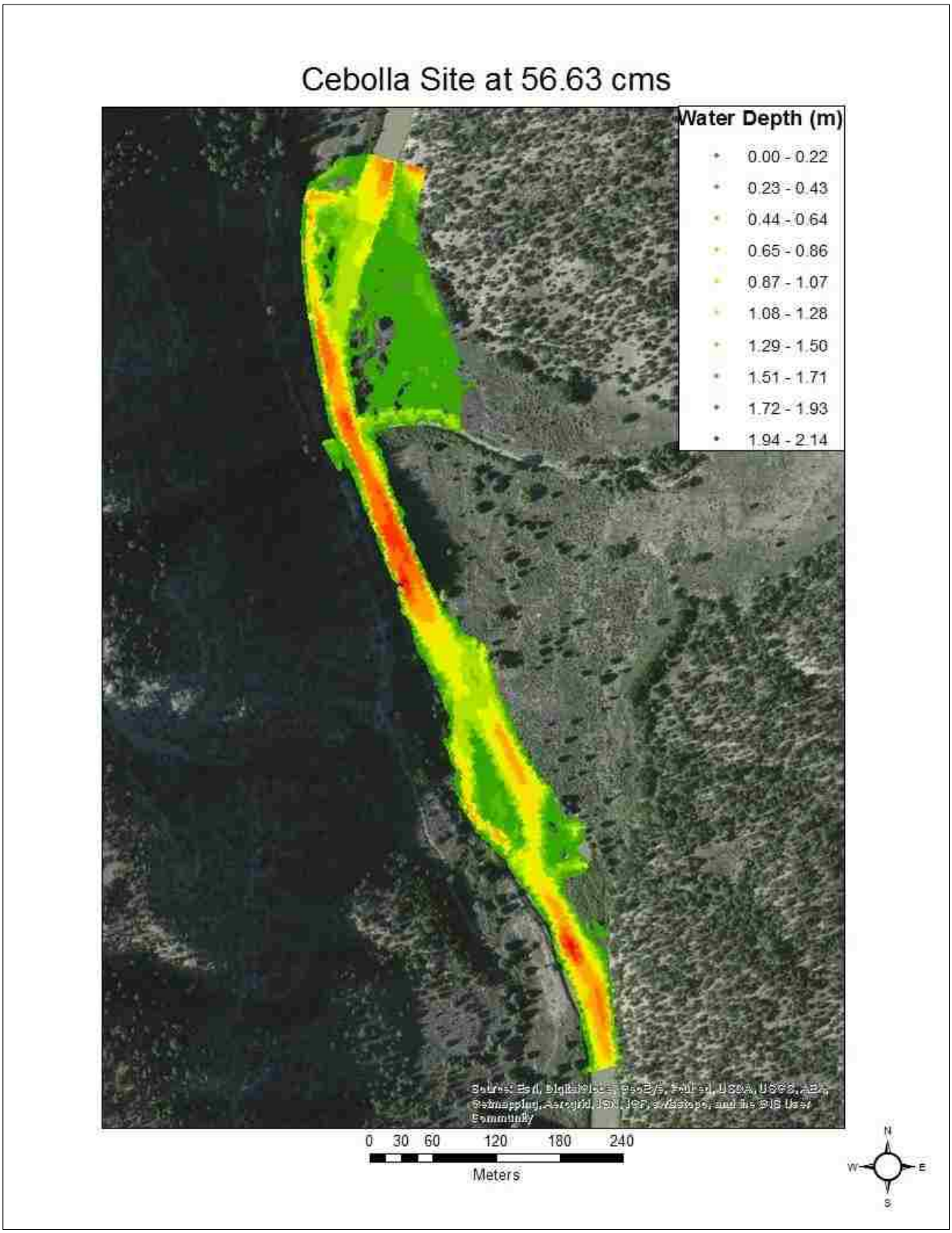

Figure 48: Cebolla Water Depth at 57 m³/s

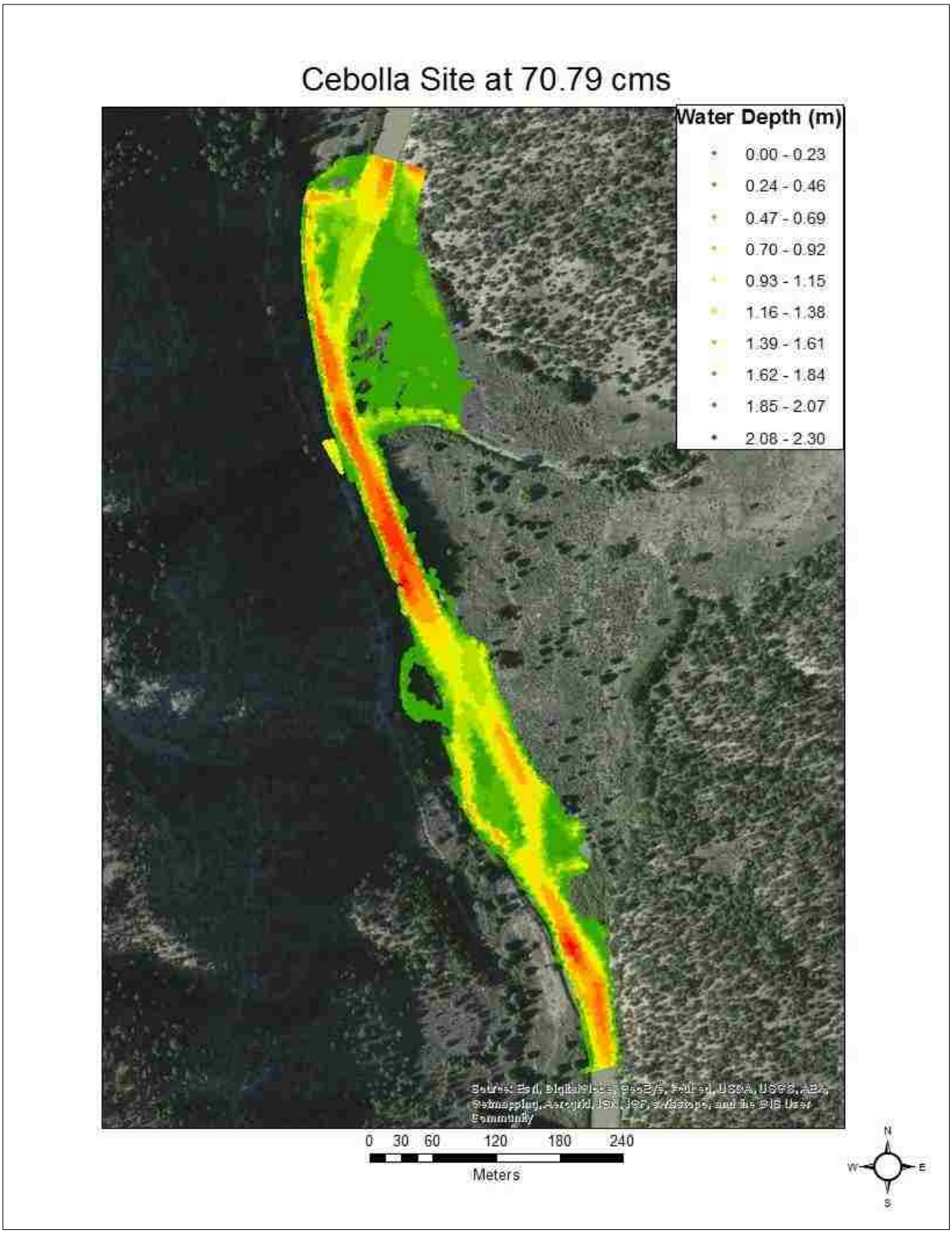

Figure 49: Cebolla Water Depth at 71 m³/s

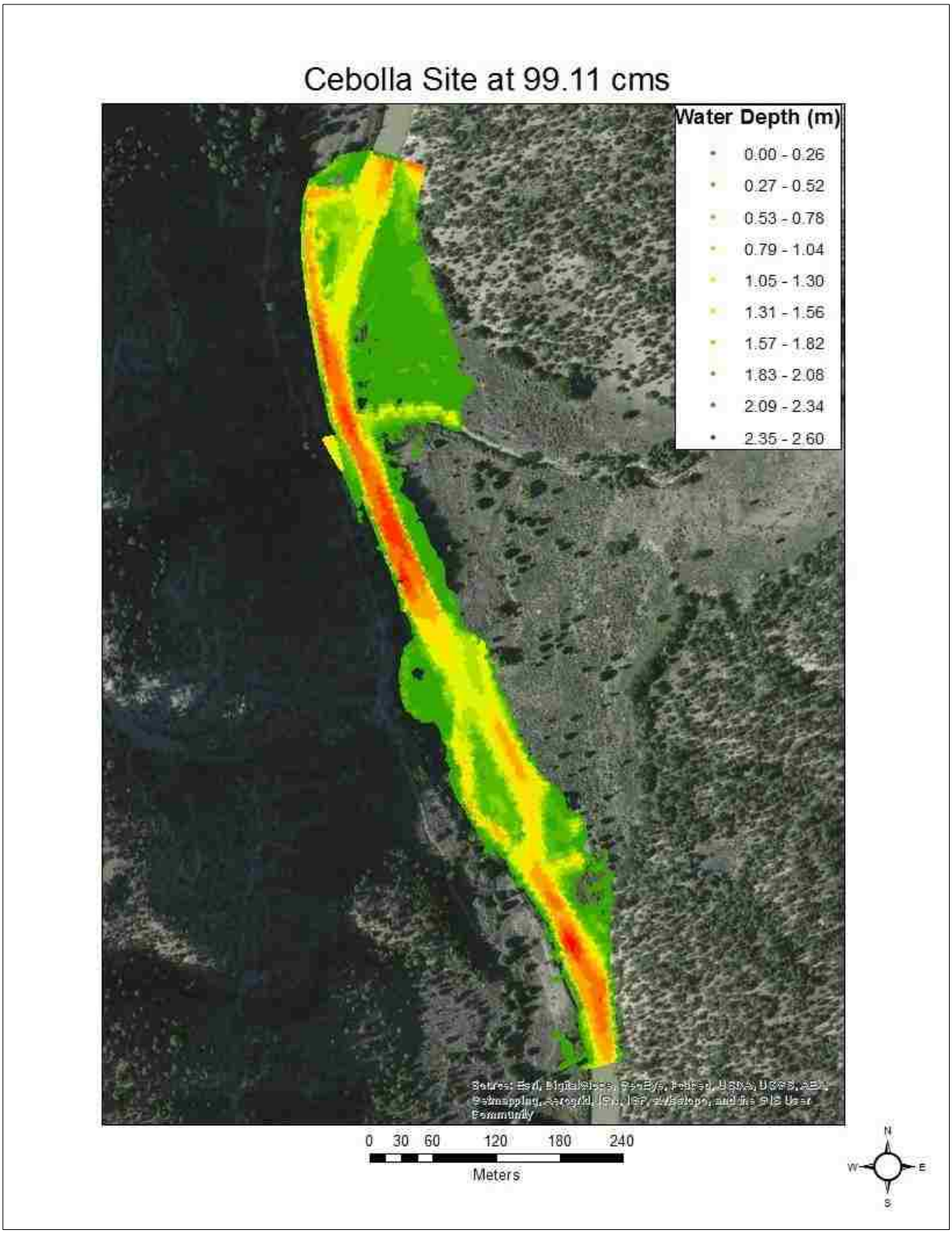

Figure 50: Cebolla Water Depth at 99 m^3/s

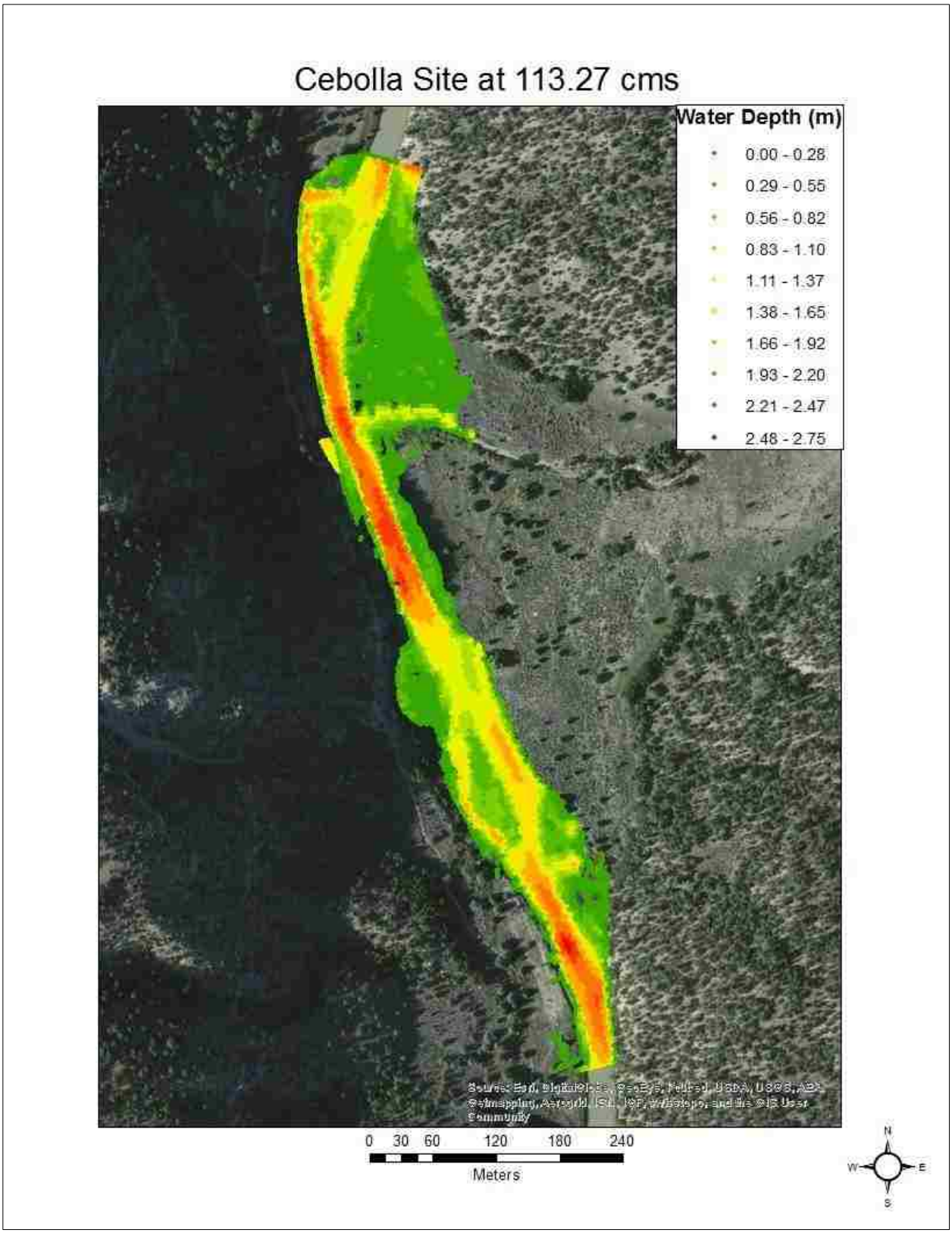

Figure 51: Cebolla Water Depth at 113 m³/s

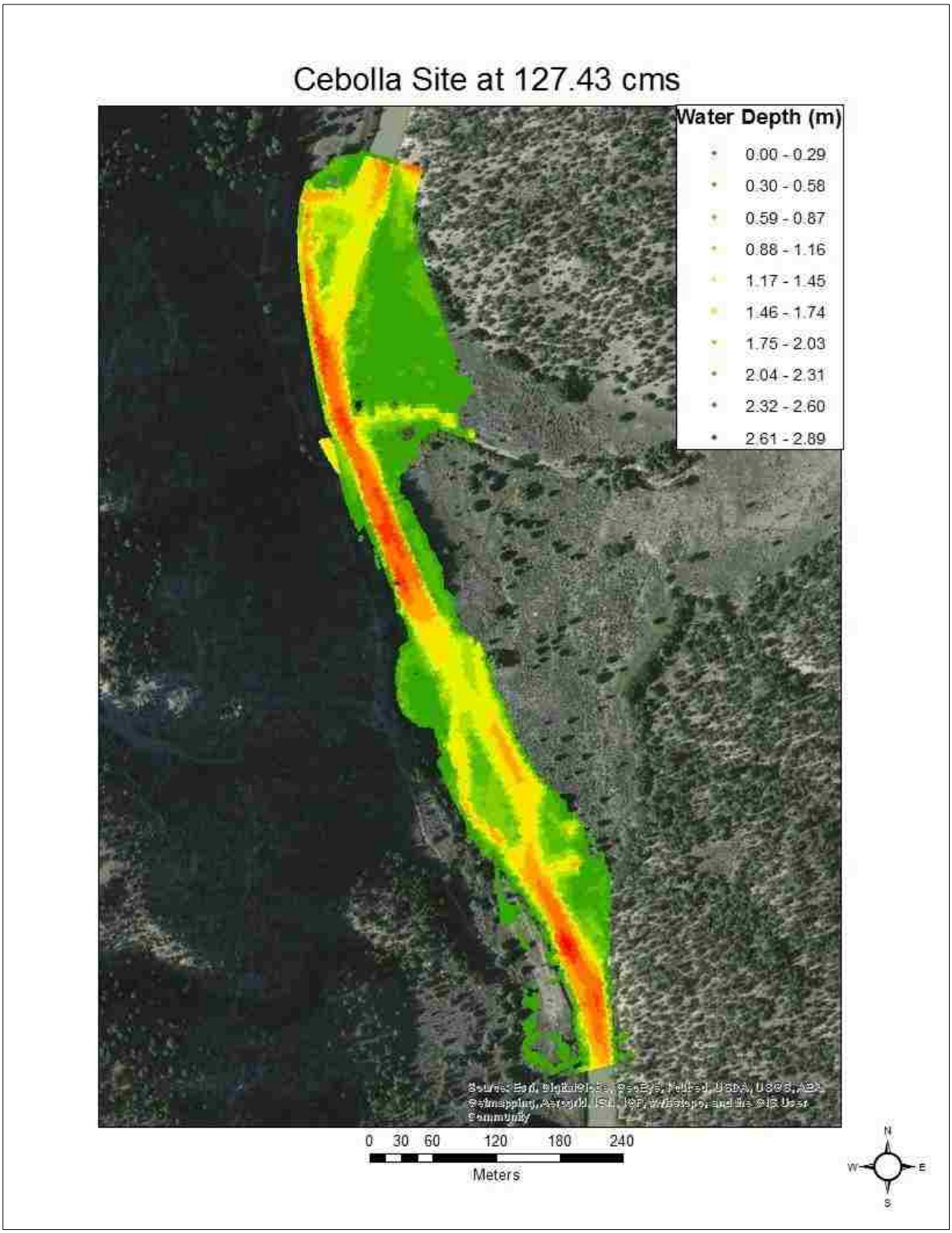

Figure 52: Cebolla Water Depth at 127 m³/s

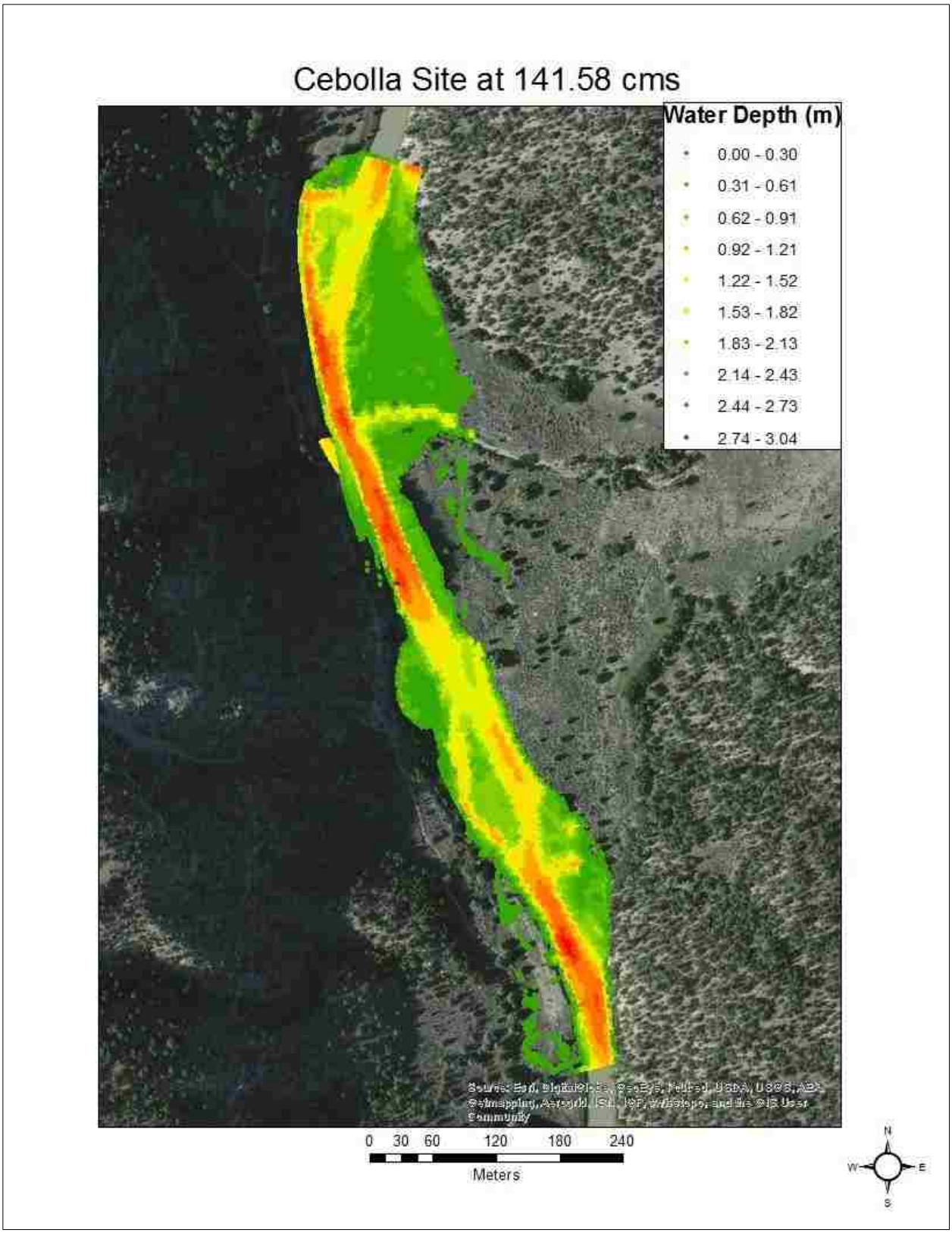

Figure 53: Cebolla Water Depth at 142 m³/s

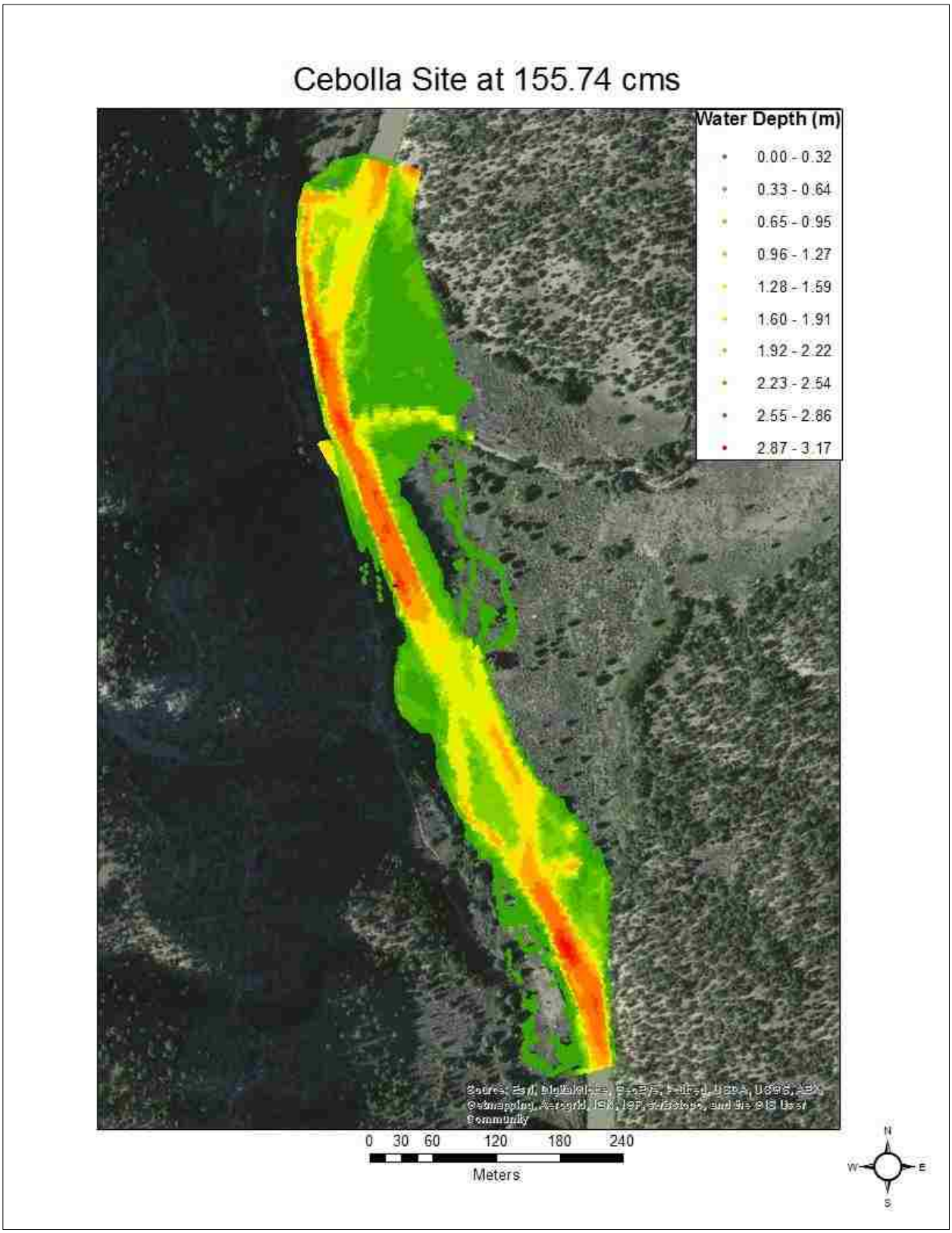

Figure 54: Cebolla Water Depth at 156 m³/s

Appendix H: Flow Results, Floodplain *n*=0.060

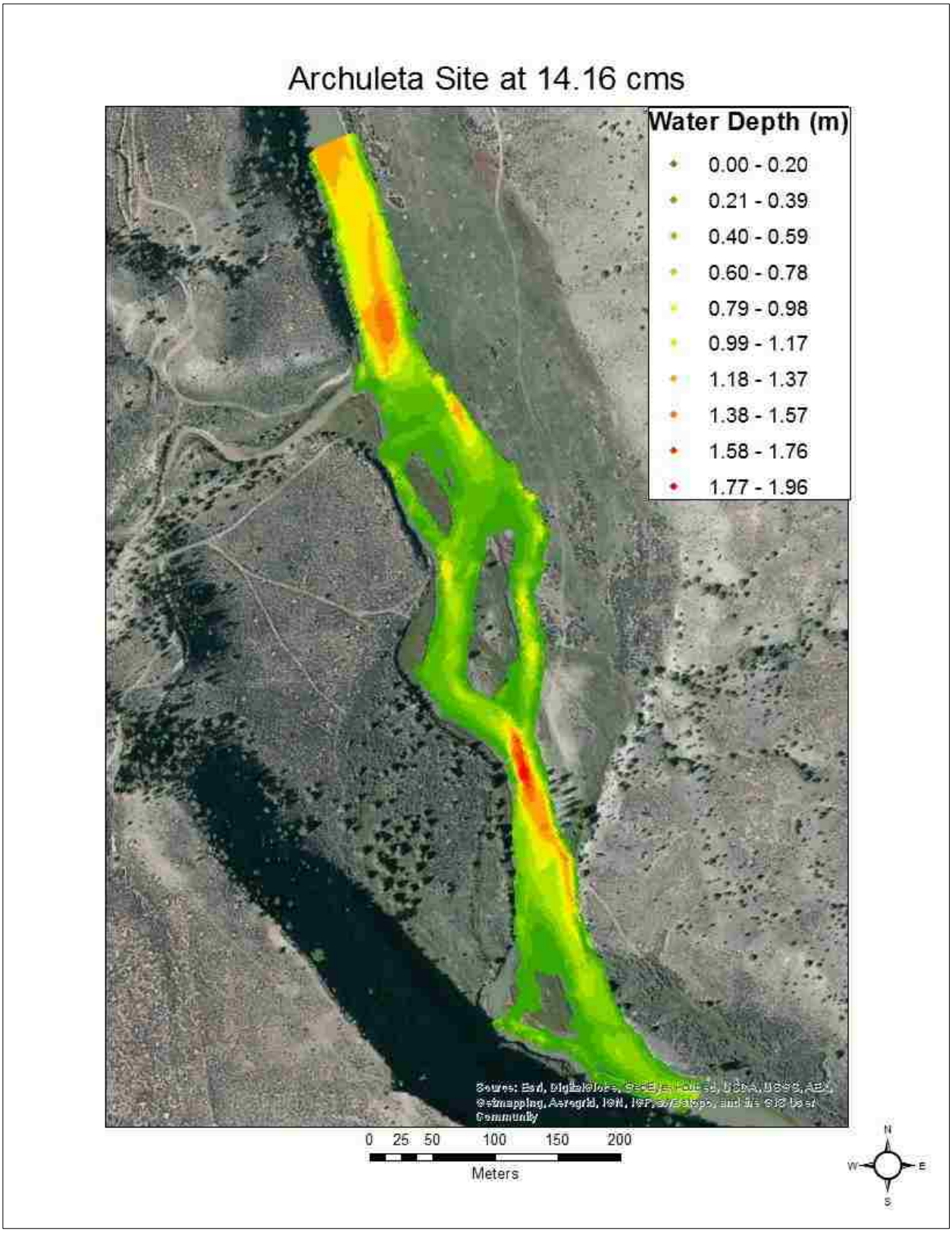

Figure 55: Archuleta Water Depth at 14 m³/s, floodplain *n*=0.060

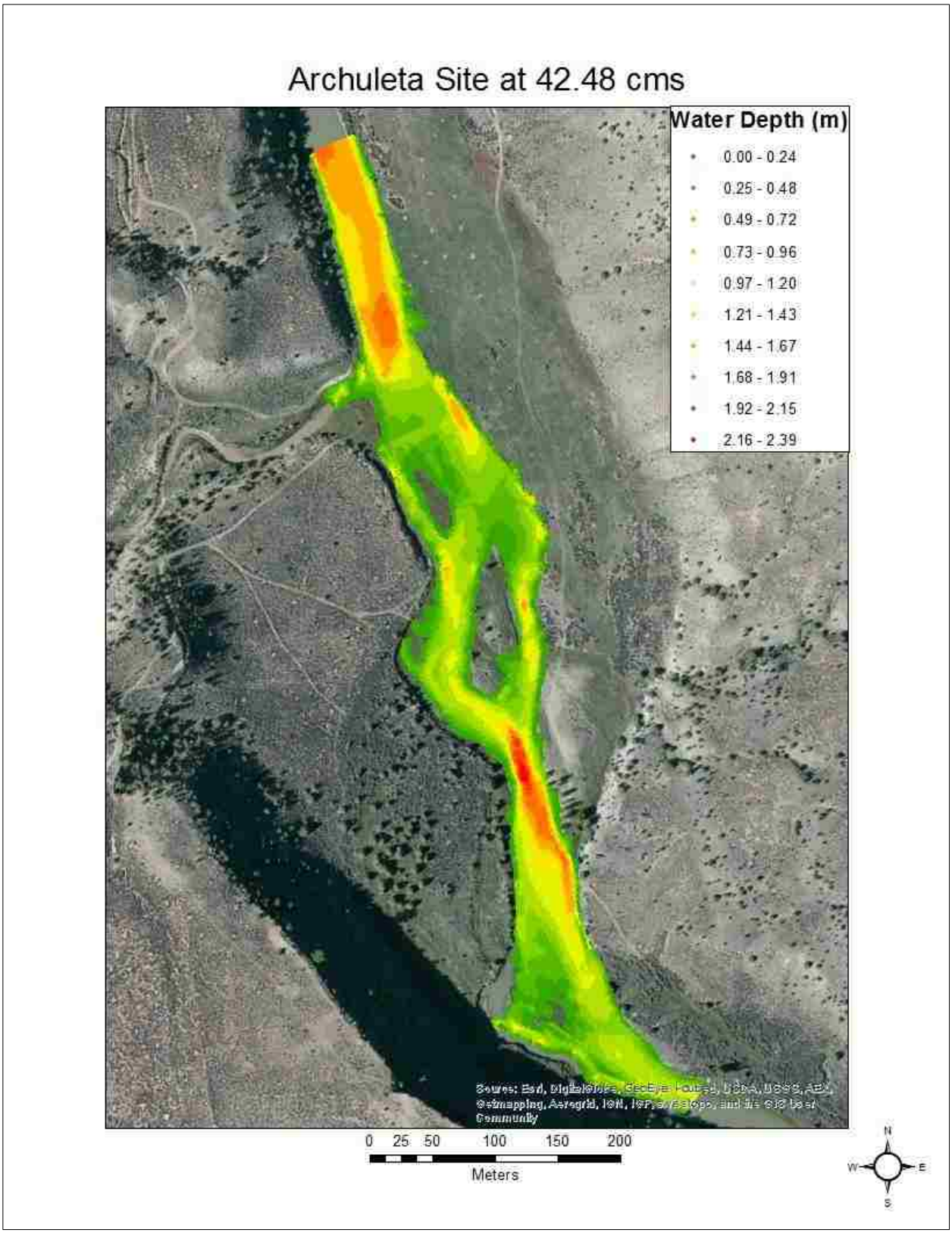

Figure 56: Archuleta Water Depth at 43 m³/s, floodplain *n*=0.060

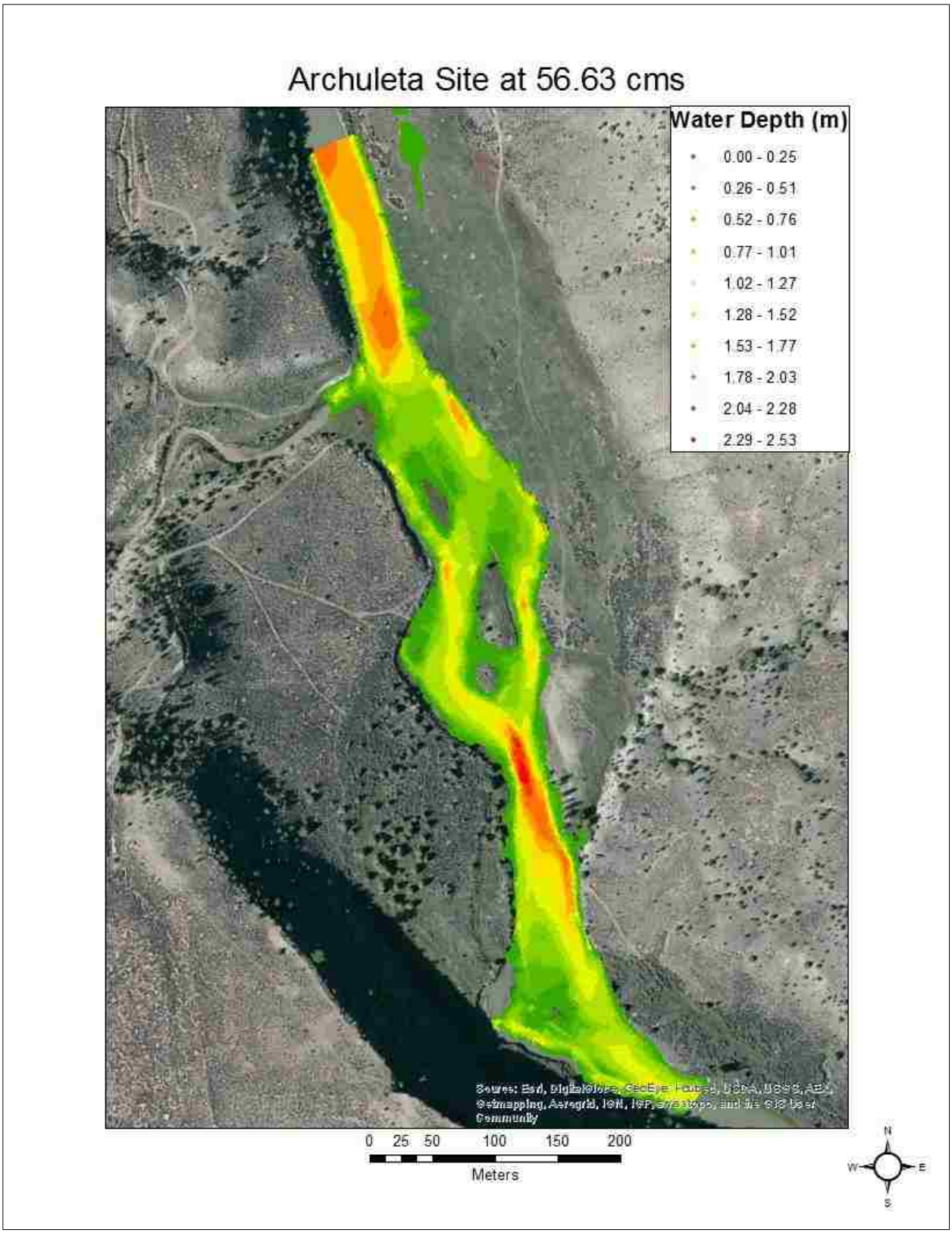

Figure 57: Archuleta Water Depth at 57 m³/s, floodplain *n*=0.060

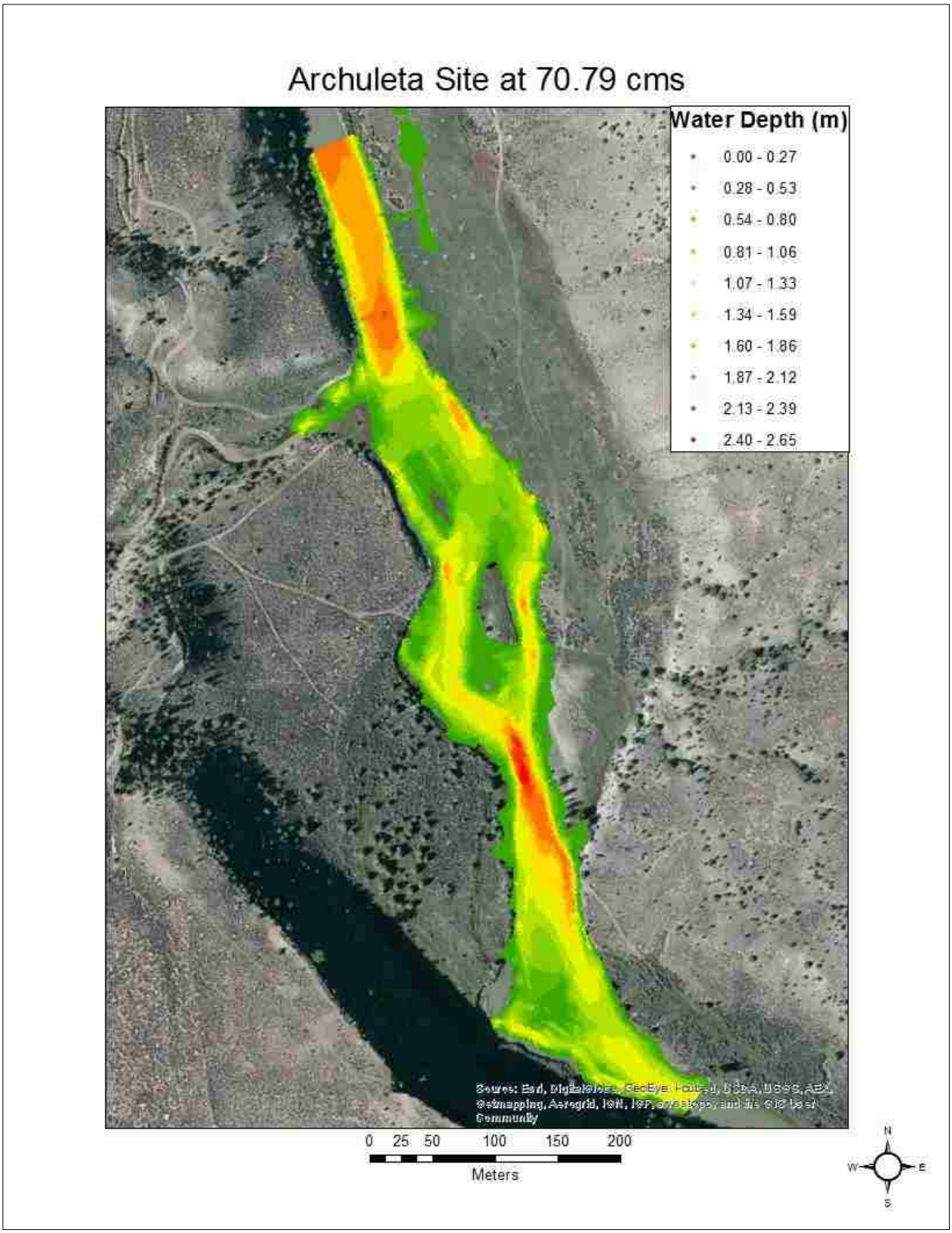

Figure 58: Archuleta Water Depth at 71 m³/s, floodplain *n*=0.060

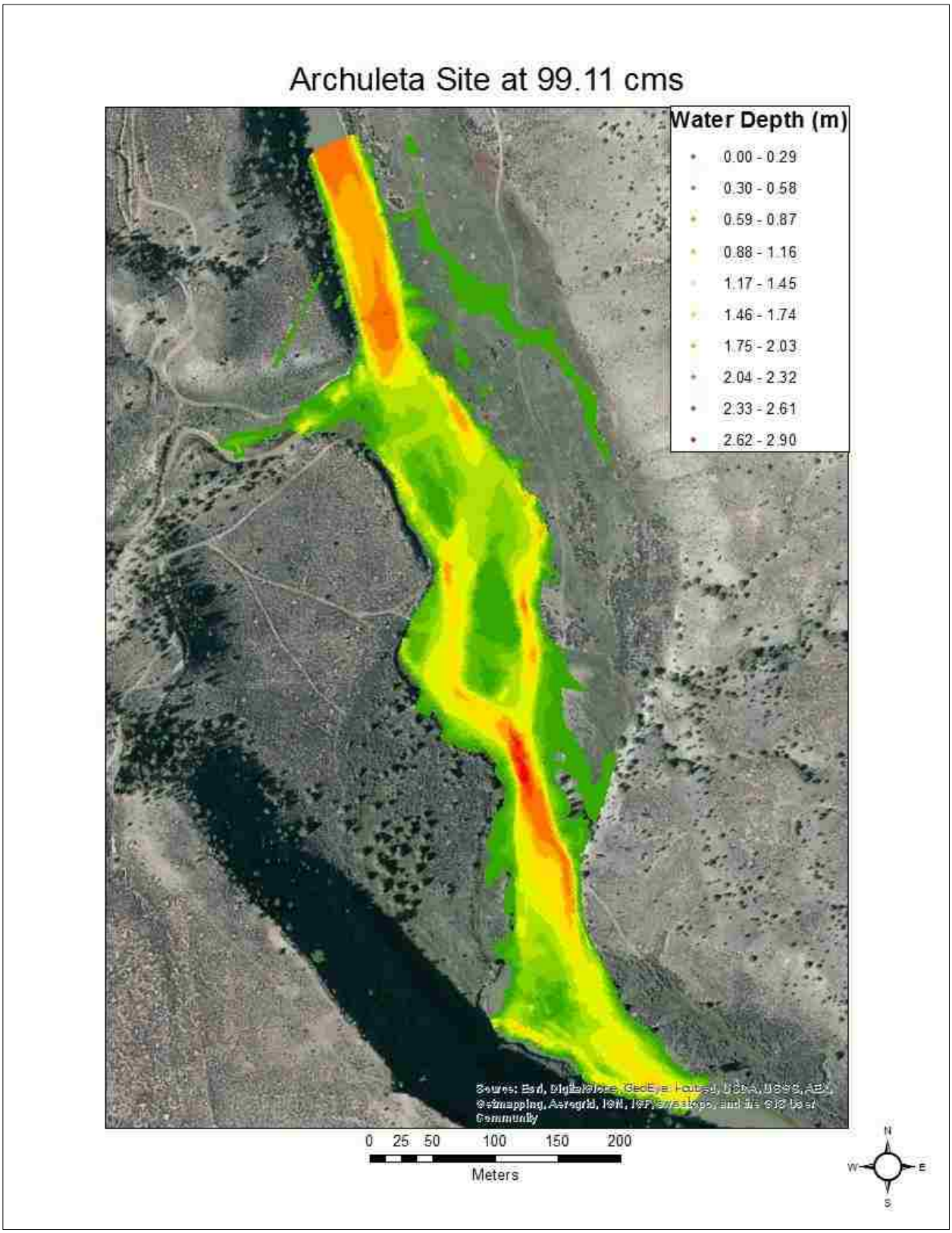

Figure 59: Archuleta Water Depth at 99 m³/s, floodplain *n*=0.060

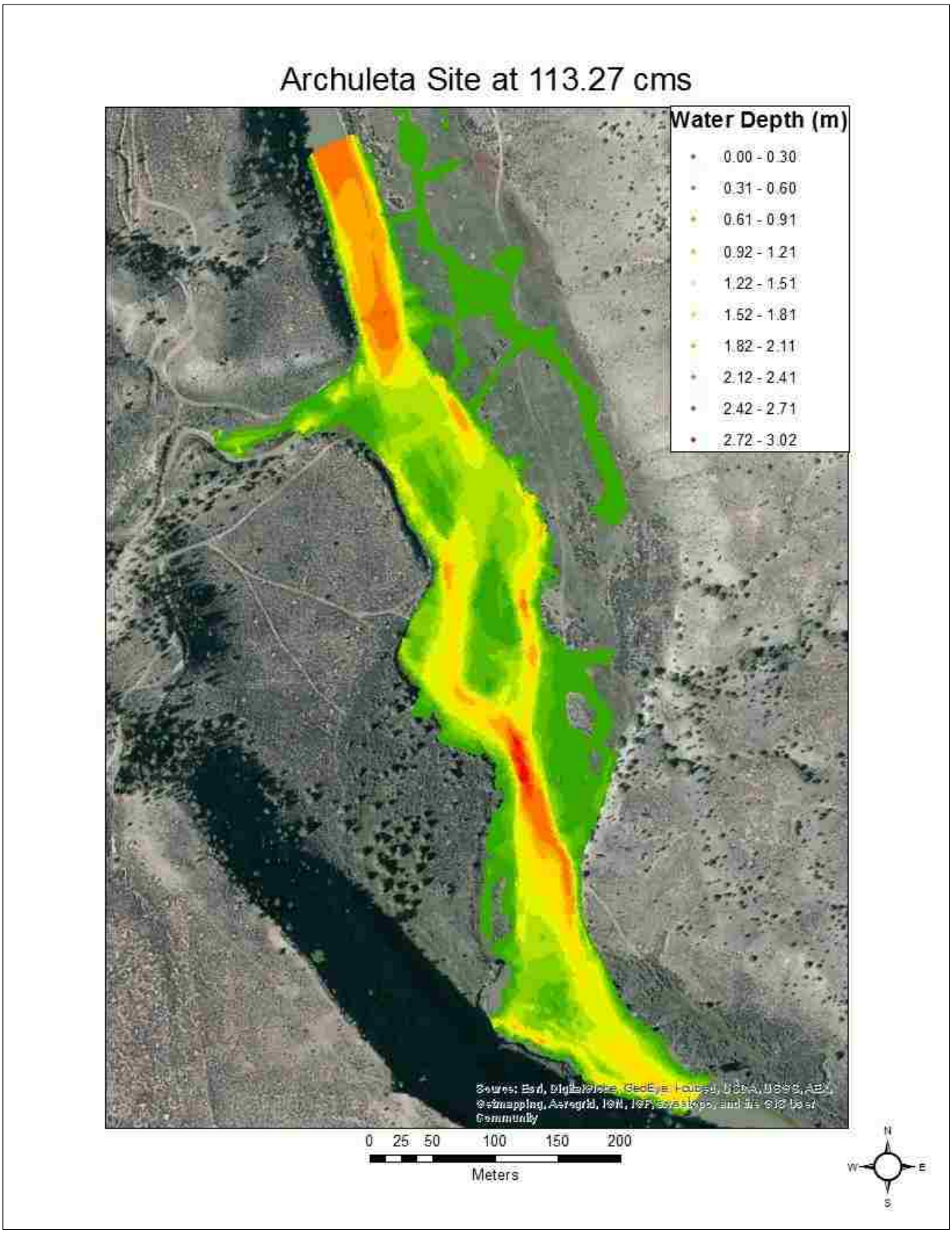

Figure 60: Archuleta Water Depth at 113 m³/s, floodplain *n*=0.060

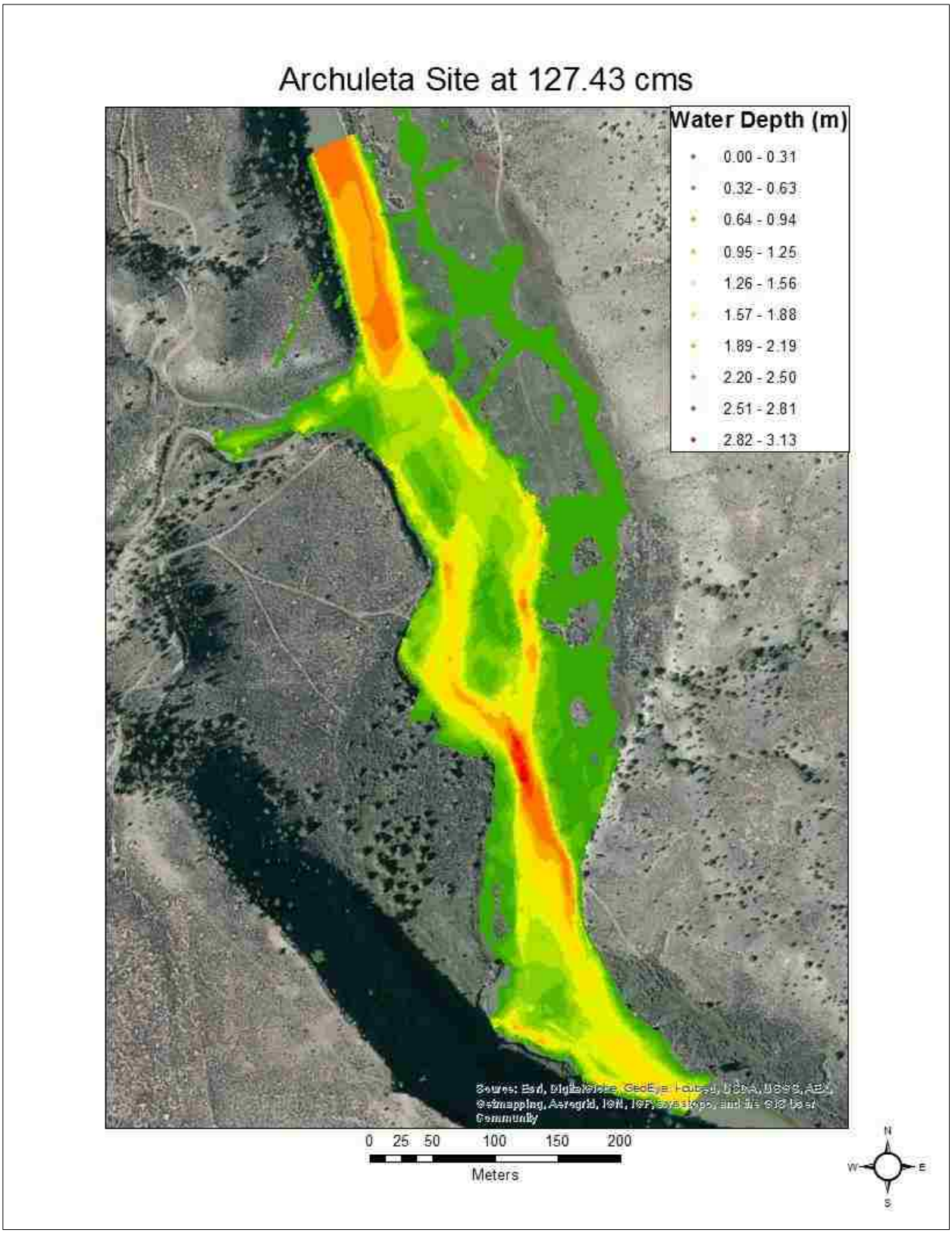

Figure 61: Archuleta Water Depth at 127 m³/s, floodplain *n*=0.060

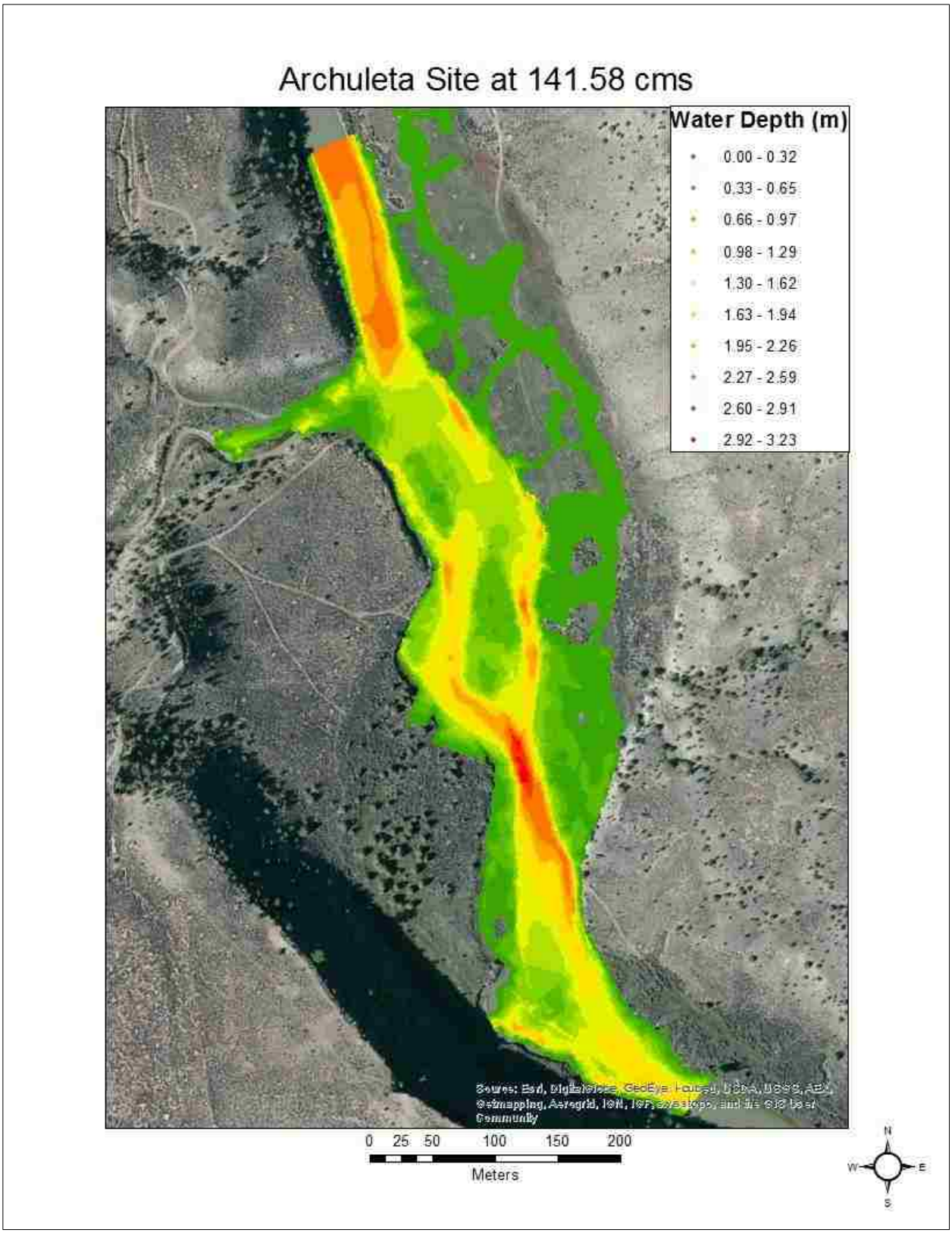

Figure 62: Archuleta Water Depth at 142 m³/s, floodplain *n*=0.060

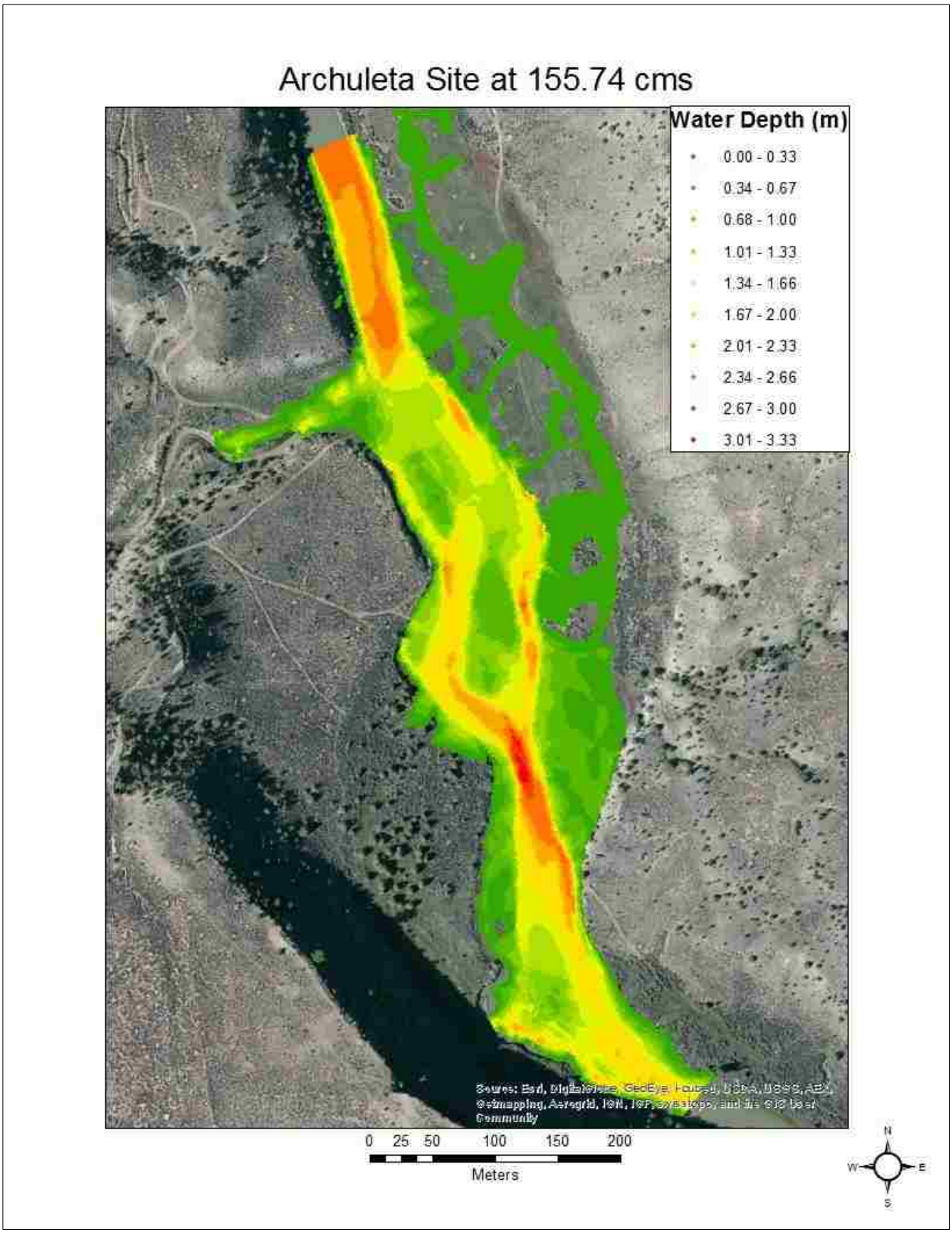

Figure 63: Archuleta Water Depth at 156 m³/s, floodplain *n*=0.060

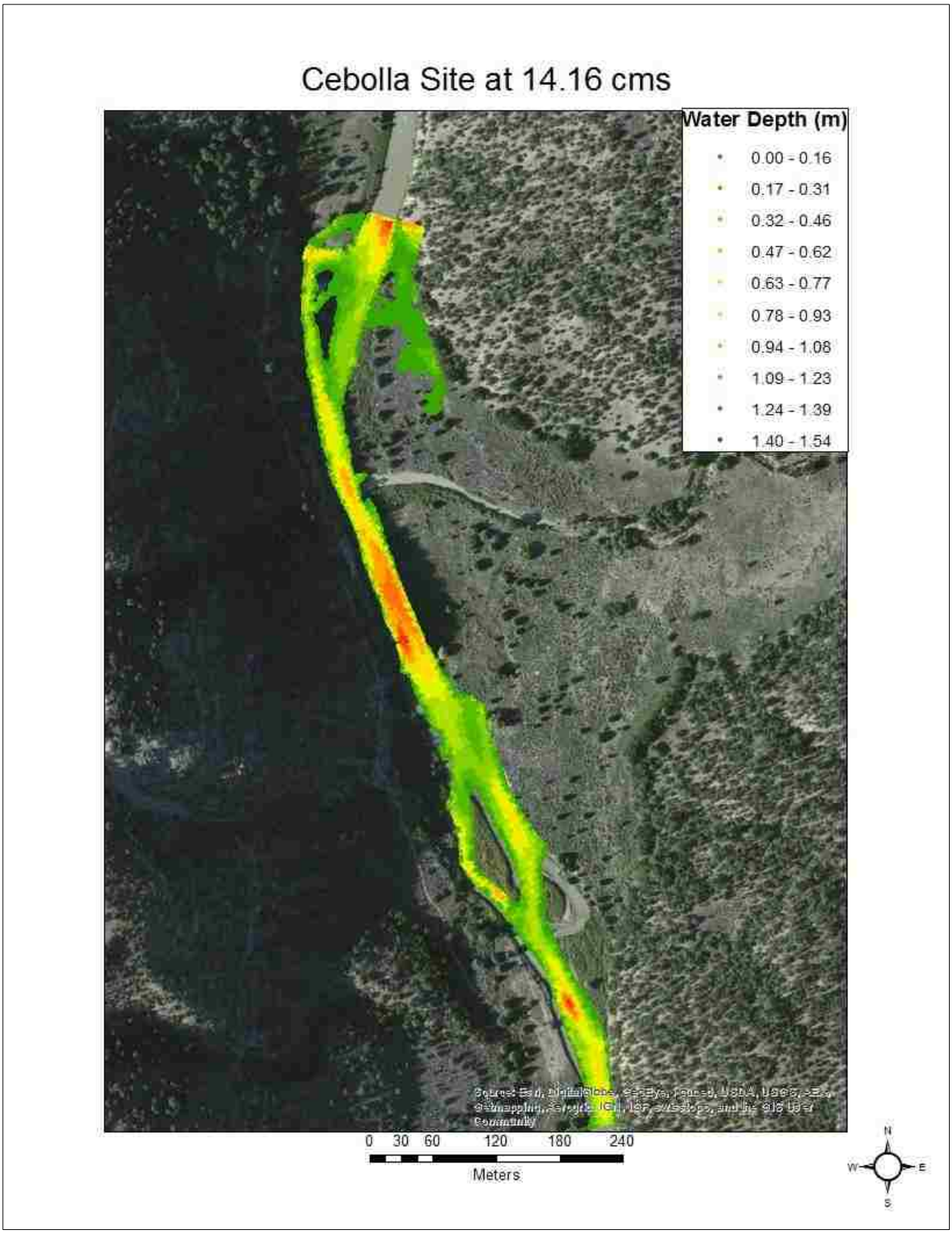

Figure 64: Cebolla Water Depth at 14 m³/s, floodplain *n*=0.060

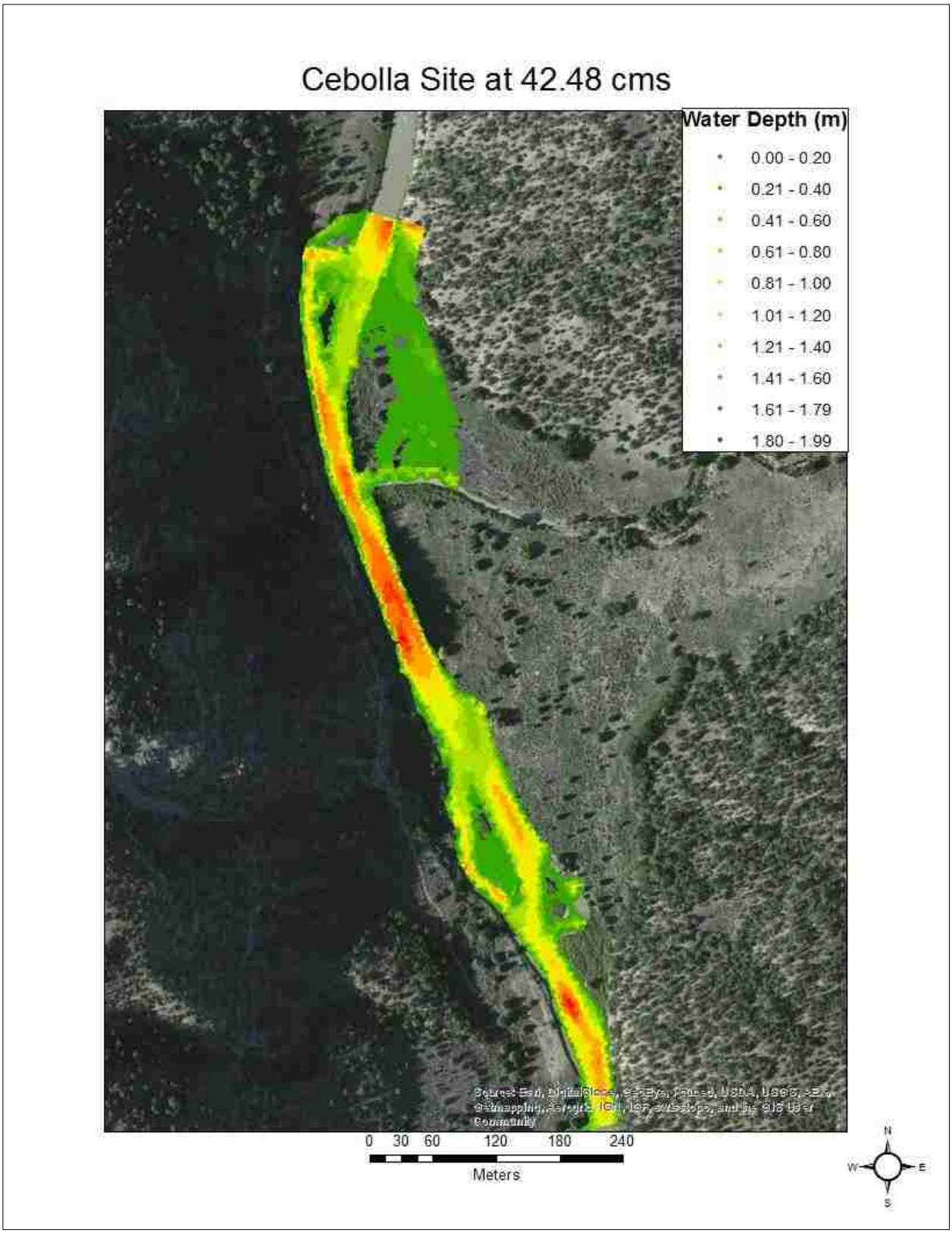

Figure 65: Cebolla Water Depth at 43 m³/s, floodplain *n*=0.060

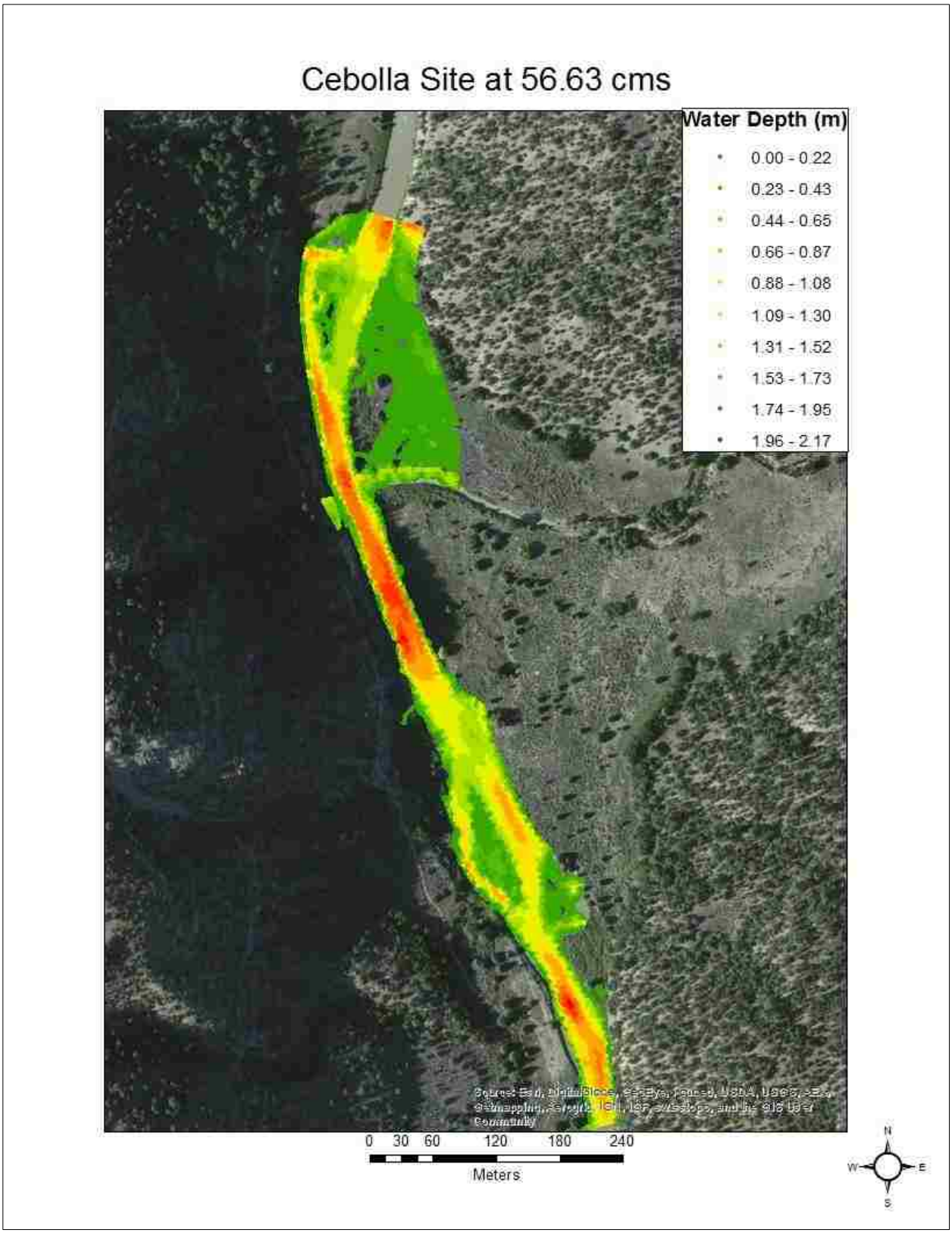

Figure 66: Cebolla Water Depth at 57 m^3/s, floodplain *n*=0.060

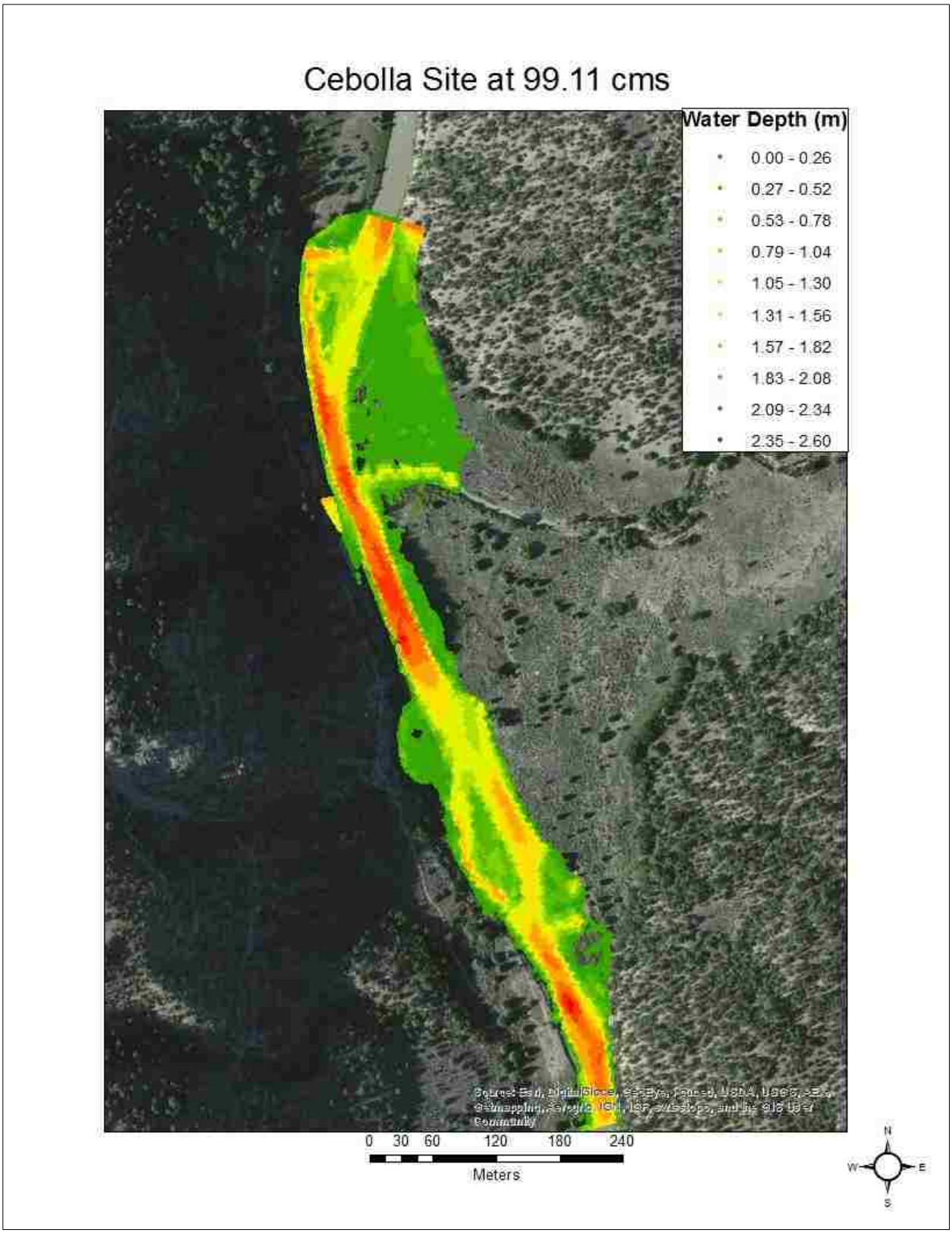

Figure 67: Cebolla Water Depth at 99 m³/s, floodplain *n*=0.060

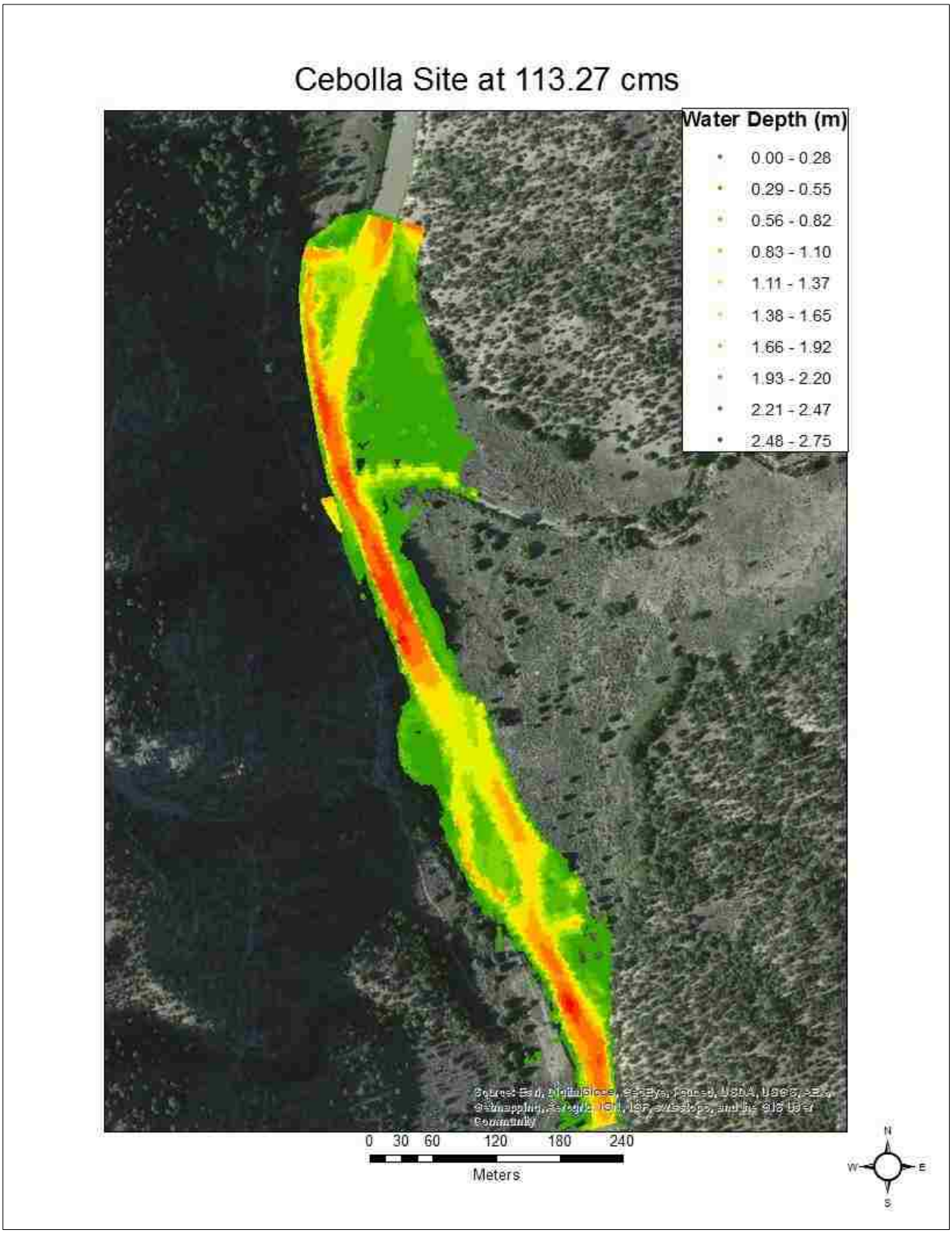

Figure 68: Cebolla Water Depth at 113 m³/s, floodplain *n*=0.060

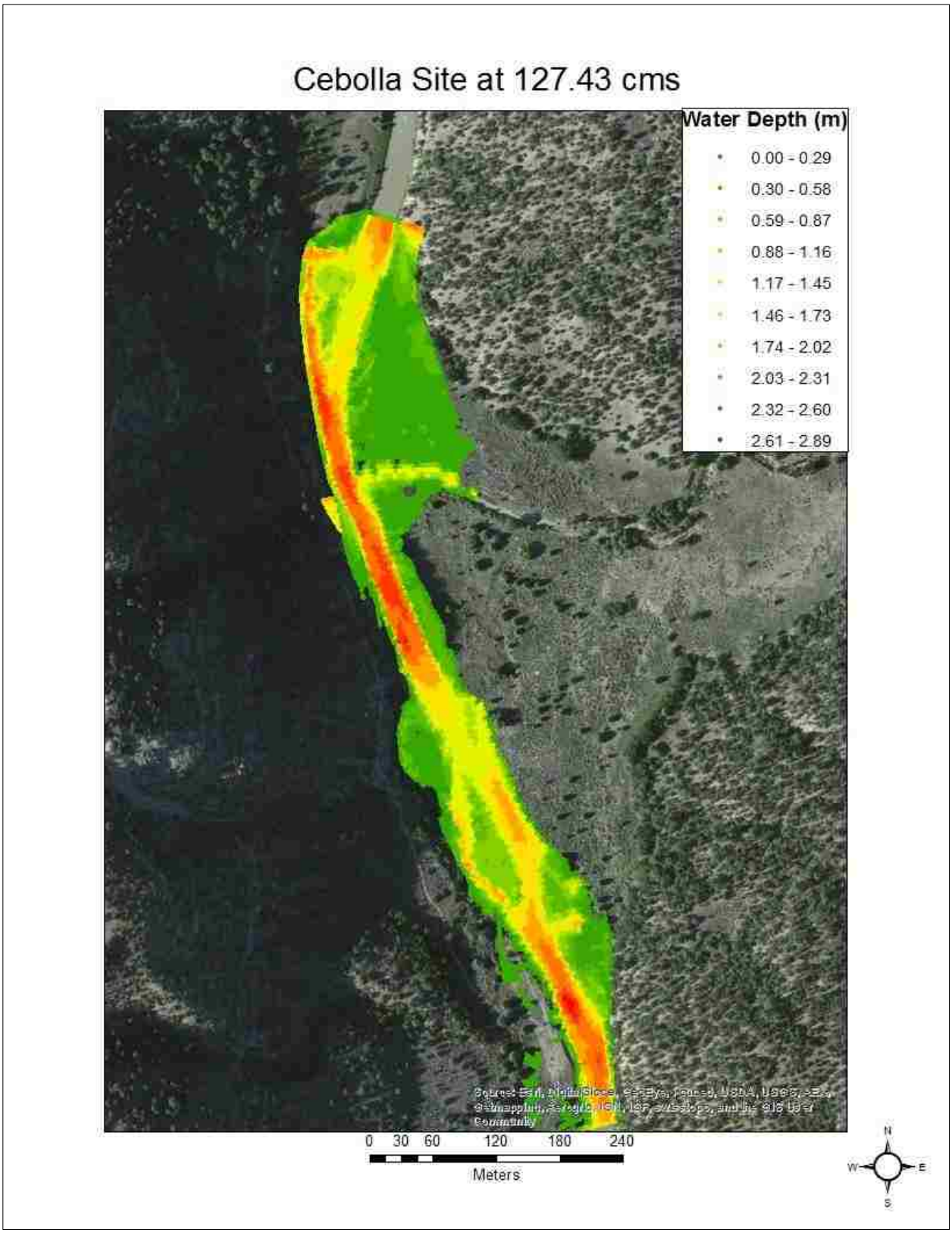

Figure 69: Cebolla Water Depth at 127 m³/s, floodplain *n*=0.060

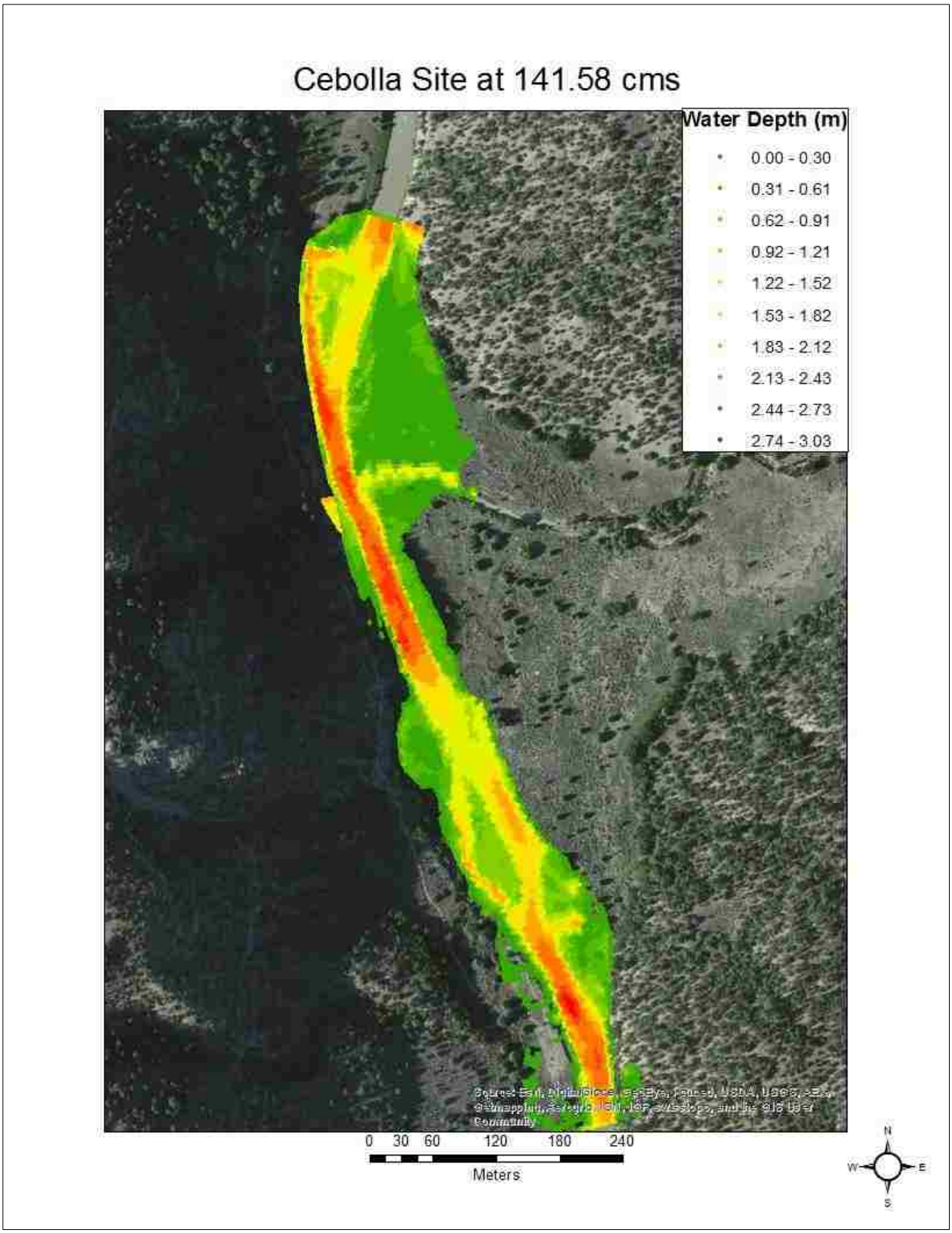

Figure 70: Cebolla Water Depth at 142 m³/s, floodplain *n*=0.060

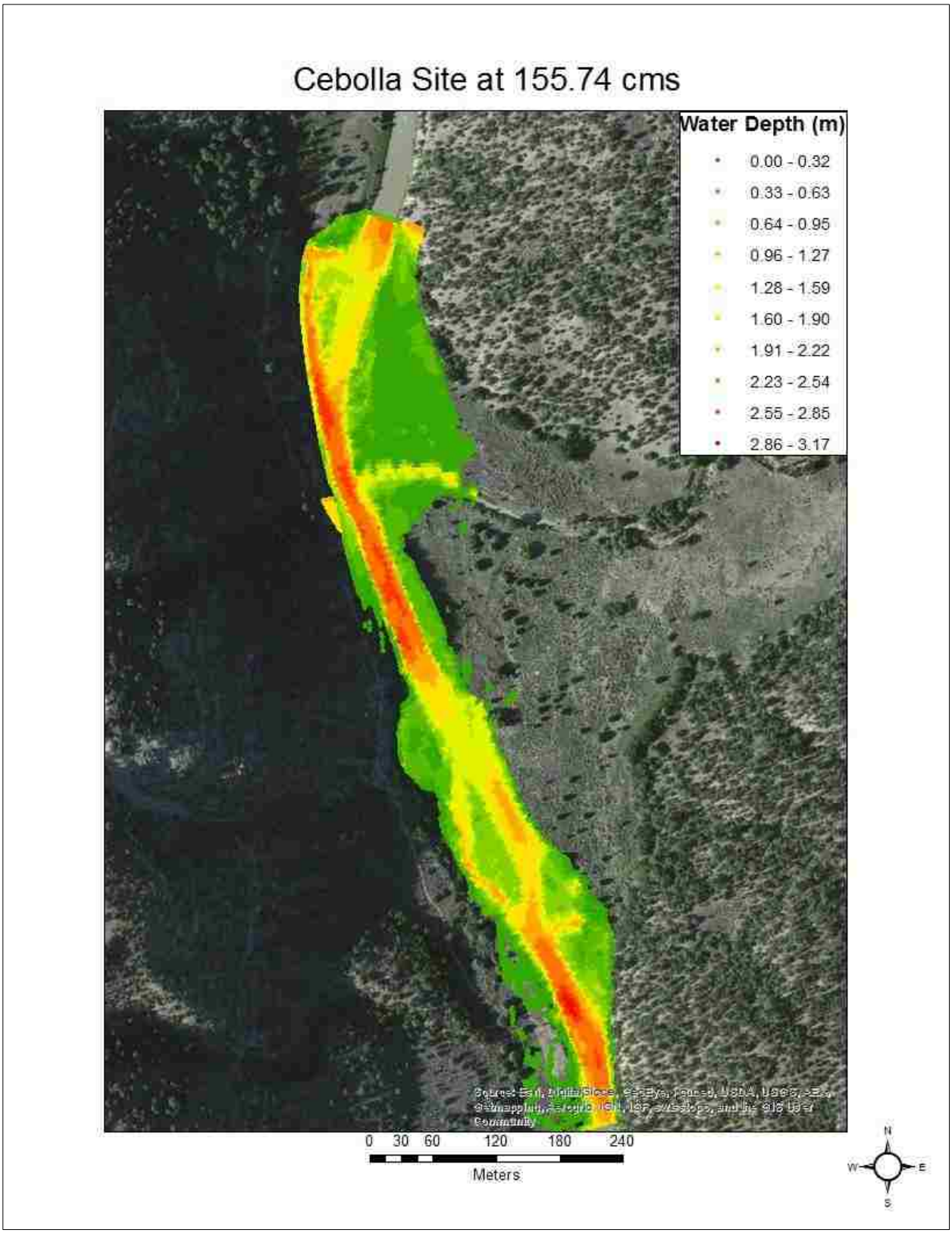

Figure 71: Cebolla Water Depth at 156 m³/s, floodplain *n*=0.060

Appendix I: Velocity Profiles

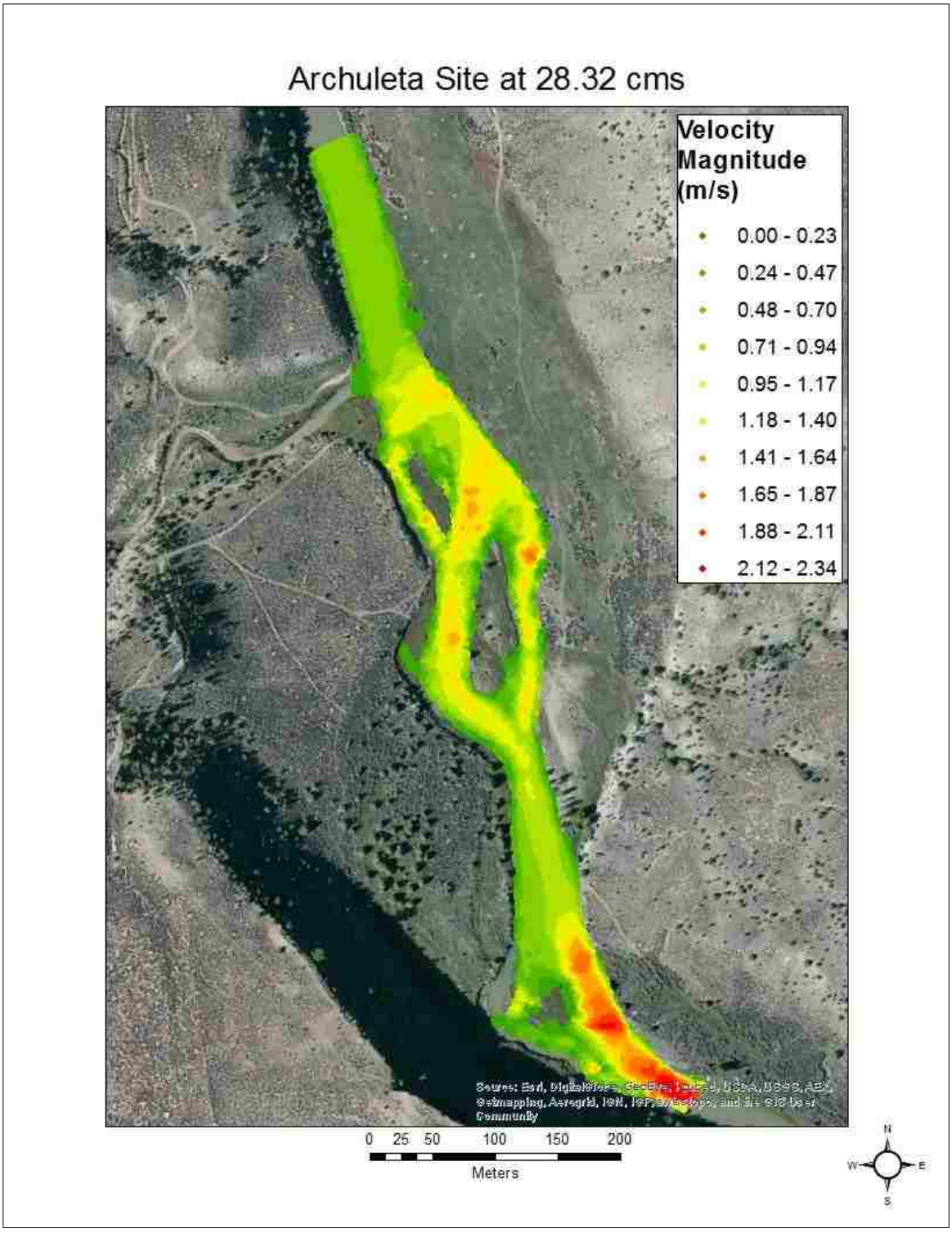

Figure 72: Archuleta Velocity Plan View at 28 m^3/s, floodplain *n*=0.060

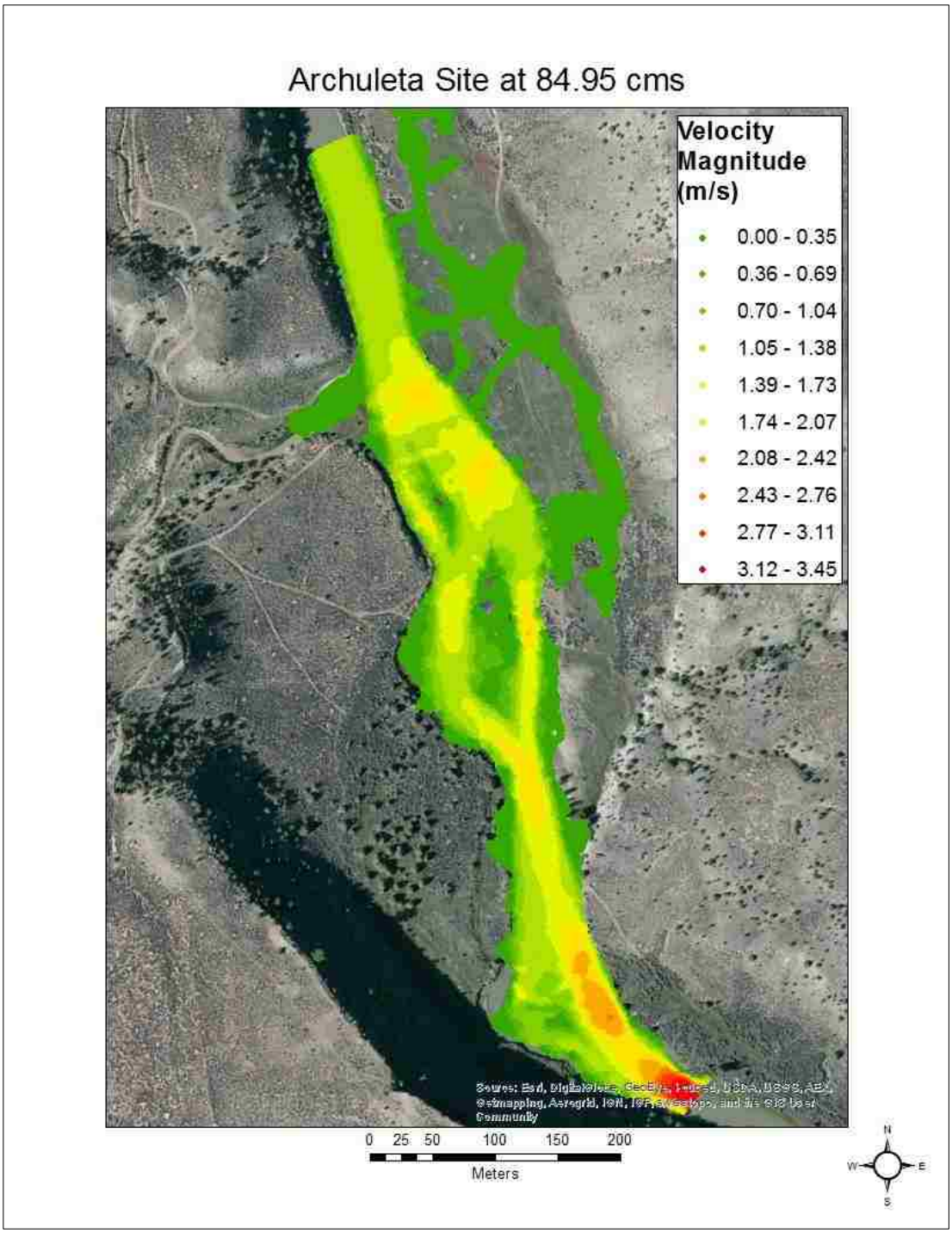

Figure 73: Archuleta Velocity Plan View at 85 m^3/s, floodplain *n*=0.060

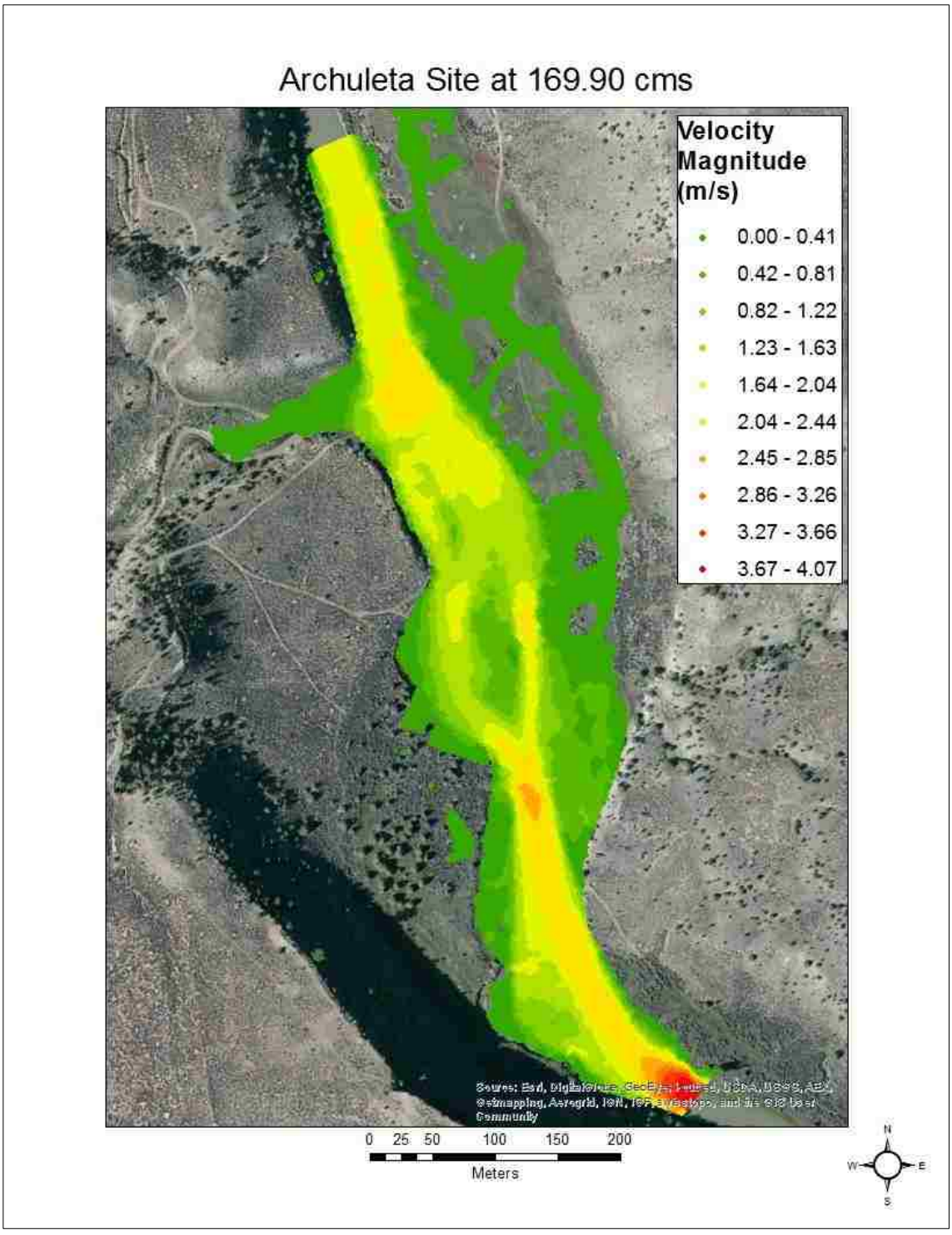

Figure 74: Archuleta Velocity Plan View at 170 m^3/s, floodplain *n*=0.060

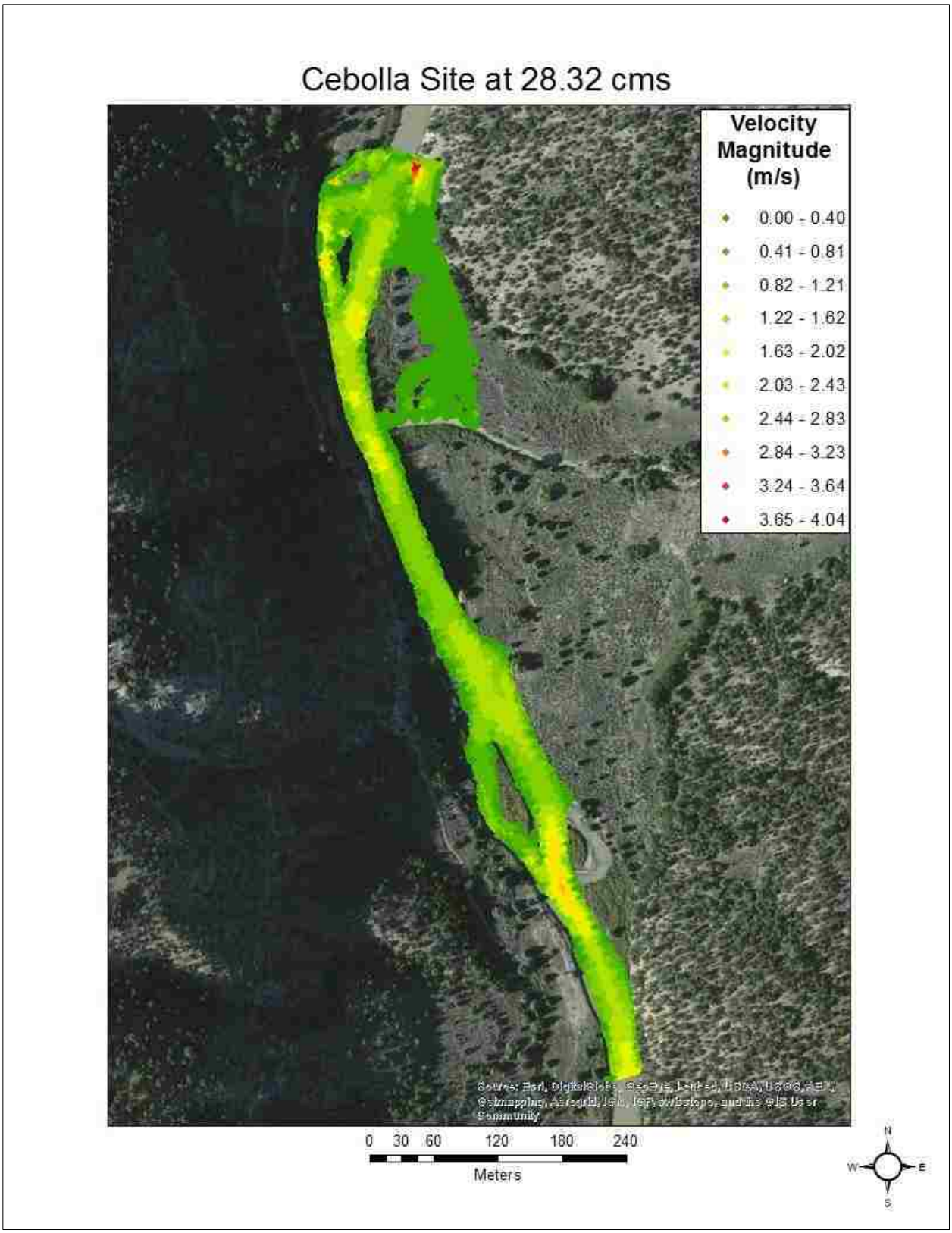

Figure 75: Cebolla Velocity Plan View at 28 m³/s, floodplain *n*=0.060

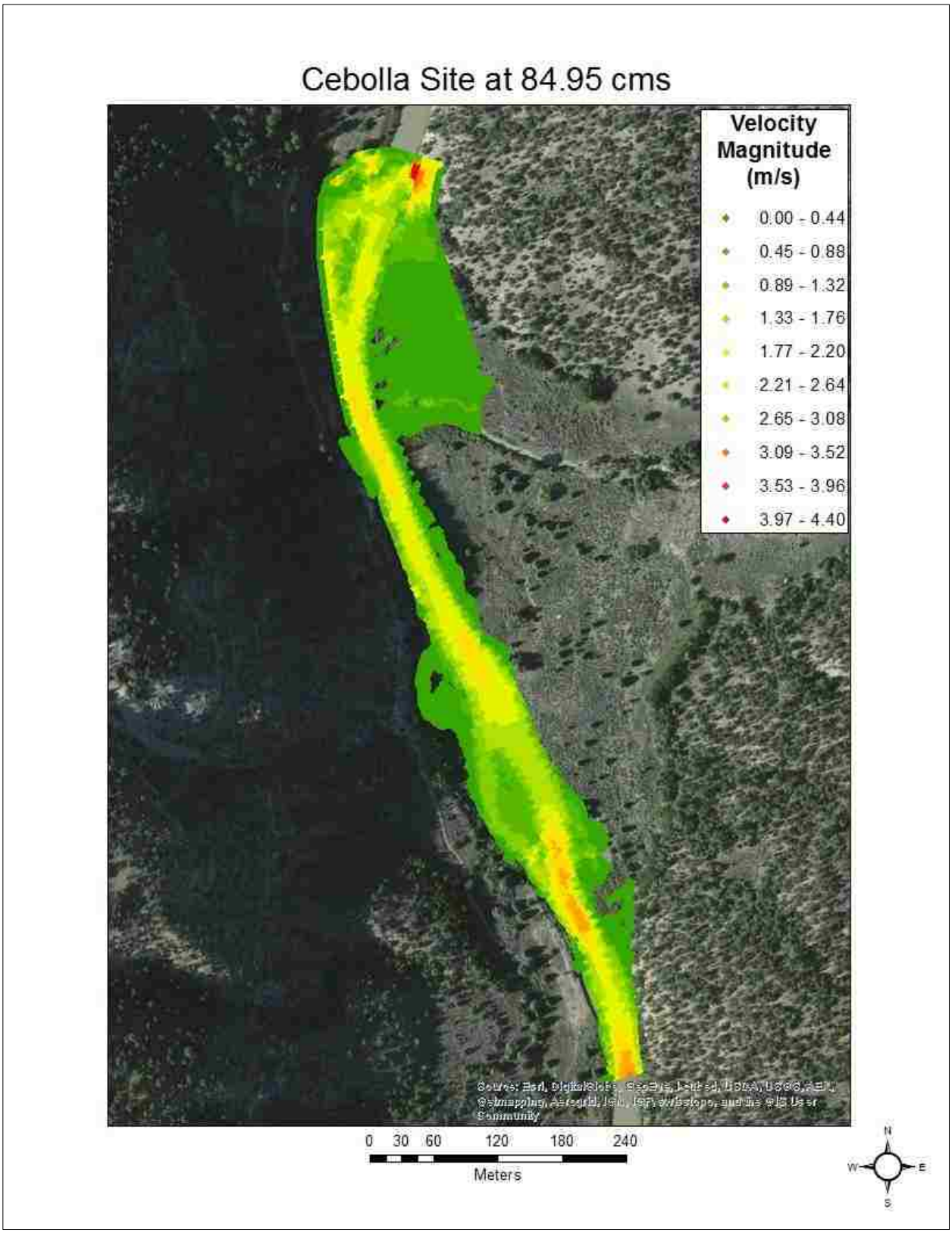

Figure 76: Cebolla Velocity Plan View at 85 m³/s, floodplain *n*=0.060

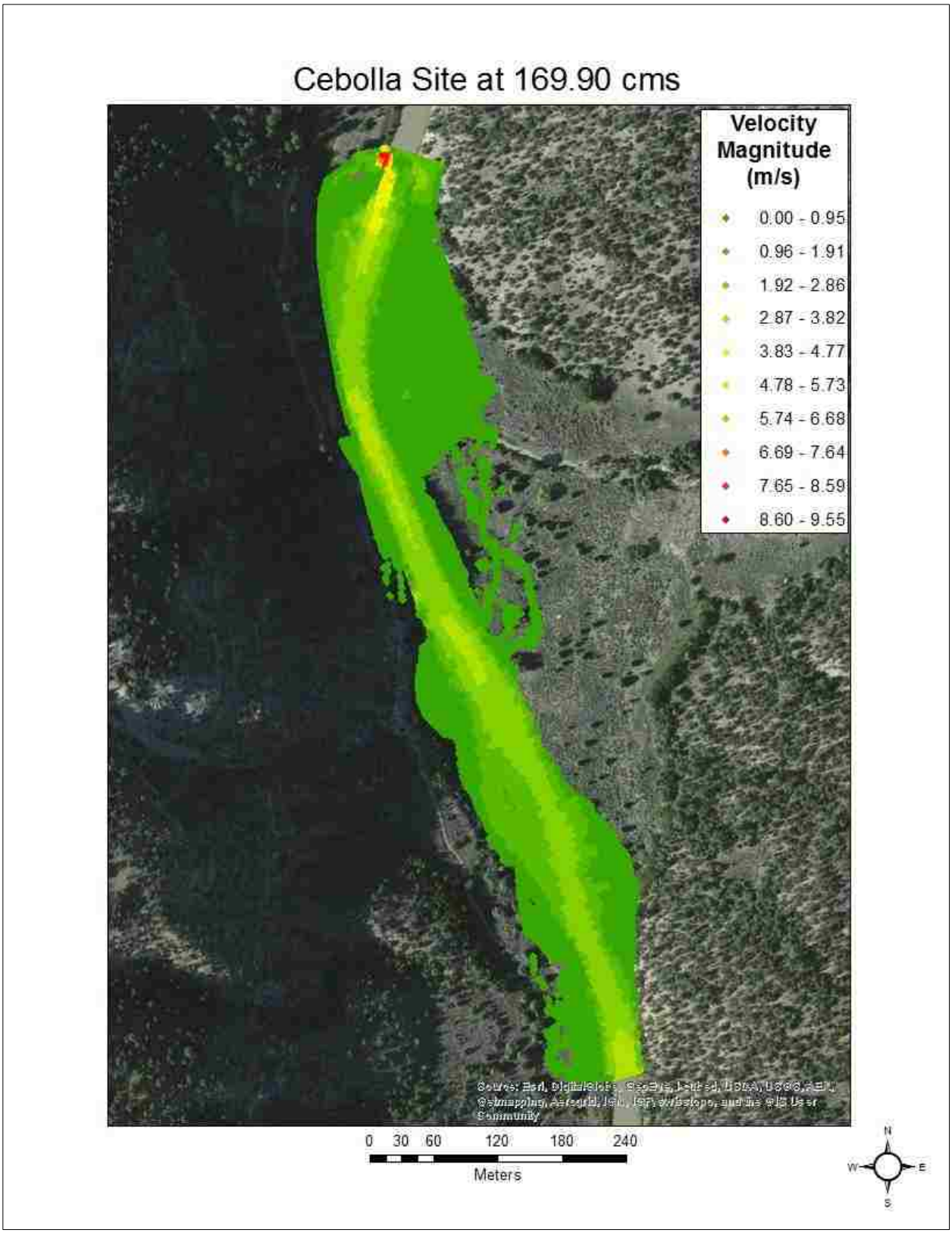

Figure 77: Cebolla Velocity Plan View at 170 m³/s, floodplain *n*=0.060

Appendix J: Sensitivity Analysis

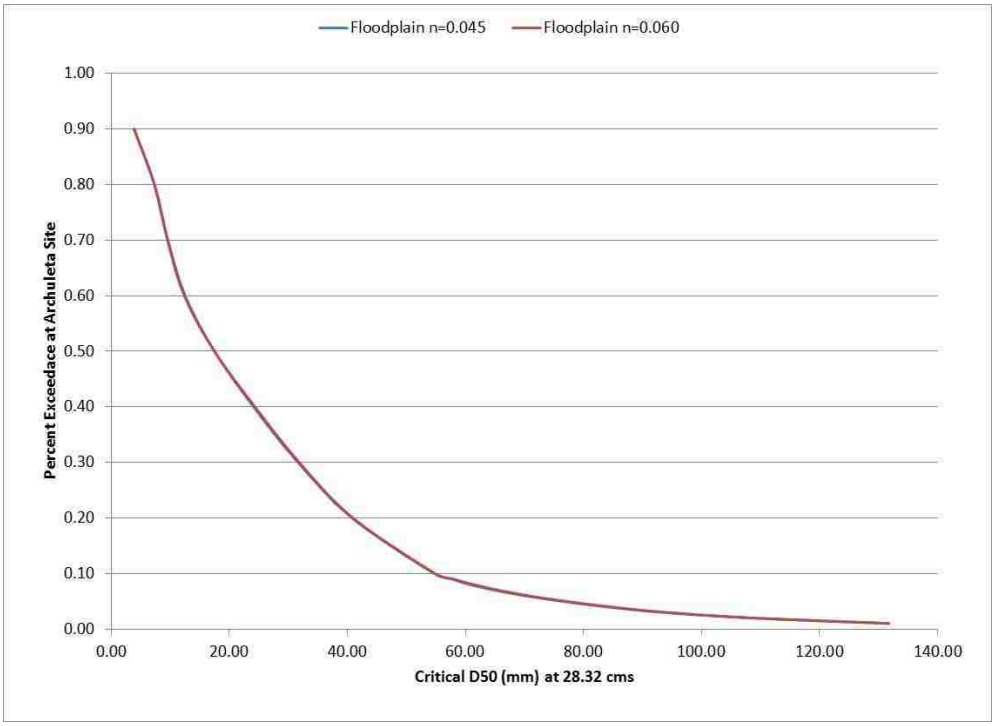

Figure 78: Comparison of Percent Exceedance Curves for Archuleta at 28 m^3/s

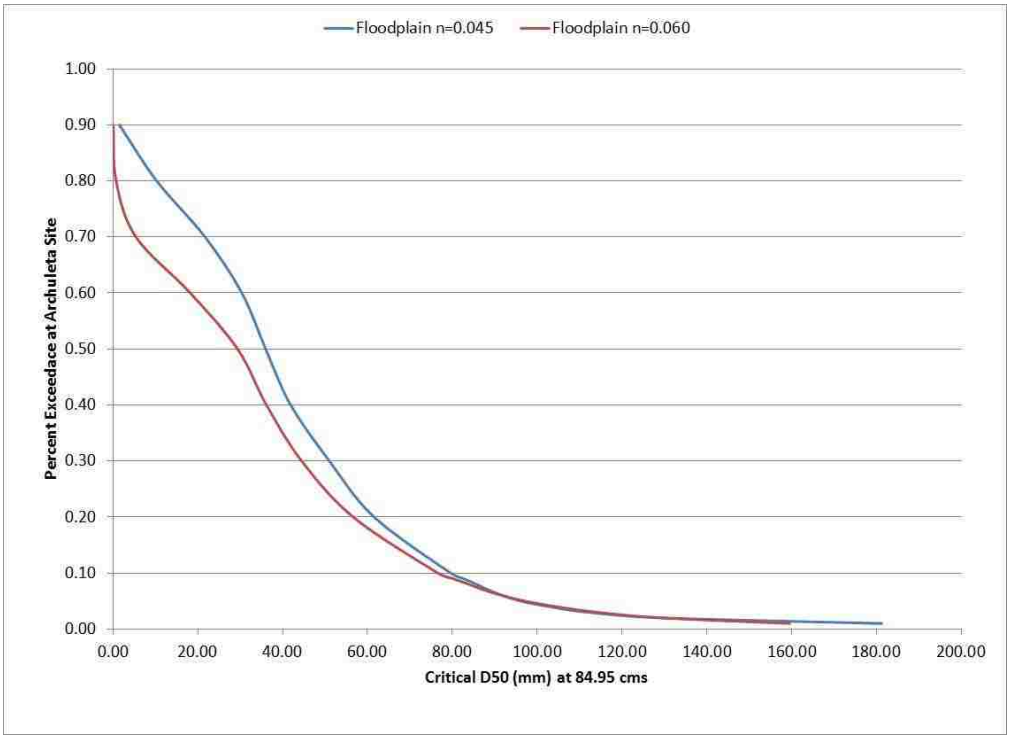

Figure 79: Comparison of Percent Exceedance Curves for Archuleta at 85 m^3/s

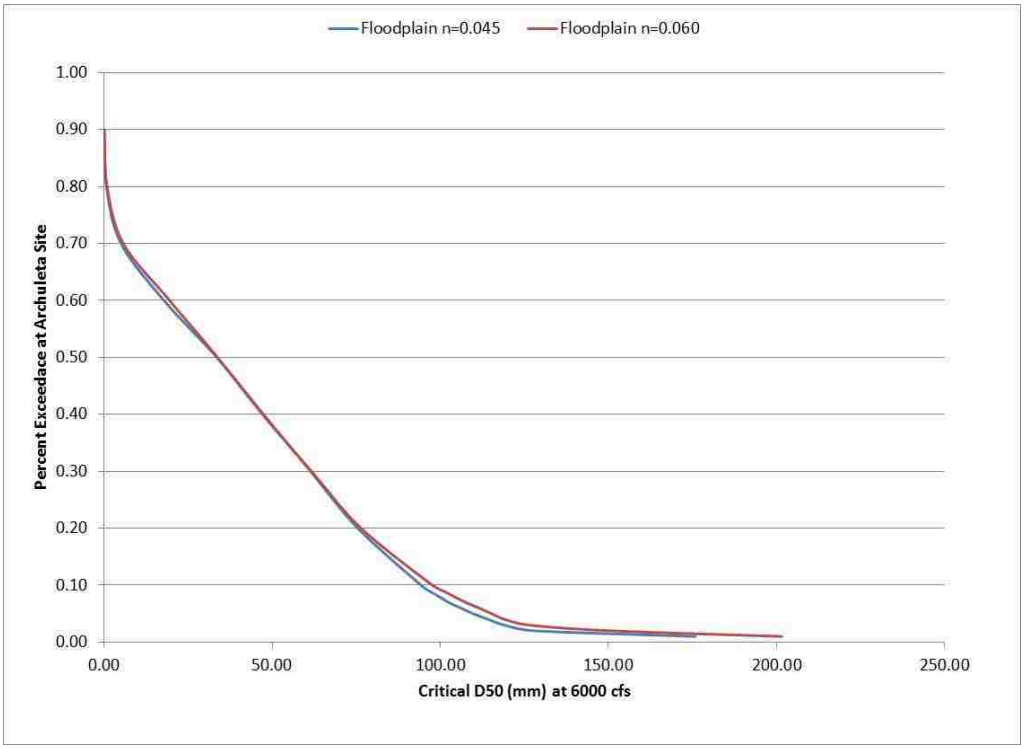

Figure 80: Comparison of Percent Exceedance Curves for Archuleta at 170 m^3/s

Table 18: Archuleta Percent Exceedance for full range of flows, floodplain n=0.045

Archuleta, Floodplain n =0.045	Discharge m^3/sec											
D50 (mm)	14.16	28.32	42.48	56.64	70.8	84.96	99.12	113.28	127.44	141.6	155.76	169.92
Max	100.69	164.34	211.44	250.28	310.05	654.93	607.59	343.53	352.51	359.90	729.27	1153.53
Average	13.79	25.74	31.28	35.34	38.34	40.63	39.64	37.90	37.55	38.37	40.17	41.26
90% Exceedance	1.47	3.89	4.07	2.94	1.99	1.50	0.14	0.03	0.04	0.05	0.05	0.04
80% Exceedance	2.76	7.34	10.69	12.25	11.71	10.30	3.83	0.74	0.60	0.59	0.67	0.70
70% Exceedance	3.49	9.60	14.70	18.90	21.20	21.70	15.41	7.00	4.15	3.78	4.97	5.05
60% Exceedance	4.07	12.53	17.82	23.27	27.50	30.38	27.49	21.36	16.98	15.95	17.73	17.83
50% Exceedance	7.68	17.46	24.01	29.36	32.24	36.00	36.36	33.83	31.90	32.04	33.29	33.54
40% Exceedance	12.91	24.10	30.58	35.77	39.41	41.88	43.22	43.45	43.58	44.50	46.54	47.43
30% Exceedance	18.92	31.62	37.76	42.76	46.80	51.03	52.62	52.03	54.45	56.72	59.49	61.41
20% Exceedance	24.91	40.78	46.56	51.54	56.74	61.58	63.69	64.69	65.27	67.14	71.98	75.46
10% Exceedance	34.69	54.66	62.41	68.67	74.72	79.61	82.42	84.71	86.49	88.86	91.75	94.26
9% Exceedance	35.93	57.71	65.20	71.34	77.43	82.71	85.12	87.60	89.44	92.31	95.05	96.66
8% Exceedance	37.38	60.74	68.68	74.45	80.22	85.74	87.87	90.54	92.75	95.50	97.87	99.67
7% Exceedance	39.07	64.98	72.73	78.45	83.57	88.48	91.22	93.49	96.12	98.67	100.94	102.38
6% Exceedance	40.88	69.96	78.05	83.23	87.83	91.94	94.57	96.99	99.61	102.27	104.61	106.07
5% Exceedance	43.14	76.31	84.84	89.20	93.43	96.12	98.27	100.32	103.52	105.98	108.54	109.78
4% Exceedance	46.12	83.81	92.67	97.43	101.62	102.95	102.88	104.63	107.62	110.37	112.16	114.25
3% Exceedance	49.21	93.22	103.51	110.51	112.27	111.98	110.56	110.30	112.31	114.66	116.91	119.06
2% Exceedance	52.78	108.20	121.60	129.53	131.54	129.41	123.83	118.90	118.94	120.19	124.35	127.83
1% Exceedance	56.47	131.72	153.97	162.78	176.06	181.26	176.23	166.08	163.26	166.51	174.32	175.78

Table 19: Archuleta Percent Exceedance for full range of flows, floodplain n=0.060

Archuleta, Floodplain n =0.060	Discharge m^3/sec											
D50 (mm)	14.16	28.32	42.48	56.64	70.8	84.96	99.12	113.28	127.44	141.6	155.76	169.92
Max	127.39	164.33	211.44	250.30	284.20	651.53	600.02	343.52	352.63	360.21	365.84	1184.87
Average	17.38	25.85	31.45	35.02	37.87	33.88	39.98	38.49	38.05	39.24	41.14	42.58
90% Exceedance	1.36	3.85	3.85	2.06	1.24	0.06	0.16	0.04	0.05	0.07	0.07	0.08
80% Exceedance	2.89	7.29	10.52	10.87	9.57	0.73	3.71	0.84	0.68	0.76	0.81	0.90
70% Exceedance	3.89	9.53	14.57	17.93	19.49	5.39	14.97	7.17	4.25	4.49	5.39	5.70
60% Exceedance	5.94	12.37	17.50	22.63	26.50	18.22	26.79	21.46	16.66	16.55	18.43	19.49
50% Exceedance	8.95	17.48	23.78	28.29	31.13	29.37	35.78	33.42	31.41	31.40	32.78	33.74
40% Exceedance	14.10	24.33	30.72	35.08	38.23	36.18	42.70	43.03	42.97	44.05	46.06	47.10
30% Exceedance	20.99	31.83	37.99	42.52	45.99	44.49	51.63	51.98	54.01	56.81	59.57	61.70
20% Exceedance	29.05	40.93	47.54	51.96	56.64	56.65	63.22	64.16	65.05	67.60	72.48	76.43
10% Exceedance	43.64	54.83	63.22	70.08	77.02	76.61	84.59	86.26	87.76	91.30	94.72	97.65
9% Exceedance	45.75	57.96	66.30	72.97	79.78	80.18	88.08	89.58	91.59	94.83	98.16	100.85
8% Exceedance	48.19	61.39	69.66	76.33	83.03	83.94	91.69	93.31	95.36	98.57	101.73	104.17
7% Exceedance	51.19	65.58	73.69	79.92	86.70	87.46	95.45	97.21	99.77	102.47	105.44	107.45
6% Exceedance	54.02	70.63	79.53	85.00	91.46	91.74	99.83	101.31	103.98	106.68	109.54	111.48
5% Exceedance	58.17	76.95	86.83	91.88	97.95	97.09	105.09	106.06	107.88	110.82	113.20	115.30
4% Exceedance	64.17	84.51	94.59	100.23	106.03	104.62	112.73	112.88	113.43	115.22	117.20	119.15
3% Exceedance	72.75	94.07	104.83	112.04	117.03	114.34	121.54	121.35	120.89	121.95	123.96	126.44
2% Exceedance	86.33	108.53	122.67	131.47	134.16	129.48	135.72	133.44	135.35	139.72	146.58	150.45
1% Exceedance	102.20	131.77	155.43	164.21	174.20	159.52	179.89	178.41	181.30	187.02	195.15	201.51

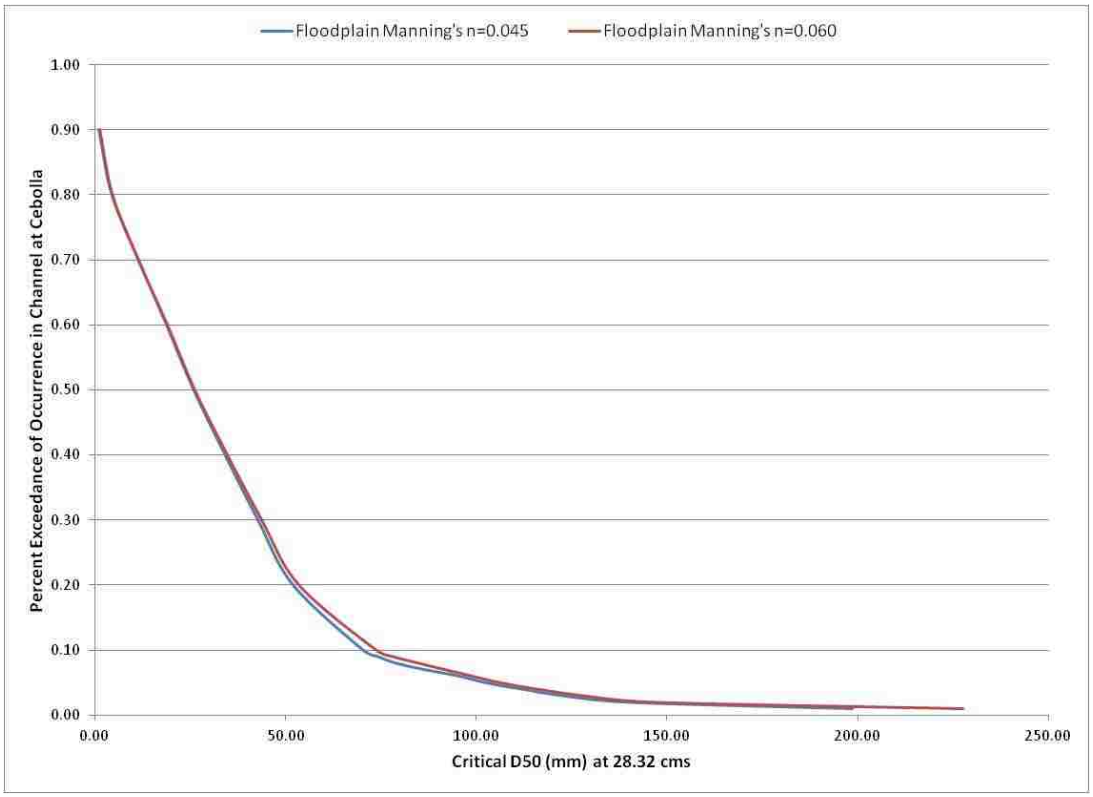

Figure 81: Comparison of Percent Exceedance Curves for Cebolla at 28 m^3/s

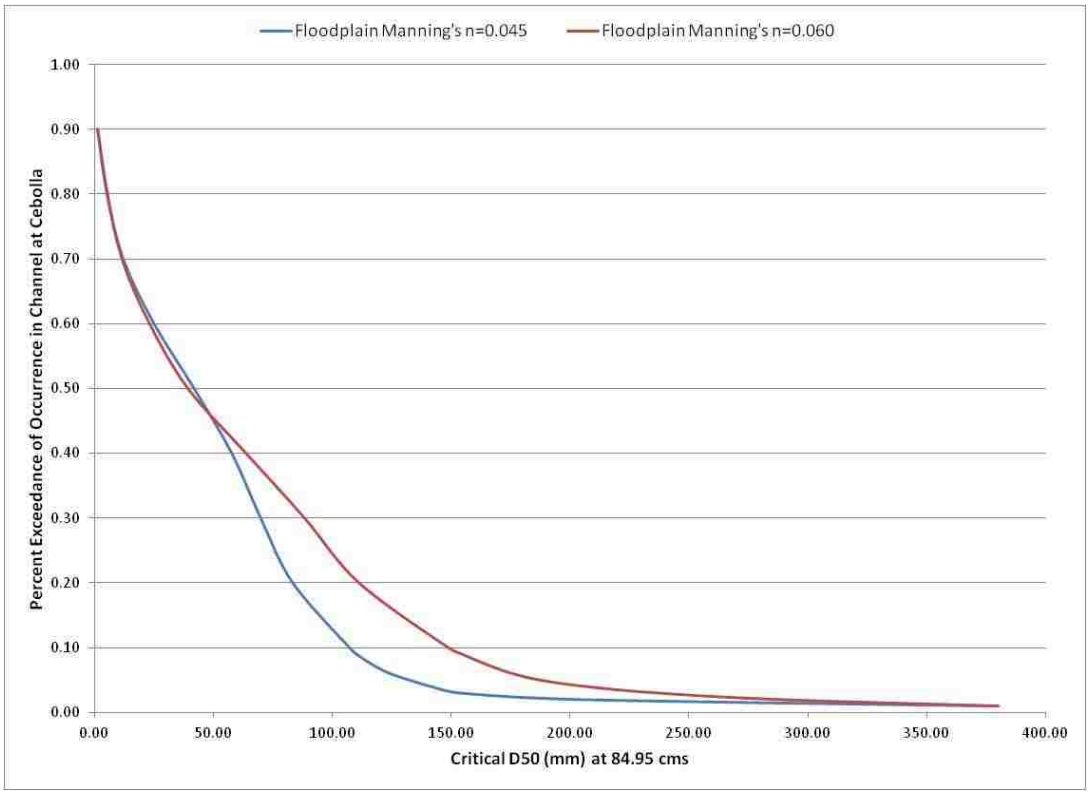

Figure 82: Comparison of Percent Exceedance Curves for Cebolla at 85 m^3/s

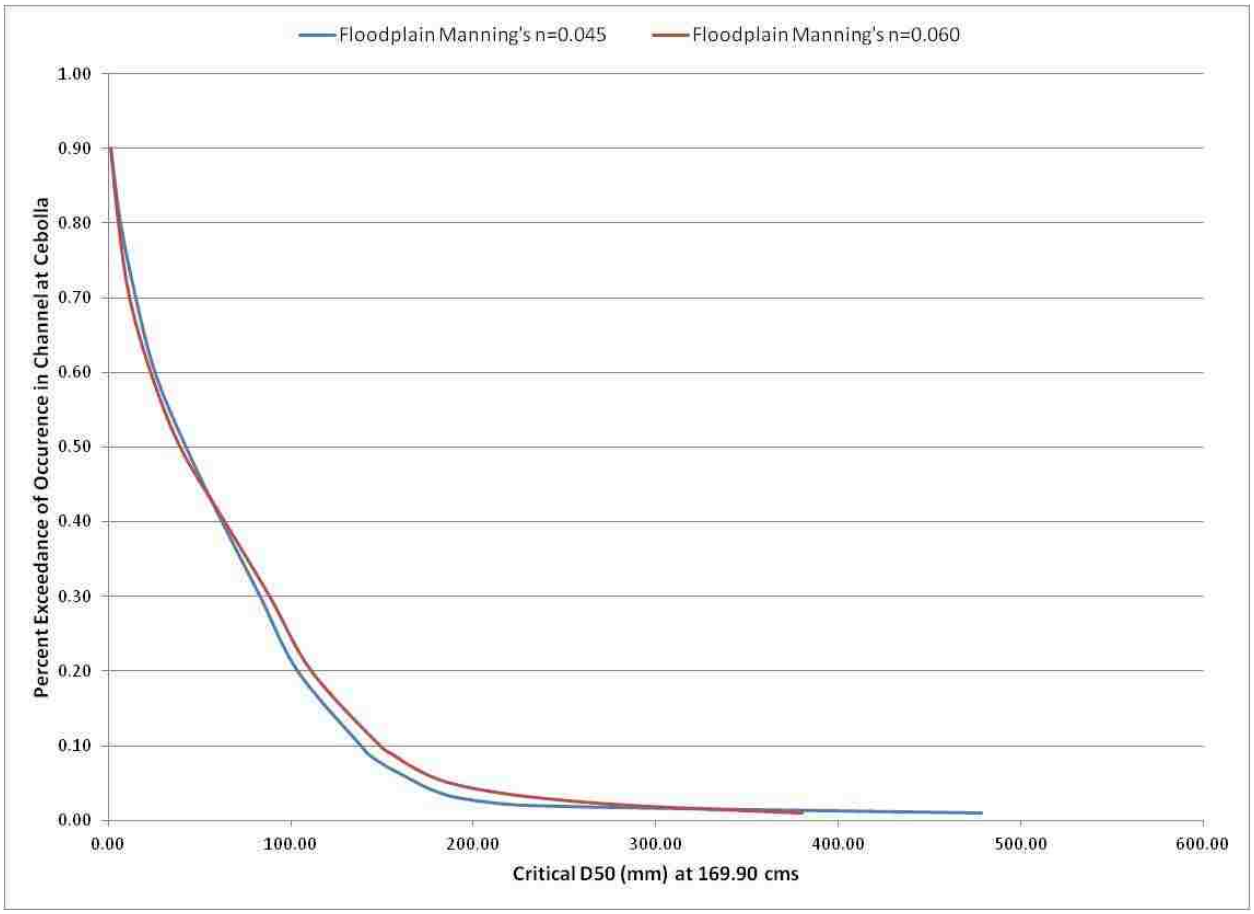

Figure 83: Comparison of Percent Exceedance Curves for Cebolla at 170 m^3/s

Table 20: Cebolla Percent Exceedance for full range of flows, floodplain n=0.045

Cebolla, Floodplain n=0.045	Discharge (m^3/sec)											
D50 (mm)	14.16	28.32	42.48	56.64	70.8	84.96	99.12	113.28	127.44	141.6	155.76	169.92
Max	735.56	823.85	924.30	1026.86	1121.20	1212.04	1289.93	1351.76	1396.63	1415.26	1397.12	1365.34
Average	26.30	35.71	41.77	46.74	50.72	54.02	57.19	59.97	61.82	63.80	64.35	64.72
90% Exceedance	0.62	1.17	1.08	1.39	1.23	1.16	1.34	1.60	1.36	1.23	0.88	1.28
80% Exceedance	3.82	4.56	4.26	4.85	4.90	5.07	5.46	6.39	6.94	7.50	6.88	6.59
70% Exceedance	8.42	11.57	11.08	11.46	11.68	11.90	12.09	12.69	13.51	14.51	14.49	14.96
60% Exceedance	12.91	18.89	22.13	23.71	25.04	24.84	25.49	25.27	24.56	25.31	25.08	25.46
50% Exceedance	18.04	26.01	32.70	36.90	40.06	41.73	43.23	44.37	44.16	44.92	43.91	42.46
40% Exceedance	23.50	34.24	41.11	47.93	53.24	57.59	61.38	62.99	62.96	63.49	63.08	62.18
30% Exceedance	30.03	42.84	50.87	57.92	64.32	69.76	73.15	76.07	78.49	81.32	82.89	83.14
20% Exceedance	38.85	52.06	62.68	71.51	78.83	83.26	88.08	93.55	97.59	100.69	102.52	103.73
10% Exceedance	52.71	70.41	85.22	93.24	99.49	107.12	114.37	120.13	125.61	131.00	134.22	138.36
9% Exceedance	56.03	74.33	88.47	95.78	102.59	110.06	117.51	123.35	129.57	135.67	139.29	141.89
8% Exceedance	60.47	79.08	92.67	99.94	106.54	114.14	120.68	126.83	133.88	140.39	145.10	147.41
7% Exceedance	66.96	86.66	99.46	106.34	111.74	118.57	124.75	130.88	138.38	145.38	151.09	154.21
6% Exceedance	72.36	95.68	106.21	113.61	119.97	124.33	129.58	135.59	143.12	150.75	157.69	162.11
5% Exceedance	79.64	102.49	112.69	123.13	128.77	132.42	134.87	141.91	148.75	156.52	164.26	169.58
4% Exceedance	86.96	112.20	121.70	132.37	139.17	141.56	144.69	151.37	156.74	165.01	171.69	178.61
3% Exceedance	95.58	122.72	135.19	144.84	150.09	154.01	161.30	168.69	174.48	182.57	189.77	192.75
2% Exceedance	108.59	139.82	158.14	167.33	185.93	203.74	211.99	222.75	224.75	227.74	228.55	232.37
1% Exceedance	136.36	198.55	248.66	293.77	336.23	377.26	418.44	455.96	483.76	495.36	495.47	478.46

Table 21: Cebolla Percent Exceedance for full range of flows, floodplain n=0.060

Cebolla, Floodplain n=0.045	Discharge (m^3/sec)											
D50 (mm)	14.16	28.32	42.48	56.64	70.8	84.96	99.12	113.28	127.44	141.6	155.76	169.92
Max	939.69	1152.98	1281.88	1377.26	1503.99	1613.72	1689.63	1730.01	1721.55	1656.43	1621.75	2317.00
Average	28.13	37.44	44.18	49.90	53.74	57.38	61.05	63.18	64.83	66.63	68.10	67.05
90% Exceedance	0.90	1.22	1.16	1.47	1.08	1.21	1.58	1.58	1.63	1.58	1.77	1.16
80% Exceedance	4.90	4.53	4.58	5.30	4.83	4.97	5.71	6.21	6.94	7.64	8.03	5.29
70% Exceedance	9.13	11.31	11.04	12.23	11.73	11.90	12.39	12.49	13.48	14.75	16.27	11.40
60% Exceedance	13.69	18.96	22.20	24.29	24.91	25.53	26.91	25.34	25.03	26.54	28.22	23.00
50% Exceedance	19.11	26.11	32.76	37.61	40.69	42.53	44.85	45.19	45.49	45.94	46.71	39.16
40% Exceedance	24.96	34.68	41.82	48.30	53.34	58.07	62.58	64.24	64.54	65.94	67.02	63.63
30% Exceedance	31.40	43.70	51.93	59.30	65.10	70.83	75.02	78.03	80.78	83.66	86.05	88.28
20% Exceedance	39.75	53.47	64.35	73.59	80.12	84.71	90.20	95.77	100.51	104.42	106.93	111.20
10% Exceedance	54.28	73.76	88.36	96.03	103.61	111.32	118.54	124.20	128.91	134.08	138.27	148.77
9% Exceedance	57.65	78.24	92.74	99.93	107.52	115.87	122.52	127.58	132.54	138.30	142.38	154.65
8% Exceedance	64.03	84.90	98.70	106.01	112.34	120.61	127.43	131.51	136.95	143.09	147.94	160.95
7% Exceedance	69.98	91.87	105.38	113.68	120.52	126.57	132.85	136.83	142.29	148.15	153.97	167.87
6% Exceedance	75.38	98.99	113.39	122.60	129.70	135.59	138.88	142.75	148.41	154.21	160.50	175.93
5% Exceedance	83.46	106.28	121.03	132.32	140.65	144.61	147.32	151.63	156.48	161.54	168.15	187.54
4% Exceedance	91.30	116.16	133.78	145.48	150.31	153.91	160.11	166.57	169.89	175.70	180.96	207.01
3% Exceedance	101.24	127.97	147.76	163.38	167.24	172.73	182.35	188.98	197.36	204.03	209.84	237.58
2% Exceedance	114.29	146.18	169.33	201.46	224.98	248.90	258.54	258.33	258.35	263.76	268.51	288.35
1% Exceedance	164.15	227.69	282.53	327.21	373.14	419.84	466.53	497.65	505.76	502.19	501.27	380.27